A STUDY OF AMORPHOUS SILICON ALLOYS

by

Paul Shufflebotham

A thesis
presented to the University of Manitoba
in partial fulfillment of the
requirements for the degree of
Master of Science
in
Electrical Engineering

Winnipeg, Manitoba, 1985

ISBN 0-315-34048-7

A STUDY OF AMORPHOUS SILICON ALLOYS

BY

PAUL SHUFFLEBOTHAM

A thesis submitted to the Faculty of Graduate Studies of the University of Manitoba in partial fulfillment of the requirements of the degree of

MASTER OF SCIENCE

The University of Manitoba requires the signatures of all persons using or photocopying this thesis. Please sign below, and give address and date.

ABSTRACT

An extensive review of amorphous silicon alloys is presented. General methods of amorphous alloy fabrication are classified and their basic operational principles outlined. The electrical and optical properties of these alloys are discussed in detail. Applications which utilize the unique properties of these alloys are described. Conspicuous gaps in the knowledge of these materials are pointed out, suggestions made for future studies and potential new applications are described. A comprehensive bibliography is presented, with references to all amorphous alloys studied up to the present date.

An experimental investigation of the fabrication of a-Si:N:H thin films by ARE with N_2 and H_2 gasses is reported. Characterization of a variety of electrical and optical properties of these films showed that no significant amounts of N or H were incorporated into the films. These films were found to possess the high dark conductivity, small activation energy and negligible photoresponse characteristic of evaporated a-Si thin films. These films were also found to contain a high concentration of defects and voids. Impurities from the atmosphere were incorporated into the films through this void network, producing O and H rich surface layers. These surface layers were found to produce thickness dependencies in the electrical and optical properties of the films. It was concluded that the lack of N or H incorporation by ARE was due to the low reactivity of the N_2 and insufficient quantities of H_2. These difficulties could be solved through the use of a more reactive gas such as ammonia.

An experimental investigation of the fabrication and properties of a-Si:Te thin films is reported. A-Si:Te thin films were produced by co-evaporation over the composition range of 0 to 82 at.% Te. Films with a greater Te concentration were subject to microcrystallization of the Te. X-ray compositional mapping showed that only films with less than 5 at.% Te or in the range of approximately 30 to 70 at.% Te were homogeneous on a macroscopic scale. All films displayed the general properties characteristic of evaporated Si (or Te) thin films; high dark conductivity, small activation energy, high density of localized gap states and negligible photoresponse. The optical energy gap was found to decrease slowly with increasing Te content. The Te was observed to produce two different behaviours in a-Si:Te. For Te concentrations of less than 1 at.%, the Te was incorporated as a four-fold coordinated substitutional double donor; decreasing the activation energy and increasing the density of localized gap states. For Te concentrations of approximately 60 at.%, the films formed a significantly less defective material, probably as an approximation to the CRN structure of a-$SiTe_4$. This produced an increase in the activation energy and photoresponse, and a decrease in the density of localized gap states. The a-Si:Te thin films also exhibited a small degree of atmospheric impurity absorption, though no thickness effects were observed.

ACKNOWLEDGEMENTS

The author would like to thank his advisor, Prof. H. C. Card, for his guidance and encouragement over the course of this project.

The author would also like to thank Prof. A. Thanailakis and Prof. K. C. Kao for their assistance and many helpful discussions. Special thanks go to S. R. Mejia and Prof. R. D. McLeod for their endless patience in helping me with the many practical difficulties encountered during this work. I also wish to thank my colleagues at the Materials and Devices Research Laboratory; especially J. J. Schellenberg, with whom I had many interesting and helpful discussions.

Financial support of Howie's Endless Loot Pile (HELP) is gratefully acknowledged.

TABLE OF CONTENTS

LIST OF FIGURES

LIST OF TABLES

CHAPTER I

INTRODUCTION

In the last decade, non-crystalline materials have become one of the most active fields of study in condensed-matter physics [1]. In particular, the study of amorphous semiconductors has been one of the most productive with respect to applications. Of the amorphous semiconductors, hydrogenated amorphous silicon (a-Si:H) is certainly the most important. This material is used in solar cells, electrophotography, image sensors, LEDs, thin-film transistors, diodes, CCDs, ambient sensors, VLSI microfabrication [2] and archival storage [3]. Recently, interest has begun to spread to other amorphous silicon alloys. Unlike their crystalline counterparts, amorphous alloys are not restricted to stoichiometric compositions. Indeed, in principle they can be produced as microscopically homogeneous alloys in *any* composition. This allows the physical properties of such a material to be varied over a wide range simply by changing the composition. A number of interesting applications have been developed that take advantage of this and other unique properties displayed by this new class of materials (see Chapter 2).

Two quite different amorphous silicon alloys were investigated in this thesis; a-Si:N:H and a-Si:Te. A-Si:N:H has become a popular subject of study as a result of its superior properties for use in electrophotography. In this thesis, a new fabrication technique called activated reactive evaporation (ARE) was used in an attempt to produce thin films of this alloy (Chapter 3). This method shows promise as an inexpensive, high-rate fabrication process — capable of producing a wide variety of alloys made from a combination of solid and gaseous components.

The fabrication and characterization of thin films of amorphous silicon telluride was the subject of the second study reported in this work (Chapter 4). This is only the third study of the electrical and optical properties of this material, and is the first to examine the composition range below 75 at.% Te. This material exhibits a number of unusual properties, and though few applications are presently foreseen, it does have potential, and is certainly interesting from a purely scientific standpoint.

1.1. Theoretical Considerations

In an amorphous material, the constituent atoms are not arranged in a periodic fashion, implying that long range order is absent. Due to the limited number of bonding configurations available to the individual atoms, however, there is short range order present in the nearest neighbour region about each atom. This short range order accounts for the fact that amorphous materials tend to resemble their crystalline counterparts in their physical properties. However, this resemblance is generally only qualitative in nature, and the presence of disorder can introduce entirely new behaviours.

The most profound effect of the presence of disorder is on the theoretical understanding of such solids. Without periodicity (and thus symmetry) one is no longer able to use Bloch's theorem, Brillouin zones, selection rules or symmetry arguments to understand their properties [1]. Indeed, the search for replacements for such powerful conceptual tools is still underway. Recently, several promising new avenues of research have arisen out of the general scientific renaissance developing from studies of nonequilibrium, evolving, interacting and other complex systems. New concepts such as fractal geometry [4], fuzzy groups [5] and cellular automata [6] have been applied to disordered systems, with varying degrees of success.

Even without such novel approaches, significant progress has been made in extending the theory of crystalline solids to amorphous materials. This effort has produced a successful, if somewhat qualitative, theoretical base upon which meaning may be given to the wealth of experimental data accumulated on amorphous semiconductors over the last two decades. In order to understand their results, experimenters utilize this theory (most of which is described in the landmark book by Mott and Davis [7]) as a standard method of evaluating and comparing their results. This procedure has also been used throughout this thesis. A brief summary of the theoretical concepts utilized in the evaluation of the experimental data obtained in this research will be presented in the following.

1.1.1. X-Ray Diffraction

The absence of lattice periodicity in an amorphous material means that the Bragg or von Laue conditions (for constructive interference of X-rays reflected from a lattice) cannot be satisfied. This implies that no sharp peaks will occur in an X-ray diffraction pattern of an amorphous material, although

broad peaks are sometimes produced as a result of short range order or the presence of microcrystallites As a result, X-ray diffraction has become a universal method of ascertaining whether or not (or to what extent) a sample is amorphous.

1.1.2. Electrical Properties

In the analysis of the electrical and optical properties of any material, one naturally starts with Schrödingers' equation:

$$H\psi(\mathbf{r},t)=E\psi(\mathbf{r},t) \tag{1.1}$$

where $\psi(\mathbf{r},t)$ is the electron wavefunction, H is the quantum mechanical Hamiltonian (eigenfunction) and E the energy (eigenvalue). In a crystalline material the solutions to this equation are in the Bloch form, which is a basic tool of solid state theory. Unfortunately, without periodicity one cannot write solutions in such a form. However, solutions to (1.1) must still exist, if not in a convenient form. Therefore, the concept of the density of states (DOS), $N(E)$, can be carried over from crystalline theory [7]. Since, of course, this is an electronic DOS, the occupancy of these states must still be described by the Fermi-Dirac distribution, $f(E)$.

In an ideal crystalline semiconductor the density of states has the form of Fig. 1.1(a); where bands of extended states are separated by a forbidden energy gap. This picture is subject to considerable modification in an amorphous semiconductor.

In 1958, Anderson [8] recognized that the random potential produced by an amorphous lattice produces spacial localization of the electronic wavefunctions. Later it was shown that if one state at a given energy is localized, then all states at that energy must be localized [7]. These localized states, said to be due to Anderson localization, occur as tail states at the edges of the conduction and valence bands, extending into the energy gap, as shown in Fig. 1.1(b). These localized states are separated from the extended states by the so-called mobility edge.

If, in the amorphous network, all bonds are satisfied, then that network is referred to as a continuous random network (CRN), and the material is called a Fermi glass [7]. This is not the case for the materials studied in this thesis. These evaporated amorphous silicon alloys are highly defective because of the highly strained nature of tetrahedral networks, the high growth rate and

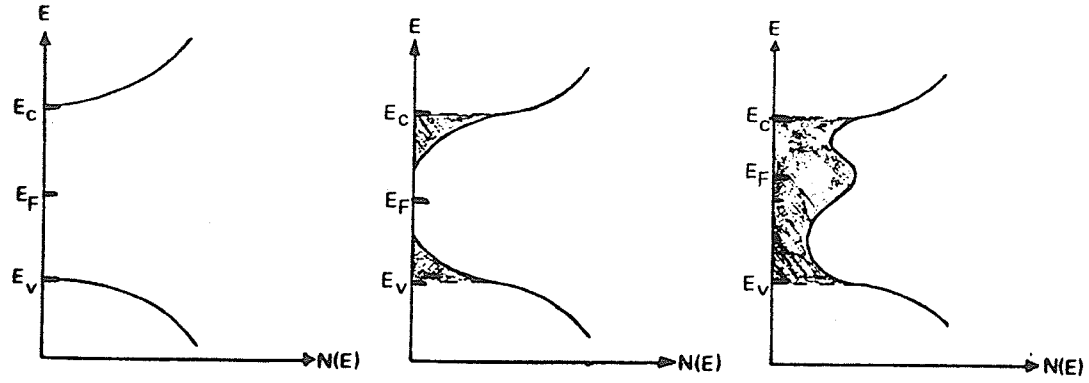

FIGURE 1.1: Density of states models: (a) is for an ideal crystalline semiconductor, (b) shows additional structure in the form of localized tail states due only to disorder and (c) shows the case of a highly defective material producing additional localized states throughout the gap. Regions of localized states are indicated by shading.

bombardment of the growing film by X-rays and energetic Si atoms from the melt. Such films contain a significant number of voids and dangling bonds. These defects produce additional localized states throughout the energy gap, producing a DOS as in Fig. 1.1(c) [7], which is the model used throughout this thesis.

The high density of localized gap states pins the Fermi level in the gap near E_c (making pure a-Si intrinsically n-type), and makes doping control of the carrier concentrations impossible. This problem was solved in 1975 when Spear and Le Comber [9] discovered that incorporation of hydrogen into a-Si films satisfied the dangling bonds, greatly reducing the density of gap states, making effective doping of this material possible. This has made a-Si:H a very useful material, and it has since become the most extensively studied and applied amorphous semiconductor.

Electronic conduction in amorphous semiconductors usually takes place through a combination of three distinct processes, each of which dominates in different temperature ranges. At room temperature and above, conduction proceeds via electrons and holes thermally stimulated into the extended states. For electrons, This type of conduction is described by the expression [7]

$$\sigma = \sigma_0 \, e^{-(E_c - E_f)/kT} \tag{1.2}$$

where σ_0 is a constant. This type of conduction is thermally activated with

activation energy $E_a = E_c - E_f$, and shows up as a linear graph of $\ln\sigma$ vs $1/T$. The slope of such a graph is proportional to E_a, which is usually obtained in this manner. This parameter is widely used in the analysis of amorphous semiconductors.

At somewhat lower temperatures, conduction is often dominated by variable-range hopping of electrons between localized tail states of similar energy. This hopping process is phonon-assisted in that phonons are emitted or absorbed as an electron hops between states of slightly different energies. This type of conduction is described by expression [7];

$$\sigma = \sigma_1 e^{-(E_1 - E_f + w)/kT} \tag{1.3}$$

where w is the hopping activation energy and E_1 is an arbitrary (but constant) energy within the range of tail states. This is also an activated process, though if w is significant it will decrease with T, producing a decreasing slope in a plot of $\ln\sigma$ vs $1/T$ with decreasing T.

When the temperature is low enough such that the DOS can be considered constant over an energy range comparable to kT (which can be near room temperature in evaporated thin films), the expression for variable range hopping, now within the defect states near the Fermi level, becomes [7]

$$\sigma = \sigma_2 e^{-T_0/T^{1/4}} \tag{1.4}$$

where T_0 is a constant. This constant is a function of the DOS at the Fermi level, $N(E_F)$, and is given by [7]

$$T_0 = \left[\frac{16\alpha^3}{kN(E_F)}\right]^{1/4} \tag{1.5}$$

where α is a constant related to the rate at which the wavefunction of an electron in a single potential well falls off with distance, and is usually assumed to be approximately 10 Å for a-Si [7]. Note that in this case the pre-exponential factor σ_2 contains a $T^{-1/2}$ dependence, so a plot of $\ln(\sigma_d T^{1/2})$ vs $1/T^{1/4}$ will be linear if variable range hopping conduction is dominant. The constant T_0, and thus an estimate of $N(E_F)$ can be obtained from the slope of the linear portion of such a graph.

Photoconductivity is also an important feature of an amorphous semiconductor. A great deal of information can be obtained from a detailed study,

though usually a clear demonstration of its presence and a calculation of the ratio $\frac{\sigma_{photo}}{\sigma_{dark}}$ is sufficient for a general characterization.

1.1.3. Optical Properties

A particularly important parameter characterizing a semiconductor is the size of the energy gap, $E_g = E_c - E_v$. As has already been mentioned, there is really no such gap in amorphous semiconductors, yet something plays an equivalent role. This is called the optical gap, E_o, and is obtained from measurements of the energy dependence of the optical absorption coefficient, α, in the highly absorbing region of the fundamental absorption edge. The absorption coefficient in this region is usually measured with optical and near IR spectrophotometry. E_o is related to α by the following equation for a-Si based materials [7];

$$\alpha h\nu = B(h\nu - E_o)^2 \tag{1.6}$$

where B is a constant. This equation is the consequence of a number of assumptions, making E_o useful mainly as a tool for comparison purposes (and is of great importance as such). A linear extrapolation of a plot of $\sqrt{\alpha h\nu}$ vs $h\nu$ to the $h\nu$ intercept yields the value of E_o. This technique is widely used, and was also used in this thesis. It should be noted, however, that the power of 2 in (1.6) is a result of the assumption of a parabolic DOS [7]. The validity of this assumption is still a matter of some debate. Recent inverse-photoemission studies of a-Si:H [10] have shown that the DOS is in fact *linear*, which would require the use of a power of 3 in (1.6). The form of (1.6) was retained in this thesis in order to allow comparison with the work of other researchers.

Another useful parameter is the refractive index, n. In this thesis, n was mainly used to indicate relative changes in an alloy as a function of composition. The refractive index, as well as α, were measured in the optical region by ellipsometry.

1.2. Organization of this Thesis

In Chapter I a brief review of the development of the study and application of amorphous semiconductors was given. The theoretical model used in this thesis to analyze the experimental results was also described.

Chapter II gives an extensive review of the field of amorphous alloys, using amorphous silicon alloys as a frame for discussion. This chapter was written in collaboration with Prof. A. Thanailakis and Prof. H. C. Card, and has been submitted for publication to Applied Physics Reviews.

Chapter III describes the results obtained in attempts to produce a-Si:N:H alloys using activated reactive evaporation. This technique was not successful; though through a careful analysis of the fabrication process and the films produced, it was discovered that successful production could probably be obtained with minor system modifications.

Chapter IV describes the fabrication and properties of a-Si:Te by electron beam co-evaporation. The understanding of the physical properties of this unusual material has been advanced significantly as a result of the research presented in this chapter. This chapter has been submitted for publication to the Journal of Applied Physics.

Finally, Chapter V summarizes the results of this work and presents conclusions and recommendations for further work in the field of amorphous silicon alloys.

CHAPTER II

A REVIEW OF AMORPHOUS SILICON ALLOYS: FABRICATION, PROPERTIES AND APPLICATIONS*†

Over the span of a single decade, amorphous semiconductor research has risen from almost complete obscurity to become one of the most active areas in condensed matter physics. This has largely been a result of the discovery of hydrogenated amorphous silicon (a-Si:H) in 1969 by Chittick et al. [1]. In 1975 Spear and Le Comber [2] found that efficient doping of this material was possible, resulting in a change in the room temperature conductivity by 10 orders of magnitude. As a direct result of this discovery, a-Si:H is now used in a large number of important and varied applications. Some examples are: solar cells, electrophotography, image pickup tubes, image sensors, CCDs, FET arrays, ambient sensors, LEDs, archival storage, memory switching and on-chip optical waveguides [3].

Recently, research has begun to turn to the improvement of these applications, and the development of new ones, through the use of other amorphous silicon based alloys. The great potential of amorphous semiconductor alloys lies in the fact that most of their physical (electrical and optical) properties can be varied continuously over wide ranges by changing their composition, since stoichiometry is not required. Multilayered devices can be made and inexpensive substrates used, since lattice-matching is also not required.

The purpose of this review is to catalog the present state of understanding and ignorance of the properties and uses of amorphous Si alloys. To accomplish this, we begin with a summary of the fabrication techniques that have been, or could be, used to produce amorphous Si alloys. The importance of this topic cannot be overemphasized; as anyone who has worked with amorphous materials knows all too well, most if not all of the physical properties of these materials are highly sensitive to the conditions under which they were made. One cannot, in general, separate the material from its method of fabrication. We then go on to describe the electrical and optical properties of all

* The contents of this chapter are from a paper co-authored with A. Thanailakis and H. C. Card, which has been submitted for publication in Applied Physics Reviews.
† The references for this chapter are given on pages 68-75.

amorphous Si alloys that have been studied to the present date. To our knowledge, this is the only review which covers the full range of amorphous silicon alloy behaviour. Finally, we discuss the various existing and proposed applications for these interesting materials.

2.1. Preparation Methods

There is a great variety of methods used to produce amorphous silicon alloys. The method used to produce a particular material depends primarily on two considerations:

(1) the glass-forming ability (GFA) of the alloy,

(2) the desired form of the material.

Recent results on glass-forming ability have been reviewed by Davies [5], though it should be mentioned that a deep eutectic in the equilibrium phase diagram generally indicates easy glass formation. The success of a particular deposition method depends on the cooling rate that can be obtained. The higher the cooling rate, the more alloy systems that can be prepared, and the wider the composition range possible in each system (compositions centered about the eutectic(s)). A brief review of preparation methods has been given by Lieberman [5]. These and other results will be presented in the following subsections.

Most preparation techniques are variations of a few basic schemes. Since even a moderately detailed treatment of amorphous material production processes would fill a fair sized monograph, we will discuss only the basic processes, referring the reader to more complete sources of information.

Fabrication methods for amorphous materials can be classified according to the underlying physical principles used:

(1) production by quenching from the molten phase (rapid quenching),

(2) deposition by "atomization" (evaporation, sputtering),

(3) deposition by chemical processes (CVD, glow-discharge),

(4) surface modification by diffusion or implantation.

2.1.1. Production by Quenching

These processes utilize the formation and subsequent quenching of a melt of the desired composition into an amorphous solid material. The melt is formed by one or more of the usual heating methods: resistive, electron-beam, laser, induction or plasma jet. If the melt is quenched through contact with some external cooling medium, the material will be produced in a bulk (or powder) form. If the bulk of the solid is used to cool a melted region, then the amorphous material will be in the form of a modified surface layer. Both these processes are discussed in this section.

Amorphous materials produced in bulk form are often referred to as glasses; two particularly important examples are the chalcogenide glasses and glassy metals. These terms describe the two main groups of amorphous solids that can be produced in bulk form. All bulk amorphous materials are made by some form of quenching of the melt. In these processes a liquid melt of the desired composition is formed, and then rapidly cooled so that nucleation and crystallization do not have a chance to occur. Bulk quenching methods are limited to cooling rates of less than 10^7 K/sec; so the kinds of amorphous materials that can be produced in bulk form is limited to a very few pure elements, alloys containing high concentrations of metallic elements (transition and noble metals), and the chalcogenides (alloys containing high concentrations of column 6a elements). One other general feature of quenching processes that should be noted is that the higher the cooling rate of a given process, the smaller the quantity of material that can be produced by that process [5].

The highest quenching rates of any fabrication process (excluding ion-implantation) are found in pulsed energy quenching processes. These techniques have typical cooling rates of 10^{10} K/sec. However, such processes are limited to producing thin surface layers of amorphous solid, supported by a much larger bulk region (which was used as the cooling medium) [6].

2.1.1.1. Sealed-Melt Quenching

Normal quenching methods generally do not have the high cooling rates needed to produce amorphous materials. However, alloys made from column 6a elements are often easily formed into glasses, and can be produced in large quantities by a (relatively) slow quenching process, which we will refer to as sealed-melt quenching.

Sealed-melt quenching was first used to produce a-Si alloys by Hilton et al. in 1966 [7]. In this process, high purity elements are sealed in an evacuated quartz vial (in amounts proportional to the desired alloy composition), which is then heated at high temperature (1000 °C) in a rocking furnace for long periods (16-40 hrs.). The vial is then quenched to room temperature in air or water. This process is capable of producing tens of grams of glassy material in a single run [7]. However, this process has a very low cooling rate, and thus is only capable of producing glasses of a limited type.

2.1.1.2. Rapid Quenching

Rapid quenching processes all operate on the principle of maximizing the cooling rate by changing the shape of the melt in order to maximize the contact area between the melt and the cooling medium [5]. A great variety of techniques have been developed to implement this process. Lieberman [5] has given a brief review (containing a thorough bibliography) of the commonly used techniques. The following discussion is based largely on his review.

Rapid quenching methods can be classified according to whether they are one-shot or continuous processes. One-shot techniques produce material in the form of small foils, while continuous processes produce filaments or ribbons. One-shot processes are referred to generically as "splat" quenching, while continuous processes are usually some form of "melt-spinning" technique.

Rapid quenching processes were pioneered by Pol Duwez and co-workers in 1960 [8]. They produced the first metallic glass (a-Si:Au) by a form of splat quenching known as the gun technique. This method uses a shock-tube to propel the molten alloy onto a thermally conductive substrate at high velocity. This has probably the highest cooling rate of all the rapid quenching processes, perhaps as much as 10^8 K/sec [9].

A wide range of variations of this theme have been used by other researchers [5]. Only the basic types will be mentioned here. Piston-and-anvil and twin piston methods squeeze a falling melt between colliding cooling surfaces. Arc-hammer techniques use an arc or plasma jet to produce a melt on a flat, water-cooled hearth, which is then flattened by striking with a hammer. A somewhat different method, referred to as melt spraying involves spraying the melt through a plasma flame, which breaks the melt up into droplets which then condense on a substrate. All these processes have cooling rates in the range of 10^6 to 10^7 K/sec.

Splat quenching techniques suffer from some serious limitations, despite their relatively high cooling rates. The quantity of material produced is very small, and is produced in a very irregularly shaped form (especially in thickness), which makes these materials unsuitable for many mechanical and electrical studies [5].

Considerable effort has gone into the development of new fabrication techniques designed to overcome the limitations of splat quenching processes. A major breakthrough was the invention by Pond and Maddin of a continuous

ribbon-forming process [10]. This development allowed large scale manufacture of glassy metals, and also made available large quantities of material in forms suitable for the study of their electrical, optical, magnetic, mechanical and chemical properties.

The most common form of rapidly quenched alloys is that of ribbons a few mm wide and on the order of tens of microns thick. These continuous ribbons are made by some form of "melt spinning" [5]. These processes involve ejecting the molten alloy onto a (thermally conductive) spinning surface so that a continuous stream of molten material is rapidly quenched. There have been a number of techniques developed to accomplish this. Helical ribbons are produced by injecting the melt onto a spinning disc or drum. The latter method can also be used to produce filamentary material. Straight ribbons can be made using wheels, single or twin rollers, or rapidly moving belts. These processes generally have cooling rates on the order of 10^6 K/sec.

It is often desirable to have samples in the form of wires or filaments, and several techniques have been developed to produce such samples [5]. The most common methods inject a thin stream of molten material into a gaseous or liquid cooling medium. One of the oldest methods involves rapidly pulling a glass tube containing the melt into a thin fiber [5].

Large amounts of material for use in X-ray diffraction, electrical measurements, or for compaction forming into otherwise unproducible shapes can be obtained in powder form by a variety of techniques. These techniques will not be discussed in this paper. The interested reader is referred to the recent review by Miller [5].

2.1.1.3. Formation of Melted Surface Layers

Recently, through the use of directed energy beams (lasers, electron beams), it has become possible to produce thin surface layers of amorphous materials by a new form of rapid quenching process. So far, lasers have been used in these processes, and thus these techniques are usually referred to as *laser quenching*. However, pulsed electron beams have also been shown to be viable [11]. A detailed review of this subject has been given by von Allmen [6]. We will briefly summarize his discussion in the following.

Laser quenching processes differ from the previously discussed (mechanical) forms of rapid quenching in two important respects: the material quenched is much thinner, and the melt is cooled through conduction into the

bulk. These differences, if properly exploited, can give cooling rates of 10^3 times that obtainable in mechanical quenching processes [6].

Laser quenching techniques can be classified according to whether they use a pulsed or continuous source. Continuous, fast scanning beams possess a number of advantages such as high throughput, capability of pattern generation, and use on preformed parts. However, presently available equipment does not appear to be capable of producing cooling rates exceeding those of splat quenching [6].

Pulsed laser quenching techniques have shown the most promise for amorphous alloy formation. Typically, a Nd:YAG laser (operating in the IR region) is used with pulse durations in the nanosecond range, with a corresponding energy on the order of 1 J/cm^2. Such devices are capable of producing cooling rates in excess of 10^{10} K/sec. However, this method is sensitive to a wide variety of parameters, including the duration, intensity and wavelength (determined by the target reflectivity) of the pulse used [6]. This technique has been successfully applied to a number of different target types. Amorphous layers have been produced by "skin melting" single and polycrystalline samples of both alloys and pure elements. a-Si:Al [12] and elemental a-Si [13] have been made in this manner. Powders, either crystalline or amorphous, can be quenched into surface layers or thin films by either pulsed or continuous techniques [6].

The most successful and versatile laser quenching technique, originally developed by von Allmen [14], uses a composite target made from several very thin (15 nm) alternating layers of the desired alloy constituents in the appropriate thickness ratio. These layers are deposited using conventional techniques, such as evaporation. Upon irradiation with the laser pulse, a homogeneous melt is produced which cools to form an amorphous alloy layer several hundred nanometers thick. A number of amorphous silicon-metal alloys have been made using this process, over virtually the entire composition range [6].

Although a very new technique, laser quenching has already demonstrated superiority over all rapid quenching and vapour deposition techniques in its ability to produce amorphous alloys. This process now makes it possible to study more amorphous alloys over enlarged composition ranges, and should become a widely used fabrication method for the study and application of these materials.

2.1.2. Deposition by Atomization

These processes are based on the condensation and solidification of an atomized solid into an amorphous thin film. Atomization is usually accomplished by either sputtering or evaporation. These are common methods of thin film fabrication, and are discussed in detail in most books on thin film technologies, such as the one by Maissel and Glang [15]. Ion beams are also used to fabricate thin films. The ion beam can be used to deposit the films either directly or by sputtering [16].

Obviously, if a material has been atomized, then (in analogy to quenching processes) the largest possible surface area is presented to the cooling surface (substrates), and therefore very high cooling rates are possible. Evaporation and sputtering processes are generally considered to have cooling rates on the order of 10^8 K/sec, though some results indicate that evaporation is superior to sputtering in this regard (see a-Si:Al in section 3.1, for example). To ensure that the films are deposited in an amorphous form, the substrate temperature must be selected to remain well below the crystallization temperature of the alloy. For amorphous Si, this usually means below 300 °C. For an amorphous alloy, this may imply temperatures below room temperature. In these cases the substrates must be cooled, water and liquid nitrogen being the most common coolants. Regardless of the temperature selected, it is vitally important when dealing with amorphous films that the substrate temperature be known and controlled, as the properties of such films vary dramatically with substrate temperature [4].

2.1.2.1. Evaporation Systems

It should first be pointed out that Si should always be evaporated with an electron beam for optimum film purity, because of its high melting temperature and reactivity with most resistive heating sources [15]. The most direct method of depositing an alloy by evaporation is to simply evaporate existing bulk alloy material (crystalline compounds or sintered mixtures, for example). The difficulty with this is that the different vapour pressures of the alloy constituents will not allow the evaporant to evaporate congruently (notable exceptions are the Si oxides) [15]. This results in films of different composition than the evaporant material, and can also result in compositional grading. A number of other evaporation techniques have been developed to overcome the problems associated with this simple but limited deposition process.

If the elemental constituents of an alloy are both solids, then they can be evaporated simultaneously in separate sources in a popular technique known as co-evaporation [15]. In this case, complete control of the composition is possible, and optimal evaporant sources can be used for each alloy component. However, a spatial dependence in the film composition can be produced if proper precautions are not taken [15].

If some of the alloy constituents are in a gaseous form, then some form of reactive evaporation must be used [15]. In its simplest form, evaporation is carried out in an atmosphere composed of the desired gases, rather than in a vacuum. Incorporation of these gases can be enhanced by using an activated reactive evaporation (ARE) technique, where a high voltage probe or grid is used to attract electrons from the electron beam and to encourage collisions with the gas molecules, ionizing them and making them more reactive [18,19]. This can be taken to its extreme form by firing a plasma or ion beam of the desired alloy atoms at the growing films [20]. We will refer to this process as plasma-assisted reactive evaporation (PARE). Any one of these reactive evaporation techniques can be used in conjunction with single or multi-source evaporation processes.

The various evaporation techniques described above have all been used to fabricate amorphous alloys. There are, however, other techniques that could be used (though generally are not). These unconventional methods are now briefly described.

A problem with using an electron beam to evaporate a material is that X-rays are emitted from the melt, which produce electrically active defects in the film [19]. This problem can be overcome through the replacement of the electron beam with a laser beam [21]. This technique is, naturally, called laser evaporation, and has been used to deposit a-Si:H using a pulsed Nd:YAG laser in a hydrogen ambient [21]. Greatly enhanced deposition rates of 10^6 Å/sec were obtained [21].

Compositional variations due to single-source evaporation can also be avoided by using a flash evaporation technique, where small portions of evaporant are evaporated so rapidly that dissociation cannot occur to a significant extent. In these processes a series of small pellets (or flow of powder) is dropped onto a very hot filament or plate [15]. Several techniques have been developed to accomplish this end [15]. The composition of films produced by flash evaporation is almost always the same as the evaporant material, and

excellent compositional homogeneity can be obtained [15].

There are also several more drastic evaporation methods available for the deposition of alloys. The exploding-wire technique is probably the oldest method of depositing thin films, and was apparently first used by Faraday [22]. Deposition is accomplished by exploding a conducting filament with a high current density transient [22]. Arc evaporation uses an arc between two electrodes composed of the desired alloy constituents [22]. Such methods do not produce readily reproducible results, and would normally be used as either a last resort, or in conjunction with more reliable systems.

2.1.2.2. Sputtering Systems

Like evaporation, sputtering is a popular and well understood method of thin film fabrication. Unlike evaporation, sputtering systems generally do not require extensive modification in order to produce alloys, and so have become the preferred method for thin film alloy fabrication. Because amorphous alloys are produced using standard sputtering systems, we will not discuss these systems in any detail here. We will, however, classify the basic processes and mention some specific modifications that have proved to be of particular importance in the production of amorphous alloy systems. Excellent descriptions of sputtering techniques have been given in Vossen and Kern [16]. The application of sputtering to the production of a-Si:H has been thoroughly discussed by Moustakas [17] and Thompson [23]. In the following paragraphs we will briefly summarize the principles behind the major sputtering techniques.

Sputtering can be performed through the use of either plasmas (glow-discharges) or ion beams [16]. The plasma or ion beam is used to bombard a target with energetic atoms, which "knock off" atoms from the target. These atoms are emitted from the target onto the substrates, where a thin film forms. As in the case of evaporated films, one of the most important control parameters is the substrate temperature. We restrict our discussion to plasma based systems. Ion-bean systems will be discussed in section 2.1.3.2.

Glow discharges used in sputtering can be supported by dc, rf or microwave electric fields, though rf sputtering is presently the most common sputtering technique used to fabricate amorphous Si alloy films. The glow discharge can be enhanced by increasing the electron population by heating the cathode (triode sputtering) [16] or by illuminating it with UV radiation — [15]. To increase the ionization efficiency of existing electrons, transverse

and/or longitudinal magnetic fields can be applied (magnetron sputtering) [16]. Also, if gaseous impurities are a problem, then part of the depositing film can be used as a getter (getter sputtering) [16].

In the fabrication of alloys by a sputtering technique, one can use either an alloy or compound as the target material, or a composite target. Generally, in neither case is the composition of the film the same as the targets. The first technique results in graded films as one element is preferentially sputtered away. In the second case, however, the composition of the film is directly proportional to the relative areas of the elements that make up the target. An excellent technique developed by Hanak [24] uses a split-disc target geometry to produce a film having a continuous variation in composition along its length. With this technique, the properties of an entire alloy system can be studied from single samples, so that process variations between runs are no longer a problem. A more complicated dual-target system has been developed in order to allow optimal control of most of the deposition parameters [25].

As with evaporation systems, gaseous components can be incorporated into the films by introducing the desired gases into the glow discharge. This is referred to as reactive sputtering [16]. We make no distinction here as to whether or not the reactant gas is decomposed by the glow discharge, though such processes are sometimes referred to as sputter-assisted chemical vapour deposition (SAP-CVD) [26]. Obviously, reactive sputtering can be used in combination with most other plasma sputtering systems (getter sputtering is an exception).

2.1.2.3. Ion Beam Systems

Ion beams can be used to fabricate thin films in two different ways [16]:

(1) primary deposition; where the ion beam is composed of the desired film material, and is deposited at low energy directly onto the substrate,

(2) secondary deposition; where a high energy beam of inert or reactive ions is used to deposit a film by sputtering.

A promising new primary ion beam deposition technique uses ionized clusters of atoms rather than individual ions to make up the beam. This technique is called ionized-cluster beam (ICB) deposition. The application of this process to a-Si:H thin film fabrication has been discussed in detail by Yamada [17]. In an ICB system, the beam is formed by evaporation of a solid. The vapours are then ejected through a nozzle into a high vacuum, which causes

the vapour to form clusters of 500 to 2000 atoms. These clusters are then passed through an ionization chamber, where bombardment by electrons ionizes the clusters. A strong potential then accelerates the clusters onto the substrates, where they condense to form a thin film [17]. This technique can also be used in a low pressure reactive atmosphere, as with a-Si:H production [17].

The use of an ion beam as a sputtering mechanism allows greater control over deposition conditions than is possible in plasma based systems. However, since the basic principles are not very different from plasma sputtering, we will not discuss these techniques further. The interested reader is referred to the review by Harper [16].

An obvious advantage of ion beam (especially primary) sources is that they can be used in concert with other sources to fabricate a wide range of alloys. As an example of this, a-Si:H has been produced by a combination of the two ion beam processes, called double ion beam sputtering (DIBS) [27]. In this system, an Ar ion beam is used to sputter a Si target, while a H ion beam impinges directly onto the growing film [27]. Considerable control is possible over the deposition parameters in such a system.

Though ion beam systems have seldom been used to produce amorphous alloys, they show considerable potential for such applications, and much more research should be done in this direction.

2.1.3. Deposition by Chemical Processes

There is a huge variety of fundamentally different chemical deposition processes that are in use today. We will begin by removing much of this variety by pointing out that Si, or Si based alloys, cannot be deposited from solutions [16]. Also, equilibrium reactions cannot be used to produce amorphous alloys as they can only produce stoichiometric, crystalline compounds. Therefore, we will restrict consideration to the two remaining chemical deposition categories: chemical vapour deposition (CVD) and plasma deposition (glow discharge).

Both of these remaining categories have a very important limitation in common; the requirement that suitable gases are available to be decomposed into thin solid films. This restriction implies that any films deposited by these chemical techniques will always contain contaminant elements from the gases, such as H, F or Cl. Though chemical processes produce the highest quality a-Si:H (and some related alloy) thin films, pure a-Si (and most alloys) cannot be

produced. However, since the presence of H, F and/or Cl is highly desirable (even necessary) in device quality films, this is not considered a problem at the present time. Even so, it is recommended that much greater emphasis be placed on the investigation of new gases for use in chemical deposition processes, in order to increase the very limited number of amorphous Si alloys which can presently be produced by these processes.

2.1.3.1 Chemical Vapour Deposition

The fabrication of amorphous thin films by CVD offers several advantages over other techniques; two particularly important ones are the excellent reproducibility and the absence of ion or X-ray damage in the films [16,28]. However, the production of alloys is hampered somewhat by the availability of suitable gases and the high substrate temperatures that must often be used. Much research on CVD in recent years has focussed on such considerations.

There are two main types of CVD; pyrolysis and photolysis. Pyrolytic CVD is the most common CVD process, and is discussed extensively by Kern and Ban [16]. Photolytic CVD is less common, but holds great promise for amorphous film fabrication because of the low substrate temperatures that can be used. There are also a number of CVD processes that do not rely on pyrolysis or photolysis [16]. However, these processes are usually restricted to producing stoichiometric crystals as they rely on equilibrium reactions. The interested reader is referred to the discussions by Campbell [15] or Kern and Ban [16]. In the following we will discuss the application of pyrolytic and photolytic processes to the production of amorphous Si alloys.

Pyro-CVD utilizes the decomposition of various gas species flowing through a "reactor" into solid deposits at a hot surface (substrates) [16]. Typically, this is done near atmospheric pressure, at gas and substrate temperatures above 600 °C, and with pressure control and removal of reaction products accomplished with a carrier gas. In this case, careful attention must be given to the mass transfer and surface reaction rates upon which the film quality depends [16]. This process is often referred to as heterogeneous CVD (HETEROCVD), in order to indicate that the process uses heterogeneous decomposition of the gas species, and to distinguish this technique from homogeneous CVD (discussed shortly). The application of HETEROCVD to the production of a-Si:H has been reviewed recently by Hirose [17] and Kaplan [23].

Improvements in the uniformity, structural integrity, and step coverage can be obtained through the use of low-pressure CVD (LPCVD) [16]. This process is typically performed at pressures between 0.1 and 1 Torr, requires no carrier gas, and the only rate determining process to be considered is due to surface reactions [16]. This technique has proven to be particularly successful in the case of Si and several of its alloys [16].

In the past, monosilane (SiH_4) was usually used in CVD (and glow discharge) production of a-Si:H. This gas yields a relatively low deposition rate, and requires high substrate temperatures. These high substrate temperatures prevent the use of glass and stainless steel substrates, an important drawback that has resulted in extensive efforts to lower deposition temperatures. Research into deposition with higher order silanes has been undertaken as part of this effort [28]. Disilane (Si_2H_6) has been found to produce high quality a-Si:H thin films at substrate temperatures between 400 and 600 °C [28]. Also, growth rates as much as 20 times that obtained with monosilane were found [28].

In the course of the research into high order silanes, it was found that the primary depositing species was SiH_2. Therefore, processes which use higher silanes than this are heterogeneous. Such processes have high deposition rates, but the high temperatures required drives the H out of the growing a-Si:H film [17], requiring post hydrogenation to improve film quality. To avoid this, homogeneous CVD (HOMOCVD) was developed by Scott [17], where SiH_2 is the predominant gas species present. This condition is created by holding the substrates at a much lower temperature than the gas. Though the deposition rate is much less than in a heterogeneous process, a-Si:H can be deposited at substrate temperatures as low as 100 °C, with the result that the films contain as much as 30 at.% H [17]. An excellent review of the use of HOMOCVD in the fabrication of a-Si:H thin films has recently been given by Scott [17].

It should also be mentioned that the substrates can be heated by CO_2 or Ar lasers [29], allowing complete spacial control of deposition.

Photo-CVD has also been studied as a method of fabricating a-Si:H and related alloy thin films. The chief advantage of this technique is that it is inherently a low temperature process; typical substrate temperatures being in the range of 100 to 300 °C [28]. This process uses optical energy to decompose the various gas species.

Direct photo-CVD has only recently become practical, due to the use of CO_2 lasers and/or disilane gas. Silane has been directly photodissociated with a CO_2 laser [30], which is referred to as laser induced CVD (LICVD). Disilane has also been directly photodissociated using halogen and mercury lamps [31]. The CO_2 laser uses resonant coupling of its IR energy to the Si-H bond vibrational mode to decompose the gas molecules, while UV sources use energetic photons to break the bonds of the gas molecules. These techniques are quite new, but appear to hold much promise for the fabrication of amorphous Si alloys.

The older and more common method of photo-CVD involves the addition of Hg to the gas mixture, in order to enhance absorption of the light. This process is known as mercury photosensitization and is reviewed by Aoto et al. [28]. Both silane [28] and disilane [33] have been decomposed with mercury lamps using this technique. Several amorphous alloys have also been fabricated [32]. Most of the work in this area has gone into finding the optimum wavelengths to use with the various gases. Despite the fact that negligible amounts of Hg are incorporated into films produced by this technique, direct photo-CVD is the superior deposition method as it avoids the contamination of the vacuum system produced by Hg [17].

2.1.3.2. Plasma Deposition

In plasma enhanced CVD (PECVD) (or glow discharge deposition) systems, a plasma is used to decompose gases flowing through the reactor, causing a thin film to form on various exposed surfaces. The physical properties of films grown by plasma techniques are very sensitive to the deposition and plasma parameters. Despite this, and the largely empirical understanding of such processes, glow discharge deposition has emerged as the standard to which all other amorphous Si alloy deposition techniques are compared.

Glow discharge deposition systems may be classified according to the frequency range of the electric field used to support the plasma; dc, rf or microwave. DC glow discharge (DC GD) systems are, as the term implies, systems in which the plasma is excited by a dc electric field. However, we will consider any system operating below a few KHz to be dc (as in the case of the ac (60 Hz), or audio frequency systems occasionally used) since the ions in the plasma are fully capable of following the oscillations of the electric field [17]. Radio frequency glow discharge (RF GD) systems operate in the MHz region

(13.56 MHz being most common). At these frequencies, the ions are unable to follow the electric field, and thus the primary chemical reactions occurring in the rf plasma are initiated mainly by electrons accelerated by the field [17]. Microwave glow discharge (MW GD) systems operate at frequencies above 1 GHz.

DC GD deposition systems have been discussed by Uchida [17]; we will summarize his results here. DC GD systems are generally of the flat-bed, internal electrode type, where the plasma is generated between two parallel plate electrodes. The substrates are placed on the cathode, so this basic configuration is called cathodic glow discharge. In these systems, the growing films are subject to bombardment by positive ions, which create additional defects in the films. To solve this problem, proximity DC GD was developed.

In the proximity DC GD system, a cathode screen is inserted a few centimeters above the substrates and the plasma is supported between this screen and the anode, away from the growing film. The substrates can then be biased with respect to the screen to control the ions impinging on the film. This system also has a much higher deposition rate than cathodic deposition.

In some cases, cathodic and proximity systems (and their rf counterparts) are referred to as diode and triode systems, respectively. Tetrode and pentode configurations have also been reported.

Less common DC GD techniques are multipole DC GD [17,33] and Penning DC GD [17]. In a multipole glow discharge, the plasma is supported by electrons emitted from a hot filament, and confined by a multipole magnetic structure. The films are deposited on the walls of the reactor [17]. The main advantages of such a system are the low operating pressures possible, and its suitability for plasma studies [33]. Penning glow discharge uses two cathodes surrounded by a cylindrical anode to power the plasma. A magnetic field perpendicular to the substrate (on one or both of the cathodes) forms a dense plasma between the cathodes, reducing plasma-wall interactions [17].

RF GD systems are usually classified according to how the electric field is coupled to the plasma; inductively or capacitively, as described by Spear and Le Comber in their recent review of RF GD a-Si:H [23]. However, new evidence suggests that such a scheme could be misleading (as will become clear shortly), and we will adopt the classification described by Hirose in his discussion of RF GD techniques [17]. In this case the distinction is made between tube reactors (with external electrodes) and flat-bed reactors (with internal

electrodes). This system is also valid for DC GD and MW GD systems. In the following, we will summarize the discussion presented by Hirose [17].

Tube reactors can use either capacitive or inductive coupling to excite the plasma, though it appears that in the "inductive" system the rf power is actually capacitively coupled through the dielectric tube wall [17]. Tube systems are subject to plasma-wall interactions, are limited to small sample sizes, and are not easily scaled up to industrial levels. Plasma-wall interactions can be reduced by the application of magnetic fields or by making the tube diameter much larger than the substrate holder.

More versatile systems use the flat-bed capacitive (or diode) configuration, where parallel-plate electrodes are used. The substrates can be mounted on either electrode, though films grown on the "hot" (non-grounded) plate will exhibit different properties than the grounded samples, due to the self-bias that develops [34]. As in the case of DC GD, a screen electrode can be used to keep the plasma off the growing films, and is also referred to as a triode configuration. The great advantage of flat-bed systems is that they are easily scaled up for the industrial production of large-area devices.

The ionization rate of the plasma can be increased by applying magnetic fields to produce cycloidal electron motion. This is referred to as a magnetron configuration. The use of higher silanes has also been studied in glow discharge systems. The results obtained with disilane and trisilane include a greatly increased deposition rate and less strain within the films, allowing the fabrication of much thicker samples [16,28].

Microwave glow discharge (MW GD) systems are relatively new, and have rarely been used up to the present time. Nevertheless, as will become clear shortly, recent results indicate that MW GD is remarkably versatile, and is capable of producing very high quality a-Si:H thin films. In order to classify MW GD systems, we will adopt the scheme described by Hirose [17] for RF GD systems. As this field is still very new, no review has yet appeared. Also, we feel that these systems, especially the MW ECR GD system, in which electrons achieve cyclotron resonance, show considerable promise as versatile systems in the fabrication of amorphous materials. Therefore, we will describe the various systems that have been used in somewhat more detail than that we presented for the more common and well-known techniques.

The most common MW GD systems at present are of the tube reactor type, with excitation of the plasma (enclosed in a quartz tube) performed with

microwave fields from outside the "discharge tube". In these systems, the plasma and samples are contained within a quartz discharge tube, through which gases flow. In one system, a coaxial line configuration is used to couple the field to the plasma [35,36]. The discharge tube is inserted concentrically into a cylindrical cavity. The microwave power is guided into this cavity by a rectangular waveguide perpendicular to the cavity. This system can be used to produce amorphous thin films by sputtering [35], glow discharge decomposition [36] or by a combination of the two.

A somewhat different system utilizes a slow-wave microwave applicator to couple the field to the plasma, contained within a quartz reactor vessel [37]. This system has produced high quality a-Si:H, and is capable of large area production [37]. This system is sometimes known as the large volume microwave plasma (LMP) system [37].

From the previous discussions, it should be clear that all plasma systems mentioned so far have a number of intrinsic drawbacks. The MW GD tube reactors in particular require hundreds of watts of continuous-wave power (as opposed to tens of watts in RF GD). Tube systems in general have difficulty with impurity incorporation and damage due to plasma-wall and plasma-film interactions, respectively. Flat-bed systems are subject to plasma-electrode interactions. All these systems are open; that is, they radiate electromagnetic radiation into the surrounding environment. All of these problems can be solved through the use of a microwave resonant cavity as the reactor vessel.

The development of such systems has been originated by Mejia et al. [38,39], who studied the use of these techniques in the fabrication of a-Si:H thin films. We summarize their results in the following.

The closed MW GD system is configured as a 2.45 GHz short circuited resonant waveguide cavity, within which the plasma is created, and deposition is performed. The cavity is equipped with shielded quartz windows for optical measurements. The plasma is confined through the use of an axial magnetic field provided by coils surrounding the chamber. In this configuration, the plasma can be controlled in order to prevent contact with the walls of the waveguide, resulting in an essential absence of impurity incorporation into the films. Further, with the application of a sufficiently large magnetic field, conditions of electron cyclotron resonance (ECR) can be achieved, which results in dramatic new plasma behaviour and altered film properties [39].

There are a number of features possessed by this system that are absent in all other plasma deposition systems. The system does not radiate into the environment, contamination due to plasma-wall interactions and damage due to plasma-sample interactions are minimized. Because of the greater energy of the electrons in the mw plasma, the deposition rate is higher than in DC GD or RF GD systems. Without ECR, the power required is on the order of that required for RF GD systems. With ECR the power requirements drop ten-fold, while retaining the high deposition rate. The system is extremely versatile, and the properties of a-Si:H films deposited by this method can be varied over a huge range [39].

The tremendous variety of properties that can be produced in a given material, and the high quality that can be obtained make this technique an excellent candidate for the production of materials for research purposes, especially in the area of amorphous alloys and devices. It may also be possible to scale this system up to industrial levels; this goal is presently being pursued by Mejia et al..

2.1.4 Surface Modification

There are two methods available for the production of amorphous surface layers: ion-implantation and thermal diffusion. Laser quenching and other surface melting techniques were considered in section 2.1.1.3. Materials produced by these methods will largely be neglected in the remainder of this review for the following reasons:

(1) ion-implantation is used as a doping mechanism; samples implanted to alloy concentrations are very rare,

(2) interfacial diffusion (between two solids) is usually used only as an intermediary toward crystalline silicide layers for use in microelectronics,

(3) vapour phase diffusion is also a doping technique, or is used to produce oxide or other protective surface layers.

Because of these facts, we will not discuss these methods further in the context of alloy formation. However, we suggest that of the two, ion-implantation holds greater potential as an amorphous alloy fabrication technique, since it is thought that this process has the largest "cooling rate" presently available; 10^{14} K/sec [5].

2.2. Electrical and Optical Properties

In the following sections we will describe the electrical and optical properties of the amorphous silicon alloys that have been studied to date. Table 2.1 shows all the elements that have been used in binary amorphous alloys of Si. Note that in a binary alloy we do not consider elements such as H, F or Cl, which are simply employed as "dangling bond terminators". For example, a-Si:Ge:H is considered to be a hydrogenated binary alloy.

TABLE 2.1: Periodic table of the elements showing, as shaded, all the elements that have been used to produce binary (see text for precise definition) amorphous silicon-based alloys.

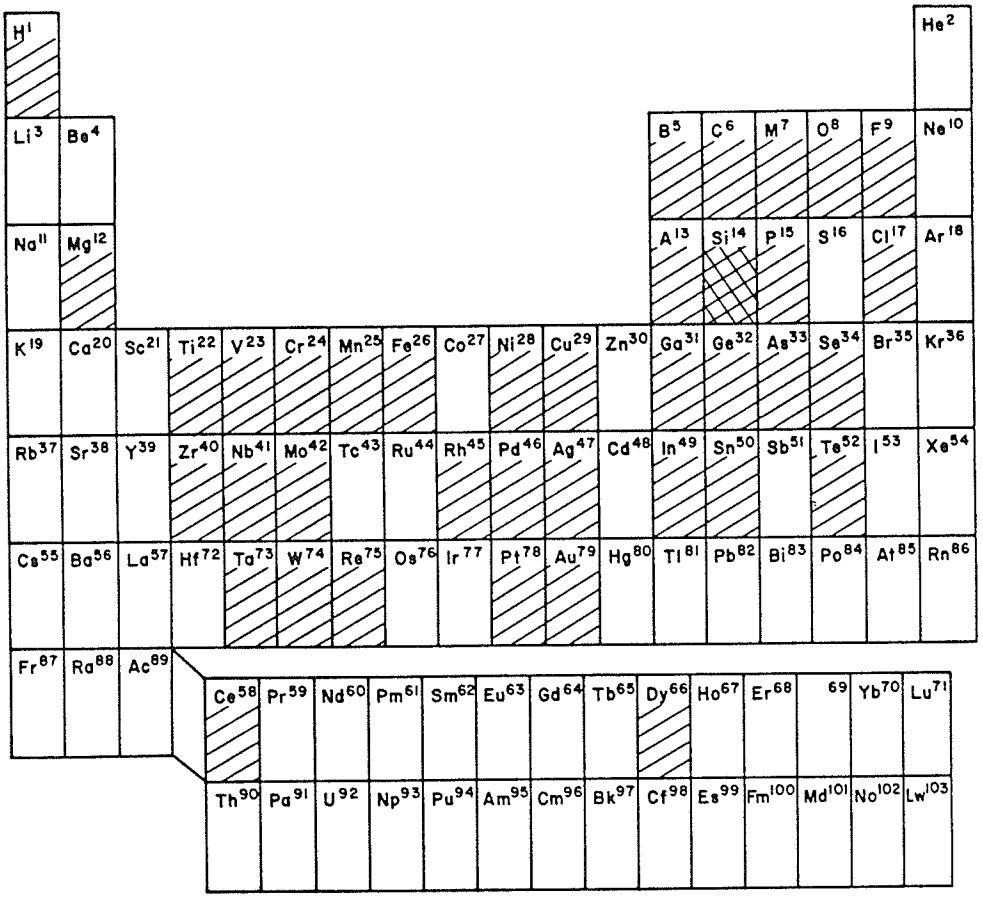

We have classified the elements according to the gross qualitative behaviours they produce in amorphous alloys of Si. All metallic elements are grouped together. Boron and column 5a elements (common dopants in Si) are also taken together. Column 4a, 6a and 7a elements each make up seperate groups. This system is perhaps not particularly satisfying in all respects, but

does reflect genuine physical and historical divisions. Any potentially more coherent system will must await the development of a stronger theoretical base for the understanding of amorphous semiconductor alloys.

2.2.1. Amorphous Silicon-Metal Alloys

Amorphous silicon-metal (a-Si:M) alloys will be discussed in this section. These include all elements to the left of column 4a of the periodic table alloyed with a-Si, excluding boron and hydrogen. The a-Si:B system will be considered along with amorphous silicon alloys containing column 5a elements. The first alloys to be considered are those which have not yet been studied.

No alkali (col. 1a) metals have been alloyed with a-Si, though most have been studied as dopants [40,41]. No column 2a, 2b or 3b elements have been reported either, except for a-Si:Mg (mentioned in [42]). This is probably due to the high quenching rates required to form these alloys, as found from failed attempts to produce a-Si:Be by melt quenching methods [43], though the application of more powerful techniques such as co-evaporation or laser quenching could probably successfully produce such alloys.

A few amorphous silicon-lanthanide alloys have been made (a-Si:Ce [44], a-Si:Dy [45]) but have yet to be studied in any detail. No amorphous silicon-actinide alloys have yet been reported.

The most extensively studied a-Si:M alloys are those made from noble, transition or column 3a metals. Most work on these materials has centered on new fabrication methods, critical-point behaviours (metal-insulator transition, superconductivity) and the formation of a detailed understanding of a few key materials (a-Si:Pd, a-Si:Au, a-Si:Al). Fabrication methods were discussed earlier in this review. The subsections on the metal-insulator transition and superconductivity portray the most important applications presently found for a-Si:M alloys, since their magnetic properties (which is *the* major field of study for glassy metals) are relatively poor.

2.2.1.1. Basic Electrical and Optical Properties

The first glassy metal ever produced was a-Si:Au, made by Pol Duwez and co-workers in 1960 by splat quenching [8]. This material has become the most extensively studied of the a-Si:M alloys. The most extensively studied transition metal alloy is a-Si:Pd, also first produced by Duwez, by splat quenching in

1966 [46]. The first amorphous silicon-column 3a alloy studied was a-Si:Al, produced by Köster and Weiss in 1975 using electron-beam co-evaporation [47]. Many other metals have been alloyed with a-Si, though few have been studied in detail. As a result, the electrical and optical properties of most of these alloys are still largely unknown. An excellent general review of the electronic structure of metallic glasses has been given by Mizutani [48].

Through extensive study of metal-insulator transitions, it has been relatively well established that a-Si:M alloys exhibit three distinct conduction regimes with composition:

(1) metal-doped semiconduction,

(2) mixed metallic and semi-conduction,

(3) mixed metallic conduction.

These regions are particularly well understood in the case of a-Si:Au, and are clearly seen in a graph of conductivity vs composition, as in Fig. 2.1. The curve for a-Si:Al:H demonstrates the behavior produced by the onset of micro-crystallization of the metallic component (at about 23 at.% Al, in this case). This curve will be discussed shortly. Because a-Si:Au has been thoroughly studied, the properties of this alloy will be discussed in detail, and any similarities or differences found in other alloys described.

The three distinct conduction regions of a-Si:Au of Fig. 2.1 are produced by the appearance of metallic conduction in Au and Si at different concentrations. For Au concentrations below 14 at.%, the alloy is a semiconductor [49]. The Au atoms act as deep acceptors in a-Si, producing p-type conduction above approximately 1 at.% Au [50]. This has also been found in a-Si:Mn, a-Si:Ni [52], a-Si:Fe [52,53] and a-Si:Al [54], though Ta has been reported to produce n-type doping [55]. The conductivity in this region shows an initial decrease (due to compensation of the intrinsically n-type a-Si), followed by a steady increase up to 14 at.% Au. Conduction is due to extended-state hole conduction above 50 K, while variable-range hopping through the Au impurity band dominates below 50 K [50]. The optical gap and activation energy show a steady decrease with increasing metal content (above $\approx$ 1 at.%), as shown in Fig. 2.2. Note that the H content of the hydrogenated samples was not measured, so only gross comparisons to pure alloys can be made. Photoconductivity has also been observed in this region at low temperatures, in a-Si:Au thin films [50], but has not been reported in any other a-Si:M alloy. The extent of the semiconducting region is limited by the concentration at which the

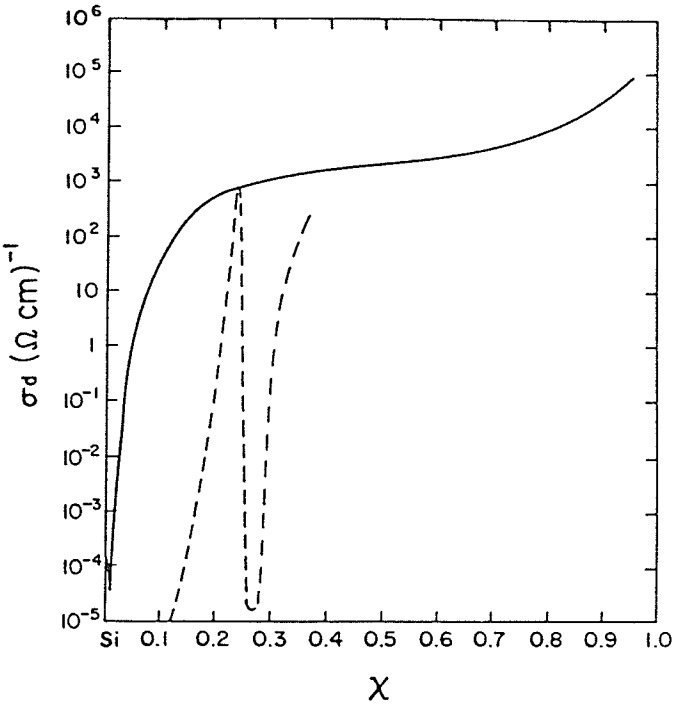

FIGURE 2.1: Dark conductivity of a-$Si_{1-x}M_x$ alloys as a function of composition. Solid line is for M = Au, which remained amorphous for all x (from Refs. 49, 50). Dashed line is for M = Al:H, in which the Al underwent microcrystallization at x = 0.23 (from Ref. 51).

metal undergoes a transition from insulating to metallic behavior, while the Si remains semiconducting [49,50]. This transition is discussed in detail in the section on the metal-insulator transition.

At concentrations above 23 at.% Al (in sputtered a-Si:Al:H samples) the expected metal-insulator transition (at about 23 at.% Al) is masked by the onset of crystallization of the Al into isolated micro-crystallites [51]. In evaporated samples this crystallization does not occur until approximately 40 at.% Al [47]. This crystallization initially depletes the surrounding material of Al (the existing crystallites acting as nucleation centers) causing the conductivity to decrease [51]. As the crystallites grow with increasing Al concentration, a broad percolation threshold occurs, which causes the conductivity to increase again [51,57]. This behavior is also shown in Fig. 2.1. The conductivity in this region is now a function of 3 processes: extrinsic activated hole semiconduction at high temperatures (>300 K), metallic conduction dominated by lattice and impurity scattering at medium temperatures ($50<T<300$ K), and electron localization which dominates at low temperatures (<50 K) [57]. This electron

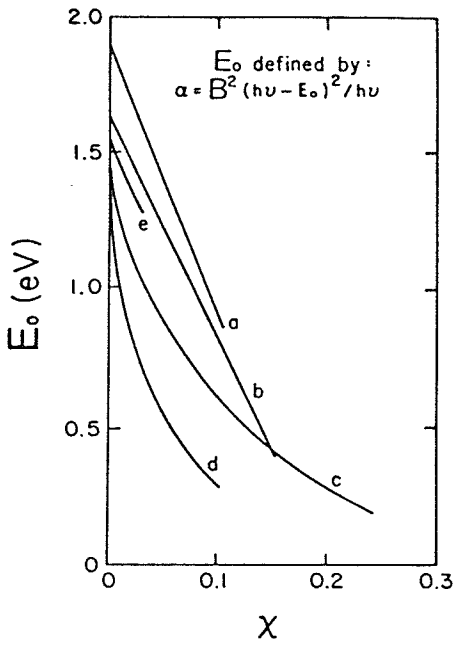

FIGURE 2.2: Optical energy gap of a-$Si_{1-x}M_x$ alloys as a function of composition. Curve (a) is for M = Al:H, from Refs. 54 and 56, (b) for M = Ga:H [56], (c) for M = Au [50], (d) for M = Fe, Mn or Ni [52], and (e) for M = Ta [55].

localization, indicative of two-dimensional behaviour (also producing a resistivity minimum, see below), is thought to occur in the fine metallic links between crystallites [57]. This subject has recently been the motivation for several studies of granular metal films [51]. The crystallization is the result of an insufficiently fast quenching rate, and can probably be obtained in many metal-insulator alloy systems.

The second conduction region extends from the metal transition to the concentration at which the Si also undergoes a transition to metallic conduction (at approximately 70 at.% Au) [49]. This transition is further described in the metal-insulator transition section. The conductivity in this region is roughly constant, as the free-electron density remains constant (at 2 electrons per atom) despite an increasing Au content [49]. Conduction in this region is independent of temperature below 50 K, but remains activated above [50].

The third region (above a Au concentration of 70 at.%) consists of an alloy of the metallic phases of Au and Si [49]. The conductivity in this region increases rapidly with increasing Au content as the free-electron concentration approaches that of pure a-Au [49].

An unusual property displayed by many amorphous metallic alloys is a resistivity minimum (as a function of temperature) at low temperatures, which also produces a negative temperature coefficient of resistance (TCR) over a wide range of temperatures and composition. Such a resistivity minimum well below a ferromagnetic transition temperature has not been observed in crystalline materials [5]. This phenomenon has been the subject of considerable study, and several theories have been proposed. No one theory has yet proven superior, and it now appears that there are several types of resistivity minima. A detailed review of the most promising theories has recently been given by Rao [5].

The resistivity minimum of a-Si:Pd has been extensively studied, and it has been concluded that the minimum in this system is due solely to the scattering of conduction electrons by trace magnetic impurities (especially Fe) [58]. This mechanism is known as the Kondo effect [5]. As expected, a-Si:Fe also exhibits a Kondo-type resistivity minimum, and corresponding negative TCR [59]. The negative TCR found in a-Si:Au alloys (for Au concentrations >50 at.%) has been explained using the Ziman model [60]. In this model, extensively discussed in Ref. [48], the resistivity of an amorphous material will exhibit a negative TCR if the following condition is satisfied [48]:

$$2k_F \approx k_P \tag{2.1}$$

where k_F is the Fermi wave-vector, and k_P is the wave-vector corresponding to the first peak in the structure factor [5]. The Ziman-type negative TCR is more a high temperature phenomenon than the other types, generally occurring above 30 K (above the Debye temperature), and is associated with a slight resistivity maximum near this temperature [48]. Resistivity minima have also been found in connection with 2-D electron localization in granular metallic films, as mentioned previously for a-Si:Al [57].

The resistivity minimum in a-Si:Zr alloys has also been studied, where a correlation between the negative TCR and superconducting properties was found [61]. Similar correlations between normal and superconducting properties have been found in a-Si:Mo alloys [62].

Finally, other a-Si:M alloys that have been made (but not studied with respect to their electrical or optical properties) are a-Si:Ti [63], a-Si:W (the only a-Si:M alloy made by RF GD) [64], a-Si:Rh [65], a-Si:Re [5], a-Si:Pt and a-Si:V [6].

2.2.1.2. The Metal-Insulator Transition

Mott was the first to consider the metal-insulator transition (MIT) via a reduction in the lattice constant for an ideal lattice of hydrogen atoms [66]. This led to the study of crystalline semiconductors heavily doped with shallow impurities, in which the MIT was observed with increasing impurity concentration in the hopping regime [66]. While this transition has not been observed in amorphous semiconductors doped with shallow impurities, it has been observed in several a-Si:M alloys [50]. In this case the metallic elements can be incorporated over a wide range of concentrations. The MIT in a-Si:M alloys was recently reviewed by Morigaki [50]. MITs in general have been discussed in great detail by Mott [66], while some of the latest advances are described in Solid State Electronics' special issue on *Heavy Doping and the Metal-Insulator Transition in Semiconductors* [67].

Amorphous alloy systems exhibit both compositional and topological disorder; therefore the theoretical analysis of these systems is very complicated. However, it seems clear that, except at high temperatures ($T \geq 50$ K), conduction in alloys such as a-Si:Au proceeds through hopping in the (Au) impurity band near midgap. The Mott criterion [66] for the MIT, in which N_c is the critical concentration of the metallic element, and a^* is an empirical atomic radius, is given by

$$N_c^{1/3} a^* = 0.26 \tag{2.2}$$

although there remains some dispute over the appropriate value on the right of the expression [50]. Table 2.2 shows examples of a^* estimated from the observed values of N_c for several a-Si:M alloys.

In the case of a-Si:Au and a-Si:Cr, the values of a^* from Table 2.2 agree exactly with the empirical atomic radius of Au found by Slater [71], but the values for Mn and Fe are somewhat low. This is presumably because of hybridization of the outer 3d, 4s and 4p orbitals which further localizes the valence electrons in alloys of these transition metal elements [50].

It has been reasonably well established, particularly for the a-Si:Au system, that the MIT is an Anderson transition [66]. Further confirmation of this behavior comes from measurements of thermoelectric power, photoconductivity, magnetoresistance, electron-spin resonance and spin-dependent conductivity [50].

TABLE 2.2: Experimental critical concentrations and corresponding empirical atomic radii for a-Si:M alloys exhibiting an (assumed) Anderson-type MIT.

Alloy	N_c (at.%)	a_c^* (Å)	Reference
a-Si:Al	23	1.15	51
a-Si:Au	14	1.35	50,68
a-Si:Cr	14	1.35	69
a-Si:Fe	>16	<1.30	50
a-Si:Mn	>17	<1.27	50
a-Si:Nb	11.5	1.45	42
mc-Si:Co	15	1.33	50,70
mc-Si:Ni	13	1.39	50,70

More recently, Bishop et al. [42] have studied the MIT in a-Si:Nb, a-Si:Al and a-Si:Mg, and have concluded that no minimum metallic conductivity existed, and that strong many-body contributions to the MIT were present. Möbius et al. did find a minimum metallic conductivity for the MIT in a-Si:Cr, though the exact nature of the transition remains to be clarified [69]. Collver, though working with Si:Co and Si:Ni in a metastable crystalline state, also found an Anderson-type MIT [70]. His values of a^* of 1.33 (Co) and 1.39 (Ni) are in good agreement with Slater [71].

A number of these alloy systems have also been studied in the metal-rich composition range, where a second MIT is observed. In this case the silicon switches from semiconduction to metallic conduction. This transition from covalent to metallic bonding of the Si atoms has been observed in a-Si:Au [49,60,72], a-Si:Ag, a-Si:Cu [72] (all at about 70 at.% metal content) and a-Si:Mo (at 37 at.% Mo) [62]. It is thought that the high concentration of metal atoms stabilizes the natural metallic state of liquid Si in the amorphous phase [72].

Another type of MIT has been observed in a-Si:Al alloys. In this system, the aluminum can be incorporated as granular crystallites embedded in a matrix of a-Si (for large Al concentrations) [51] by using quenching rates slow enough to allow partial crystallization to occur. Conduction switches from semiconducting to metallic with increasing Al content at approximately 50 at.% Al. This corresponds to a weak percolation threshold for these crystallites [51,57].

A potentially promising new material for the study of MITs is the ternary alloy a-Si:Ge:B [73]. In this case the spacial extent of the localized states in the gap can be increased directly through the addition of Ge [73]. This phenomenon is discussed further in section 2.2.6.

While appropriate theoretical descriptions of the various MITs in a-Si:M alloys are far from settled, one conclusion is clear: that unlike the case of energetically shallow impurities such as B or P in a-Si, the presence of metallic elements in large concentrations ($\geq$ 10 at.%) gives rise to a wealth of interesting transport properties involving critical behaviour. For example, many of these amorphous alloys also exhibit superconducting behaviour.

2.2.1.3. Superconductivity

Superconducting behaviour in amorphous materials was first discovered in evaporated Bi and Ga films by Buckel and Hilsch in 1954 [74]. All amorphous superconductors exhibit type II superconductivity in the dirty limit (where the electron mean free path is much less than the superconducting coherence length) [61]. A detailed review of the latest theoretical aspects has been given by Poon [5]. In amorphous alloys, superconducting properties are exhibited over a range of compositions, through which parameters such as the critical temperature (T_c), magnetic field (H_c), and current density (J_c) vary continuously.

There are two particularly interesting general results on amorphous superconductors that have arisen from previous work:

(1) The coupling between electrons and phonons in a solid is *enhanced* by the disorder present in amorphous materials. This leads to an enhanced probability of superconductivity, and a tendency towards strong-coupling behaviour [5].

(2) The amorphous phase of a metallic superconductor is stabilized through alloying, especially with metalloids such as Si. This leads to a large increase in T_c towards the maximum predicted for that metal [5]. This is particularly true for Al, where T_c increases from about 1 K to 8 K upon ion-implantation with Si [5].

For a-Si:M alloys, there are four important points to note:

(1) Superconductivity has been shown to be unaffected by long range order through studies of the Si:Pd:(H,D) [75] and Si:Zr ($T_{c\,max} \approx 3$ K for a-Si:Zr) [61] systems, where it appears that only the short range order is

important.

(2) Although amorphous materials possess a lower T_c than their crystalline (compound) counterparts, they may have *sharper* transitions, as in the case of a-Si:Pd:H ($T_{c\,max} \approx 3$ K). This is due to the greater overall homogeneity of the disordered phase [75].

(3) Some systems which are not normally superconductive can be made so through hydrogenation or deuteration, as in the Si:Pd system. Hydrogen (and Si to a lesser extent) is thought to suppress the harmful spin fluctuations in Pd which normally prevent superconductivity from occurring [75].

(4) In the section on the MIT, it was mentioned that the presence of large metal concentrations allows the Si atoms in an amorphous alloy to form metallic bonds. This implies that it should be possible to observe superconductivity due to the Si, as has been found in amorphous germanium-noble metal alloys (the noble metals Cu, Ag and Au not being superconductors) [72,76]. Superconductivity has been observed in a-Si:Au alloys ($T_c < 1$ K), but only in the range of *covalent* Si bonding [76] (the range of metallic Si bonding has not been studied at superconducting temperatures). It has been suggested that in this case the superconductivity is due to the degenerate electron system donated by the impurity (Au) atoms. If this is true, this will have been the first observation of superconductivity through an impurity band [76].

Presently, the most important application of a-Si:M superconducting alloys is in the production of ductile, high T_c materials. Applications such as Josephson junctions, superconducting magnets, motors and generators require materials with a combination of high T_c and ductility. Unfortunately, all high T_c materials are crystalline, and thus very brittle. Amorphous alloys are well known for their excellent strength and ductility, but have very low T_c. However, it has recently become possible to combine these two conflicting requirements through the production of the so called A15 (or β-W) metastable crystalline compounds (T_c expected ≥ 25 K, perhaps as much as 38 K in Nb_3Si [77]) from the amorphous phase. Such production has recently been demonstrated for A15 V_3Si (a-$T_{c\,max} < 1.2$ K) [78] and Nb_3Si (a-$T_{c\,max} = 4.5$ K [79]) [80]. The A15 phase is very difficult to form directly [77], and is brittle in its purely crystalline form. The amorphous phase is easily formed by the usual methods, and the A15 phase is then obtained by proper annealing (under pressure in the case of Nb_3Si). A high T_c can be traded off for greater ductility by leaving some of the amorphous phase present [78].

Other superconducting a-Si:M alloy systems that have been studied are a-Si:Mo ($T_{c\,max} \approx 7$ K) [62] and a-Si:Al [81].

2.2.2. Amorphous Silicon Alloyed with Column 4a Elements: The Tetrahedral Alloys

In photovoltaic solar energy conversion, the successful application of a-Si:H as a solar cell material has led to the possibility of increasing solar cell efficiency by incorporating various amounts of C, Ge or Sn into a-Si:H, thus producing tandem type solar cells (see section 4.). In the following sections we discuss in detail the results obtained for amorphous alloys of Si with the column 4a elements: C, Ge and Sn. A brief review of some of the properties of a-Si:C:H, a-Si:Ge:H and a-Si:Sn:H alloy films has been published by Kuwano and Tsuda [28]. a-Si:Sn alloys are considered here because the form of tin most commonly associated with Si is the tetrahedral semiconducting form (grey or β-Sn). However, it should be pointed out that their behaviour resembles a-Si:Al and other a-Si:M alloys more than it does the other amorphous silicon-column 4a alloys such as a-Si:Ge.

2.2.2.1. Amorphous Silicon-Carbon Alloys

The great interest shown in a-Si:C:H during the past several years has mainly been due to the electroluminescence and photoluminescence properties of this material, and its successful use in improving solar cell efficiency. a-Si:C has been studied in less detail, and only in the vicinity of the 50 at.% composition range (a-SiC).

a-SiC thin films were first produced by Mogab and Kingery [82] in 1968 by rf sputtering of a polycrystalline SiC target. The electrical and optical properties of this material have since been studied by Fagen [83] and Nair and Mitra [84]. a-Si:C:H thin films were first produced by Anderson and Spear [85] by rf glow discharge in 1977. Since then, a-Si:C:H thin films have been fabricated by glow discharge in gas mixtures of silane and a hydrocarbon such as methane, ethylene or tetramethyl-silane [85-91], pyro-CVD of SiH_4/C_2H_2 mixtures [93,94], rf sputtering [86,90,95-97], PECVD [98], and by direct photolysis of pure methylsilanes or acetone and disilane mixtures [99].

In the following discussion, it is important to realize that not all researchers measured the actual C content of their films. Generally, the compositions quoted refer to gas phase or target composition ratios, which are poor

measures of the actual composition of deposited films. The following references do contain composition values obtained from direct measurement: [86,87,89,97,100].

The electrical and optical properties of a-Si:C have not been studied as a function of composition; study has so far been restricted to amorphous silicon carbide, a-SiC [83-85]. As well, study of this alloy has essentially been abandoned in favour of a-Si:C:H. Therefore, we will not consider a-SiC in detail. However, it should be pointed out that conduction was found to be p-type [83], and due mainly to hopping in localized gap states even at room temperature [84,85]. The properties of a-SiC have been compared to those of a-Si:C:H, and considerable differences were found [86]. These differences appear to be a result of the presence or absence of hydrogen, and are similar to the differences between evaporated a-Si and RF GD a-Si:H [86].

The optical gap of a-Si:C:H films as a function of carbon concentration is shown in Fig. 2.3. As the carbon content is increased, E_o increases almost linearly up to a maximum at approximately 65 at.% C, before decreasing towards the value for pure C. It is interesting to note that, in glow discharge films, increasing the deposition substrate temperature, T_s, shifts E_o towards lower energies [86,87,92]. There are, however, some discrepancies among results from different workers regarding the actual value of E_o. These cannot be entirely accounted for in terms of differences in T_s, and point to the importance of other growth parameters, such as the H content. In sputtered a-SiC films, for example, increasing the deposition temperature has the opposite effect on E_o [84]. The decreasing spin density accompanying this shift in the absorption edge in sputtered films strongly suggests that this behaviour results from a reduction in the density of gap states, as structural defects, probably associated with multivacancies, are annealed out. In glow discharge films, ion-probe analysis showed that some H is incorporated even into high T_s films, but this does not appear to have a dominant effect on the observed shift in E_o with T_s. Thus, for example, the optical absorption in high T_s glow discharge and highly annealed sputtered specimens are in reasonable agreement [86].

It has been suggested [86] that a completely random alloy, in which one constituent is present in considerable excess of the stoichiometric composition, must contain regions in which four or five atoms of that element are bonded together. Such regions of C are more likely to bond graphitically than

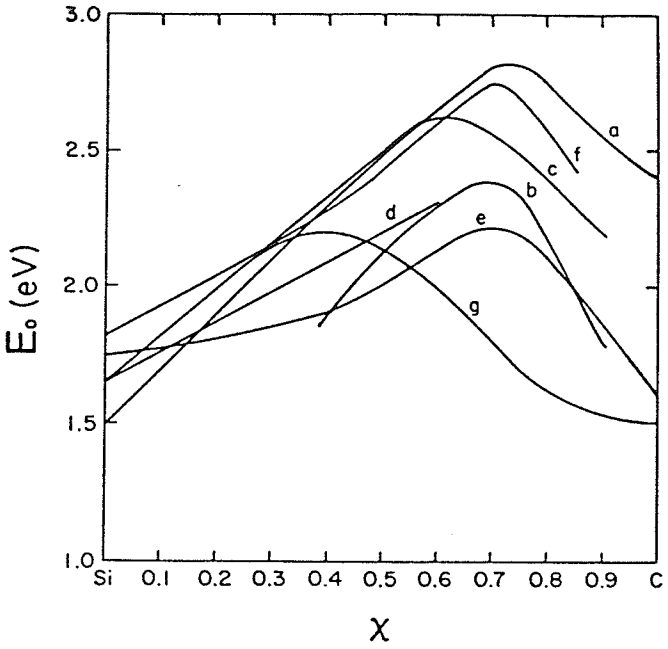

FIGURE 2.3: Optical energy gap of a-$Si_{1-x}C_x$:H alloys as a function of composition. Curves (a-f) are for glow discharge samples, while (g) is for reactively sputtered samples. Curves (a,b) are from Ref. 85, (c) from [87], (d) from [89], (e) from [91], (f) from [92] and (g) from [97].

tetrahedrally, and their probability of occurrence can be shown to rise rapidly with increasing C content. It appears that the effect of graphitic regions is to increase the density of gap states, thus shifting the fundamental optical absorption to lower energies, as shown in Fig. 2.3. Work on glow discharge carbon showed that as the deposition temperature was increased, E_o decreased, implying that the structure becomes more graphitic. The change from fourfold to threefold coordination with increasing C content was found to occur at about 50 at.% C [97,102,103]. This is believed to contribute to the observed shift of E_o to lower values in a-Si:C:H films with decreasing T_s.

It is worth noting that the optical gap results obtained by Tawada et al. [88] and Yamada et al. [101] are profoundly different from all other published results. In this case, it was found that E_o increased monotonically with an increase in the methane or ethylene fraction in the gas phase. The problem in comparing these results with those of Fig. 2.3 is that the actual C content of the films (certainly greater than the gas phase ratio [92]) was not determined. Therefore, their results were not included in Fig. 2.3.

The effects of B doping were also studied by Tawada et al. [88] and Yamada et al. [101]. They found that B doping in a-Si:C:H thin films reduces the amount of H bonding to the C atoms (H bonding to Si is apparently unaffected) producing widening (Si rich region) or narrowing (C rich region) of the optical gap. This was also found in photo-CVD produced films [101].

The refractive index of a-Si:C:H thin films varies from about 3.8 (for pure a-Si) to about 1.8 for C rich samples [87,92], as shown in Fig. 2.4.

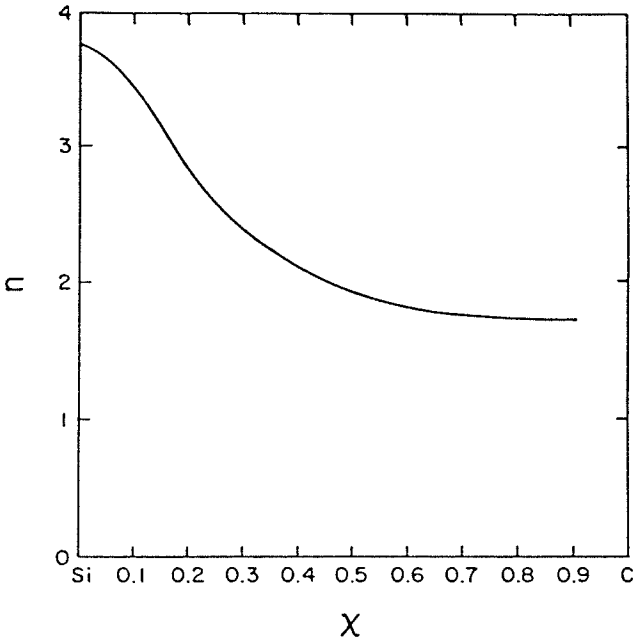

FIGURE 2.4: Refractive index of a-$Si_{1-x}C_x$:H alloys as a function of composition. Taken from Ref. 87.

Dutta et al. have studied the effects of hydrogenation [95] and flourination [104] in a-Si:C:H thin films. They found an unexpectedly high total atomic concentration of these elements in the films, with F being the most easily incorporated (40 at.% with 6 % SiF_4 in the gas phase). The effect of introducing H or F into a-Si:C:H is similar to annealing. H, and F especially, tend to bond preferentially to C over Si, with the C-F bond being very strong. This makes a-SiC:F a very thermo-stable material, with no deterioration exhibited up to 800 K [104]. The H concentration of a-Si:C:H increases as the C concentration increases [88,94,96,97]. Although the number of C-H bonds per C atom is larger than that of Si-H bonds per Si atom, the unpaired spin density increases from 10^{16} to 10^{20} cm^{-3} as the C content increases from 0 to 77 at.%. This increase is attributed to the change of the incorporation scheme of

the H atoms, the difference in bond lengths between Si-Si and C-C, or to the tendency of the coordination number of C to be three [90]. The presence of C atoms in the amorphous network makes the the Si-H bond more stable in a-Si:C:H than in a-Si:H, making a-Si:C:H films more heat resistant.

Photoinduced changes in a-Si:C:H have been studied by Iida and Ohki [96]. They found two types of photoinduced changes in these alloys:

(1) photobleaching; a shift in E_o to higher energies upon exposure to bandgap illumination in the presence of O,

(2) photodarkening; a shift in E_o to lower energies upon exposure to bandgap illumination in a vacuum.

These effects were accompanied by changes in film thickness: an increase with photobleaching, and a decrease with photodarkening. These effects became more pronounced as the C content increased. It was found that photobleaching (upon O exposure) also resulted in the appearance of a C=O stretching mode in IR measurements. However, no satisfactory explanation could be found to account for both phenomena. It should be pointed out that thermal effects were ruled out by experiment, and sub-band gap illumination failed to produce any photoinduced changes.

The dc dark conductivity of a-Si:C:H thin films is due primarily to extended state conduction at and above room temperature [85,95], while hopping within localized gap states dominates below [95]. The conductivity parameters σ_d, σ_o and E_a for the high temperature regime are shown in Fig. 2.5. At about 80 at.% C, there occurs a precipitous decline in E_a and σ_o, suggesting that hopping within gap states has begun to dominate conduction even at room temperature [85]. Completely different results were obtained by Bullot et al. [91], who reported two regions of extended state conduction, possessing different activation energies, above and below 350 K. No trends in E_a or σ_o were found as a function of composition [91]. Because interest in a-Si:C:H has focussed on optical properties, little work has been done on dc conductivity, and considerable uncertainty remains about the nature of this fundamental property. We strongly suggest that that studies of this easily measured parameter be included in all work on this material, at least until it is reasonably well understood.

The photoconductivity of a-Si:C:H thin films has been extensively studied [86-88,91]. Unfortunately, quantitaive comparisons would be misleading, as each study has used different illumination methods. However, a number of

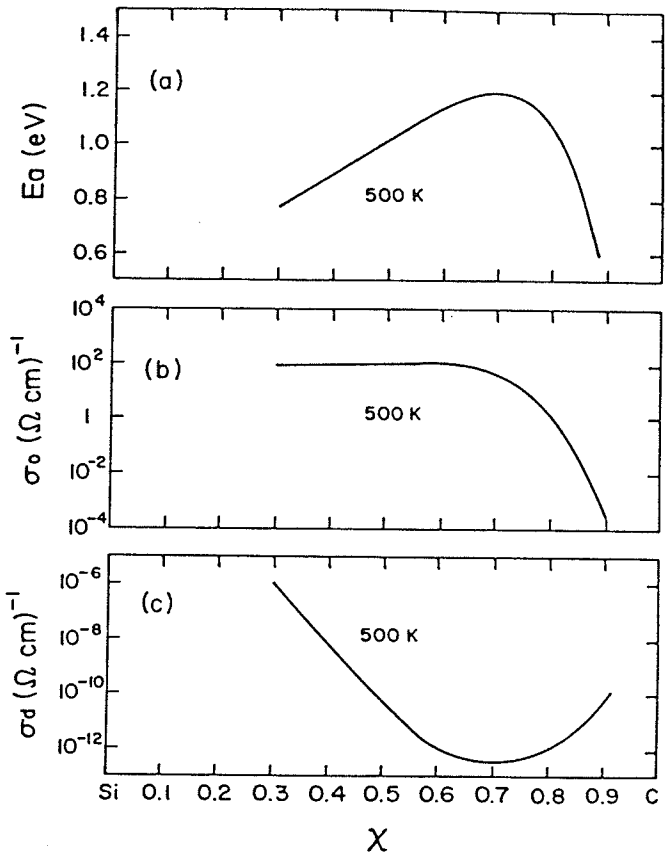

FIGURE 2.5: Dark conductivity parameters of a-$Si_{1-x}C_x$:H alloys as a function of composition. (a) is the activation energy, (b) the pre-exponential factor and (c) the conductivity. Taken from Ref. 85.

important trends have been clearly identified. The photoconductivity is strongly dependent on composition; decreasing by between 3 to 8 orders of magnitude as the C concentration increases above 10 at.%. The consensus on this phenomenon tends to favour the worst case [86,87,91] rather than the best [88]. The shape of this dependence also varies between researchers. The decrease has been attributed to an increase in localized tail states, producing a decrease in the mobility-lifetime product [86,87]. Below 10 at.% C, it is possible to have the photoconductivity reach a maximum value which can be greater than that of pure a-Si:H films [86].

The decrease in σ_{ph} can be partially compensated for by B or P doping. Tawada et al. [88] found that a-Si:C:H films produced from methane (CH_4) exhibited a stronger σ_{ph} recovery with doping than did ethylene-produced (C_2H_4) films. It was also found that even undoped methane-produced films had a stronger photoconductive response than did ethylene-produced films.

Because of these facts, it is suggested that methane is to be preferred over ethylene in glow discharge fabrication of a-Si:C:H for optical applications [88].

The energy dependence of σ_{ph} has also been studied [86,91]. As would be expected, the maximum value of σ_{ph} shifted towards higher energies, following E_o, with increasing C content [91]. More interesting however, is a shoulder in the energy dependence of σ_{ph} at 1.2 eV (below the peak value), indicative of a local maximum in the density of states (DOS) [86]. The strength of the photoconductive response was found to be directly related to the height and intensity of the corresponding 1.2 eV peak found in photoluminescence measurements [86]. Indeed, the existence of the peak (or shoulder) appears to be a necessary condition for the existence of photoconductivity in these films [86].

The photoluminescence (PL) properties of a-Si:C:H were first studied by Engemen et al. [100], whose results stimulated some controversy in this area. They found two distinct peaks, and attributed these to emissions from separate Si and C clusters [100]. Later researchers [87,89,105] found only one peak (albeit usually with some structure) which shifted to higher energies with increasing C content. This was found to be satisfactorily explained as being due to the greater disorder in C rich films extending the range of localized states into the gap [87,89,105]. However, through the use of peak deconvolution techniques, other researchers have pulled peaks similar those seen by Engeman out of single asymmetric peaks [86]. Thus it appears that this controversy has yet to be brought to a satisfactory conclusion. Nonetheless, the fact that PL in a-Si:C:H can be efficiently produced at room temperature, and can also be made to appear "white" [106] means that this area will continue to remain active for some time yet, especially in conjunction with studies on electroluminescence.

A promising and possibly unique (among a-Si alloys) property of a-Si:C is visible, room temperature electroluminescence (EL), first observed in a-SiC by Hartman et al. in 1968 [93]. They found "blue-white" EL to occur in sandwich structures subjected to relatively large dc voltages (of either polarity) [93], but did not report any detailed study of this phenomena. Recently, the possibility of creating large area EL display devices has motivated some detailed studies into ac EL in a-Si:C:H thin films [106,107]. In both cases, ac EL was produced in Y_2O_3/a-Si:C:H/Y_2O_3 structures. These devices use C rich materials, and produce "blue-white" [106] or "orange-white" [107] EL at room temperature. The voltage and frequency behaviours were found to be quite similar to those of

conventional ZnS:Mn cells, and due to similar causes [106,107]. However, a-Si:C:H devices have higher threshold voltages ($3-5\times10^6$ V/cm) [106,107]. Considering the early stage of research in this area, the results are quite encouraging.

2.2.2.2. Amorphous Silicon-Germanium Alloys

a-Si:Ge:H alloy films have been fabricated by rf glow discharge decomposition of SiH_4 /GeH_4 mixtures [108-119], dc sputtering in a triode system [120], rf sputtering [121,122], reactive sputtering [123] and dual magnetron sputtering [25]; whereas a-Si:Ge alloys have been fabricated by co-evaporation [124].

The optical gap of a-Si:Ge:H films decreases smoothly with increasing Ge concentration, as shown in Fig. 2.6. Note that von Roedern [112] obtained a nonlinear trend, while the remaining researchers found a linear dependence of E_o on composition. This difference is attributable to concurrent changes in the H content with changing Ge content. The "inconsistent" results obtained by von Roedern were found to be a result of a rapid decrease in the H concentration as the Ge content increased above 60 at.% [112]. However, the relatively small change in E_o at lower Ge concentrations, where the H content is constant, remains unexplained. Other researchers made no attempt to distinguish the effects of alloying with Ge or H. However, since the quoted gaps are, for all compositions, smaller than von Roedern's results, it is inferred that the H content was also smaller and the energy gap less susceptible to variations in the H concentration. One should note that the total change in E_o in all cases is about 0.8 eV. These results make it clear that a separation of changes in the intrinsic band structure of the amorphous alloy from the extrinsic effects of H concentration, defect density or microstructure should be regarded as a major element of analysis. We underline the importance of this point for future experimental investigations. It should also be noted that the films produced by reactive sputtering [123] have comparable, or larger, optical gaps than RF GD produced material, which implies that the reactive sputtering method can be as, or more, efficient than RF GD in incorporating H into a-Si:Ge:H thin films.

The variation of E_o (and other parameters) as a function of H content (at a fixed Ge content of 50 at.%) has been studied by Banerjee et al. [121]. It was found that, with increasing H content, the absorption edge exhibited an initial blue shift (increase in E_o), followed by a small red shift at high

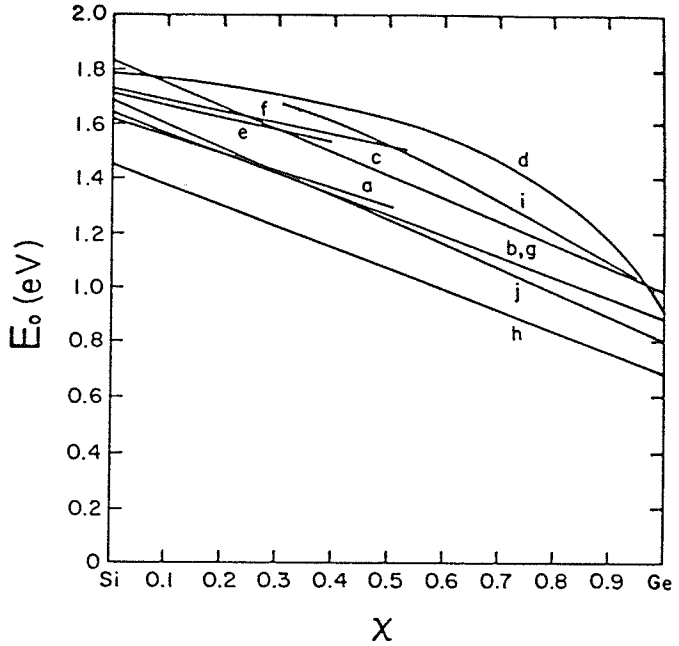

FIGURE 2.6: Optical gap of a-$Si_{1-x}Ge_x$:H alloys as a function of composition. Curves (a-g) are for glow discharge samples and curves (h-j) for reactively sputtered samples. (j) shows the dependence of the mobility gap, as derived from the dc dark conductivity activation energy [120]. Curve (a) is from Ref. 108, (b) from [109], (c) from [111], (d) from [112], (e) from [114], (f) from [115], (g) from [117], (h) from [122] and (i) from [123].

concentrations. This result is consistent with conductivity data which shows a corresponding minimum in the dark conductivity, and a maximum in the mobility gap. It was also found that the density of states at the Fermi level varied considerably with changes in H content; 10^{25} $eV^{-1}cm^{-3}$ for low H concentrations, approaching a more reasonable 10^{18} $eV^{-1}cm^{-3}$ at the concentration corresponding to the conductivity minimum [121].

The optical constants of a-Si:Ge:H films, such as the refractive index, extinction coefficient and loss factor have been measured as a function of composition by Kao et al. [122], and were found to vary approximately linearly with composition. The refractive index and extinction coefficient are dispersive and exhibit two peaks in their spectra; one above and one below the optical absorption edge. The first peak has been attributed to interband transitions and the second to transitions involving localized states in the mobility gap [122].

The spectral dependence of the optical absorption coefficient, α, has been studied by several researchers, and is shown in Fig. 2.7. It is remarkable to see

that the same feature in the density of localized states, at the same energy as in a-Si:H, still exists in the alloy. This shoulder has been attributed to a local maximum in the density of localized states in the gap, at ≈ 0.5 eV above the valence band. The proportion of characteristic defects responsible for this behaviour increases with increasing Ge concentration. Disorder-induced effects at the band edges do not seem to be significantly enhanced, as evidenced by the small modifications of the exponential part of the absorption edge. For large Ge concentrations, however, the shift of the optical absorption shoulder by about 0.15 eV and the broadening of the exponential edge suggest a modification of the distribution of localized states at the band edges. In such concentrated alloys, changes are expected in the nature of defects, introducing localized states in the lower part of the pseudo-gap. These alloys are also probably more disordered.

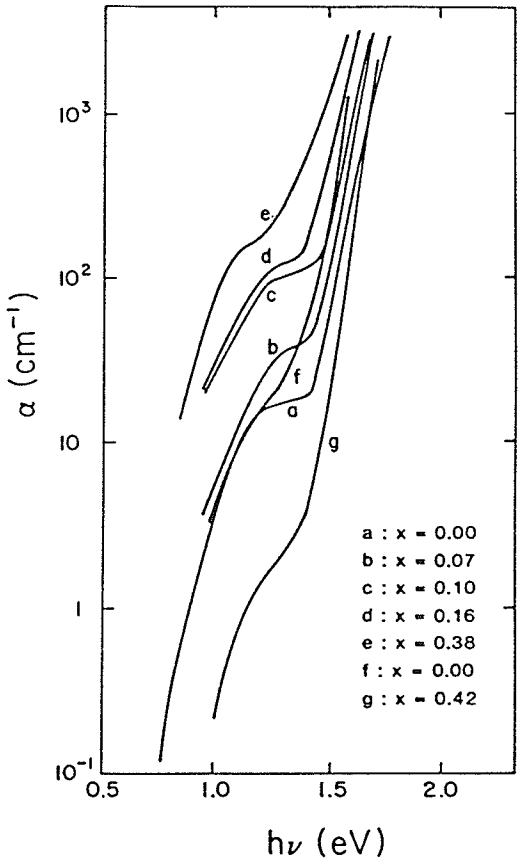

FIGURE 2.7: Optical absorption edge of a-$Si_{1-x}Ge_x$:H alloys as a function of composition, as obtained from photoconductivity measurements. Curves (a-e) are taken from Ref. 114, while (f, g) are from Ref. 112.

Conduction in a-Si:Ge is n-type over the entire composition range. Increasing Ge concentrations in the Si rich region moves the Fermi level first towards midgap, and then, in the Ge rich region, moves it back toward the conduction band [121]. Dark conductivity measurements as a function of temperature showed that the conductivity is singly-activated over a wide temperature range (room temperature to 500 K) [111,112,120]. This behaviour is attributed to extended state conduction. The room temperature σ_d increases monotonically with increasing Ge content, not only due to a decreasing activation energy, but also due to the variation of the pre-exponential factor, σ_o. While the activation energy (considered to be half the mobility gap) varies linearly with the Ge concentration (curve (j) in Fig. 2.6), σ_o varies as shown in Fig. 2.8. The variation of room temperature conductivity σ_d, activation energy E_a and σ_o are shown in Fig. 2.8. The average value of σ_o is about an order of magnitude smaller than that for a-Si:H. The-low temperature conductivity is consistent with a hopping mechanism between states near the Fermi level.

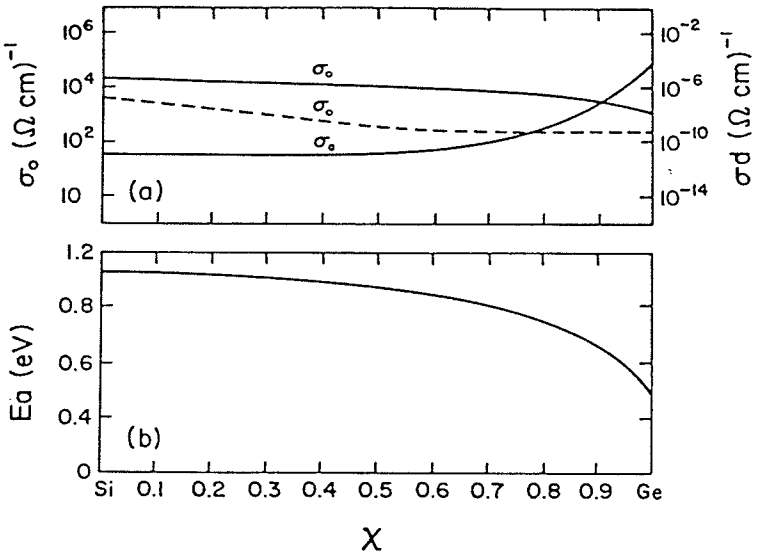

FIGURE 2.8: Dark conductivity parameters of a-$Si_{1-x}Ge_x$:H alloys as a function of composition. (a) is the conductivity and pre-exponential factor, while (b) is the activation energy. Solid lines are taken from Ref. 112, dashed line from Ref. 120.

The photoconductivity in a-Si:Ge alloys is the subject of some debate. There are significant discrepancies in experimental results, which have also led to difficulties in the interpretation of these results. In the following discussion we will concentrate on the qualitative similarities, but will also describe the differences, which seem to arise from differences in the fabrication

methods used.

At a Ge concentration of 30 at.%, the photoconductivity of dc sputtered a-Si:Ge:H decreases considerably as the Ge content increases, and there occurs a transition from monomolecular to bimolecular recombination [120]. Films with Ge concentrations less than 30 at.% were found to be highly photosensitive, while slight P doping led to more than an order of magnitude change in the photoconductivity [120]. However, it has also been reported that even small amounts of Ge incorporated into a-Si:H results in a considerable reduction of the $\eta\mu\tau$ product, which is usually taken as a measure of the photoconductivity of a material, as can be seen in Fig. 2.9. As may also be observed, this reduction appears to be dependent on the fabrication method used ([109] is RF GD, [123] reactive sputtering). In this case, the degradation of the photoconductive response has been attributed to the incorporation of structural defects [109] or the increase in the number of dangling bonds on the Ge atoms [112,118]. The latter problem is thought to be enhanced by the preferential bonding of H to Si over Ge [118,123]. The decrease in the photoconductivity may instead be due to the movement of the Fermi level towards midgap as the Ge content increases in the Si rich region. This would also be consistent with the observation that the photoconductivity increases again for increasing Ge concentrations in the Ge rich region, which is accompanied by a shift in the Fermi level back toward the conduction band [109]. The photoresponse has been found to decrease initially by 3 orders of magnitude, then to increase by a factor of about 20 as the Ge content is increased [112].

Attempts to optimize the photoconductive response of a-Si:Ge:H has resulted in various recipes, depending on the fabrication process used. The degradation of the photoconductivity has been eliminated in RF GD films by using high power [110], low substrate temperature [110] and low pressures [112], though optimized films have also been obtained at high temperatures, where the photoconductivity appears to reach a maximum in the range 5-15 at.% Ge [114]. Excellent results have also been obtained in magnetron-sputtered films, near a composition of 50 at.% Ge [25]. In this case it was found that the maximum photoconductivity was obtained when sufficient H was incorporated to produce a small amount of dihydride bonding on both the Si and Ge constituents [25]. The photoconductivity for alloys produced by this method had the highest value yet reported at this value of the optical gap (1.4 eV). These somewhat conflicting results indicate that much research remains

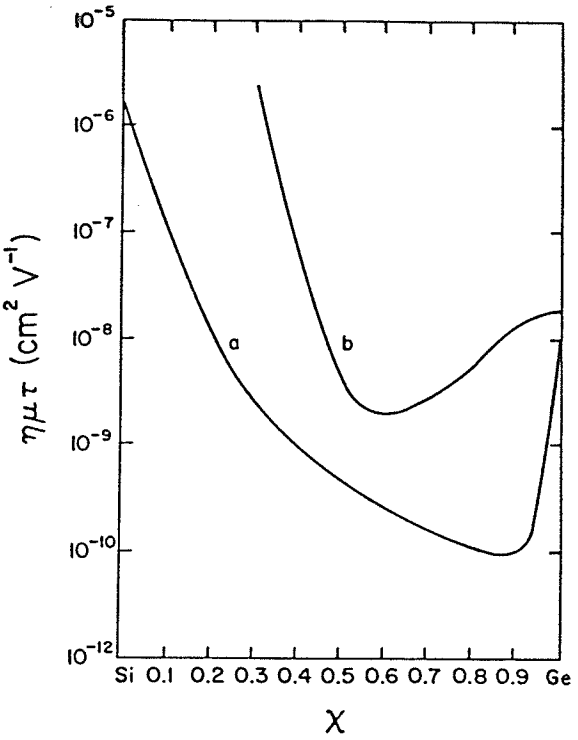

FIGURE 2.9: Photoconductivity $\eta\mu\tau$ product of a-$Si_{1-x}Ge_x$:H alloys as a function of composition, at a temperature of 300 K. Curve (a) is taken from Ref. 109, (b) from Ref. 123.

to be done in this area.

In sputtered films [120] it appears that, above a critical Ge content of 30 at.%, the band tail below E_c is gradually broadened by the addition of more Ge. This has also been found in RF GD material [112]. This broadening has been attributed to causes other than Si-Ge mixing; such as H-induced defects and/or micro-structural changes resulting from the particular combination of preparation parameters used, since despite the fact that the Ge-H configuration is much less likely than Si-H [118,123], there is not a corresponding high density of non-radiative recombination centers (dangling bonds) associated with Ge. This conclusion has been supported by ESR studies [119]. However, it has also been found that increasing the Ge concentration steepens the DOS of the tail states [109].

It appears that despite differences in the detailed changes in the DOS of samples prepared by different methods, there is an overall increase in the intrinsic state density, especially in the lower half of the pseudo-gap, which leads to a decrease in the photoelectric response. In particular, a decrease in

both $(\mu\tau)_n$ and $(\mu\tau)_p$ is indicated. The distribution of gap states in a-Si:Ge:H alloys in the upper half of the mobility gap, as a function of Ge content, was found to increase as the Ge concentration increased, and (up to a Ge concentration of 30 at.%) the general shape of their distribution found to be similar to that in a-Si:H [116]. For concentrations above 40 at.%, a hump appears in the distribution, at about 1.2 eV above the valence band edge, attributed to dangling bonds associated with the Ge atoms [116].

Light-induced defects in a-Si:Ge:H and their effect on opto-electronic properties have been studied in some detail [113,115]. A relatively small Staebler-Wronski effect was observed [113,125,126], although the density of photo-induced states is on the same order of magnitude as that in a-Si:H. This has been attributed to the fact that the large DOS created by Ge dangling bonds masks the effect of light-induced defects. Thus, the Staebler-Wronski effect cannot be observed for compositions above 50 at.% Ge. The origin of these photo-induced defects is, as in the case of a-Si:H, still uncertain. Whether these changes are a surface or bulk effect remains a matter of debate.

Although the optical gap is decreased with increasing Ge concentration in a-Si:Ge:H thin films, as required, for example, by practical applications in the field of solar cells, a decrease of photoresponse is also found, whatever the composition. It appears that only in the Si rich composition range (0 to 10 at.% Ge) can useful alloys be found with a moderate decrease in E_o. More studies are needed to improve the electronic properties; in particular by varying the deposition parameters and by trying to compensate the dangling bonds with atoms more firmly bound to Ge. The latter approach has recently been reviewed by Shimizu [28], where $SiF_4/GeF_4/H_2$ gases are used instead of hydrides. The number of dangling bonds was reduced to 8×10^{15} cm^{-3} in an a-Si:Ge:F:H film with E_o =1.4 eV [28]. It appears, therefore, that a-Si:Ge:F:H is a promising material, particularly due to the fact that the photoconductivity is almost constant as E_o decreases (with increasing Ge content). The electron drift mobility was found to be 0.2 to 0.3 $cm^2V^{-1}sec^{-1}$ in a film containing 30 at.% Ge [28]. Doping was achieved by B or P incorporation, resulting in a marked change in the number of dangling bonds [28]. At the present time however, little is known about the properties of this new and interesting material, and more work should be initiated on this problem, including in the direction of devices.

2.2.2.3. Amorphous Silicon-Tin Alloys

a-Si:Sn alloys were first prepared by Vérié et al. [127] in 1981 using a dc triode sputtering system. Non-hydrogenated a-Si:Sn alloy films have also been prepared by co-evaporation in ultra-high vacuum [128]; whereas a-Si:Sn:H films were prepared by sputter-assisted CVD (SAP-CVD) [26], glow discharge of SiH_4, H_2 and $SnCl_4$ or $Sn(CH_3)_4$ gas mixtures [129-131] and sputtering [132].

Optical absorption measurements showed that the optical gap decreases linearly with increasing Sn content, as shown in Fig. 2.10. This variation is consistent with the increasing refractive index found with increasing Sn concentration [127].

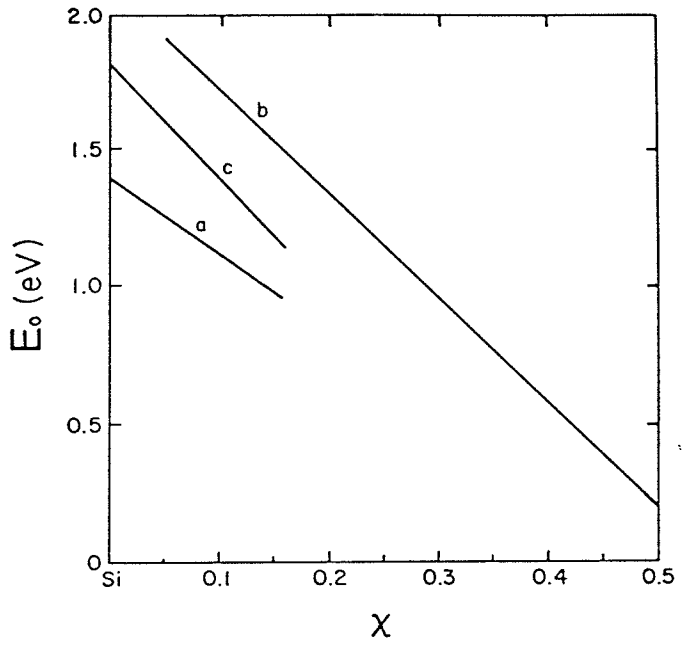

FIGURE 2.10: Optical energy gap of a-$Si_{1-x}Sn_x$ (curve (a) [127]) and a-$Si_{1-x}Sn_x$:H (curve (b) [26] and (c) [129, 130]) alloys as a function of composition.

Vergnat et al. [128] have recently investigated the structure of a-Si:Sn alloys and found that, for Sn concentrations less than 50 at.%, Sn atoms are substituted for Si atoms, and are selectively surrounded by Si atoms in almost perfect tetrahedral units forming a continuous random network. In this composition range, the alloys are amorphous and homogeneous. As the Sn content increases, small crystallites of β-Sn appear in an amorphous Si matrix. For Sn concentrations above 75 at.%, a mixture of Si and β-Sn crystallites occurs, and the amorphous phase disappears. This is probably due to an insufficient cooling rate during deposition, similar to the situation in a-Si:Al.

The dark conductivity of a-Si:Sn:H alloys was found to increase exponentially as E_o decreased [26]. These films contained oxygen, which must presumably be eliminated if films suitable for multi-gap solar cells are to be obtained. Oxygen contamination was also found in sputtered a-Si:Sn:H films [132]. Substantial progress in eliminating O from a-Si:Sn:H films has not yet been reported.

The incorporation of Sn into a-Si and a-Si:H changes the predominant conduction mechanism from n-type to p-type at about 5 at.% Sn [129,130,133]. This is similar to the effect of metals added to a-Si. This transition can explain the accompanying loss in photoconductivity, as well as the poor performance in solar cell device structures. Fig. 2.11 illustrates the transport behaviour of the a-Si:Sn:H alloys as a function of E_o [130] The minimum in the (room temperature) dark conductivity has been attributed to a change in conduction mechanism from n-type extended state conduction to p-type hole hopping behaviour [130]. The activation energy also indicates the change of conduction mechanism to hopping via the lower E_o values. Fig. 2.11(c) illustrates the drastic drop in photoresponse with Sn incorporation. These workers also suggested that with the addition of Sn atoms, states of indeterminate character are created above the valence band; with sufficient Sn incorporation the conduction mechanism is then changed to hole hopping within these states [130]. This interpretation was confirmed by the positive Seebeck coefficients for a-Si:Sn:H films with small E_o (1.3 eV). Only a small percentage of the incorporated Sn atoms are deposited as impurities, producing localized states that cause the n to p-type transition. The majority of the remaining Sn atoms are incorporated substitutionally, as shown by Mössbauer results [130], and play a crucial role in band gap narrowing.

The conduction mechanism was found to reverse to n-type with phosphorus doping, while retaining the narrow band gap. This was accompanied by a recovery in the photoconductivity response.

2.2.3. Amorphous Silicon Alloyed with Column 3a/5a Elements

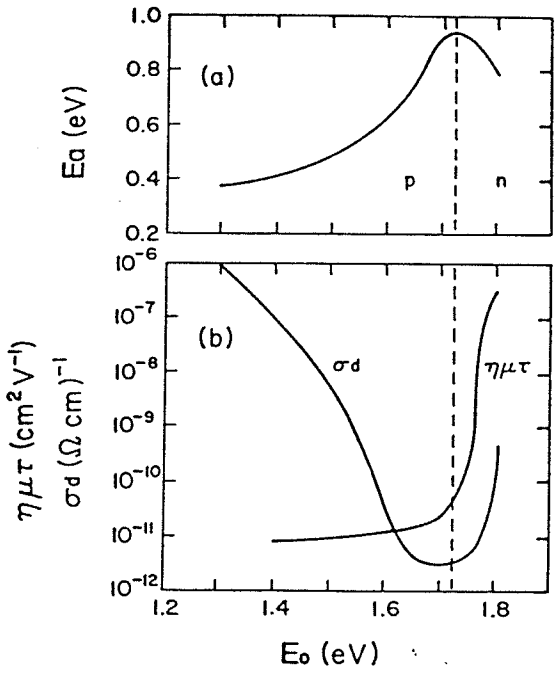

FIGURE 2.11: Conductivity parameters of a-$Si_{1-x}Sn_x$:H alloys as a function of the optical energy gap. (a) is the activation energy and (b) the dark conductivity and photoconductivity $\eta\mu\tau$ product. Taken from Ref. 130.

2.2.3.1. Amorphous Silicon-Nitrogen Alloys

Apart from a-Si:O alloys, a-Si:N alloys appear to be the most extensively studied of all amorphous silicon-nonmetal materials. We will not discuss the amorphous insulator Si_3N_4 in this review; although this material is well studied and of great technological importance in VLSI, such topics depart from the present theme of the modification of a-Si through alloying. a-Si:N:H alloys have been prepared by rf glow discharge in $SiH_4/NH_3/H_2$ and $SiH_4/N_2/H_2$ ambients, by sputtering in $Ar/H_2/N_2$, and by chemical vapour deposition [134-146].

The presence of nitrogen has little effect on the optical gap below 40 at.% N. For larger concentrations E_o undergoes a precipitous increase as the structure converts from a tetrahedral to a Si_3N_4 network [138,140]. This is shown in Fig. 2.12.

The dark conductivity of undoped a-Si:N:H initially increases with increasing N content, followed by a dramatic decline above 40 at.%, as the optical gap increases. There is some debate as to whether N acts as a n-type dopant in small concentrations [135,136,140]. The mobility for electrons in the

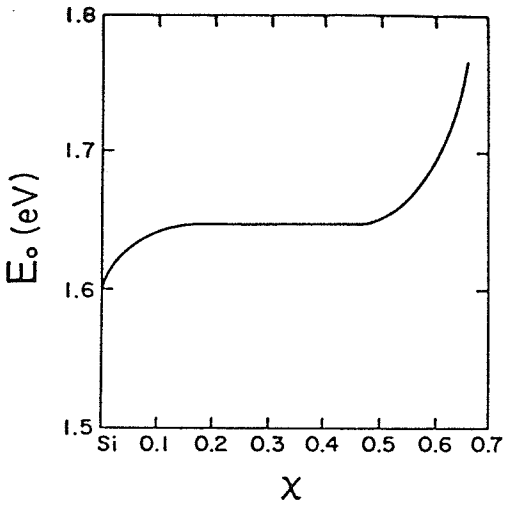

FIGURE 2.12: Optical energy gap of a-$Si_{1-x}N_x$:H alloys as a function of composition. Taken from Ref. 140.

extended states has also been reported to increase by as much as an order of magnitude due to N incorporation [140]. Sasaki et al. have shown that N incorporation into a-Si:H causes an appreciable reduction in hopping conduction at the Fermi energy [146,147]. The $\eta\mu\tau$ product obtained from photoconductivity measurements is not sensitive to N incorporated in concentrations below 40 at.%, a conclusion shared by other workers [140]. N also reduces the number of ESR centers, as expected [147].

a-Si:N:H films have been doped efficiently with both boron and phosphorous; as a result of which the Fermi energy can be varied widely in the upper portion of the energy gap [136]. Boron doped a-Si:N:H exhibits a larger ratio of photo to dark conductivity than a-Si:H [137], which is of great interest in xerography and a great many other applications (see section 4.).

Kurata and co-workers [144] have identified the stretching and bending modes of the N-H, Si-H and Si-N bonds in this material. The Si-N lattice vibrational mode corresponds to 3-fold coordinated N for concentrations above 20 at.% N. They believe that relatively little N is tetrahedrally coordinated, in contrast with the opinion of other workers. Lucovsky and Pollard [148], in reviewing the vibrational properties of a-Si alloys, point out that both N and H can bond to the same Si sites. The Si-H can also adopt a polysilane configuration. The structural model for a-Si:N:H, for small N concentrations, includes isolated Si-H and Si-N bonding sites within a connective polysilane network, as reported by Lucovsky and Pollard [148].

In their recent summary of tetrahedral amorphous alloys, Kuwano and Tsuda [28] concluded that the balance of published literature on a-Si:N:H alloys supports the following view:

(1) for small N concentrations, E_o increases modestly with increasing N; the dark and photo-conductivity remain in the semiconducting range rather than the insulating range,

(2) some atoms are 3-fold coordinated and some 4-fold; as the N concentration increases 3-fold coordination becomes dominant,

(3) a-Si:N films with modest B doping, corresponding to a Fermi energy at midgap, provide optimum optoelectronic properties for a wide range of applications,

(4) the Si-H bonds in a-Si:N:H are stronger than in a-Si:H. a-Si:N:H is therefore expected to be a more thermally stable amorphous semiconductor than a-Si:H (the H not being as readily expelled at high temperatures as it is from a-Si:H).

2.2.3.2. Other Amorphous Silicon-Column 3a/5a Element Alloys

This section is included for completeness, since very little work on a-Si:B, a-Si:P and a-Si:As has been published, apart from the extensive literature for minute (doping level) concentrations, which are not within the scope of this review. To our knowledge, a-Si:Sb and a-Si:Bi have not been reported in alloy concentrations. The other column 3a elements (Al, Ga, In) are metallic, and were covered in section 2.2.1.

a-Si:B:H alloys have been systematically studied by Tsai [149]. These films were prepared by RF plasma decomposition of SiH_4/B_2H_6, and covered the entire compositional range. These films also contained 10 to 40 at.% H in various bonding arrangements at both Si and B sites. Three-center bridge bonds involving B and H as well as three-center B covalent bonds give rise to a wide spectrum of bond strengths. Tail states from the conduction and valence bands penetrate deep into the energy gap. This property is exhibited in an extreme form in a-Si:B:H films deposited by low-pressure CVD, where the density of localized states is so great that no optical gap can be measured [73]. This is discussed further in section 2.2.6 on a-Si:Ge:B:H ternary alloys.

The optical gap is in the range from 1.4 to 2.0 eV; this initially decreases, and then increases again with increasing B concentration. The minimum is reached at about 40 at.% B, and the maximum at 90 at.%, as seen in Fig. 2.13.

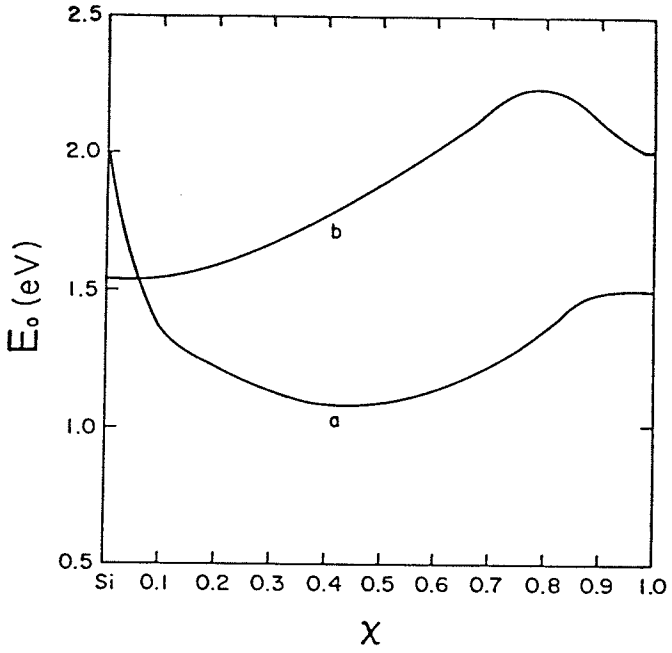

FIGURE 2.13: Optical energy gap of a-$Si_{1-x}B_x$:H (curve (a), from Ref. 149) and a-$Si_{1-x}As_x$:H (curve (b) [150]) alloys as a function of composition.

a-Si:As:H alloys have been studied as an extension of As doping into alloy concentration levels in a-Si:H [150]. The optical gap of a-Si:As, shown in Fig. 2.13, initially increases, and then decreases as the composition of the films approaches that of pure a-As. Over the same range the dc conductivity initially increases with increasing As content by 7 orders of magnitude (doping effect), then decreases by approximately 5 orders of magnitude with further increases in the As content. For As concentrations of 10 at.% and above, there is an As-As interaction which affects E_o and shifts the Fermi level back towards midgap [150]. The absence of donor state formation when Si is incorporated into a-As, which should parallel the case of As incorporation into Si, remains unexplained.

a-Si:P alloys have been prepared over the full compositional range [151]. The concentration of P atoms acting as donors is a very small fraction of the total P concentration, which implies a small doping efficiency. The conductivity initially increases dramatically due to the doping effect, and the activation energy for extended state conduction decreases to 0.15 eV. With further increases in the P content, E_a increases very gradually until, at a critical concentration in excess of 90 at.% P, E_a increases rapidly by 1 eV or more. This marks the transition from a doped semiconductor to an alloy with a modified

bonding structure [151].

2.2.4. Amorphous Silicon-Column 6a Element Alloys

The most widely studied alloy in this category is, of course, a-Si:O. This material is of interest for both very low O concentrations, since small amounts of oxygen are often unavoidable in a-Si:H, and for large O contents, in which the SiO_2 network is encountered. Because of the extensive literature available on SiO_x we do not include this material in our review; a brief account is bound to be misleading in its conclusions. Instead, we refer the reader to the many books and reviews available on this important material. In passing, we might point out that recent work has demonstrated that incorporated O has a generally detrimental effect on the optoelectronic properties of a-Si:H, except perhaps in extremely small concentrations (< 0.01 at.% O) [152]. To our knowledge, neither a-Si:Po or a-Si:S have been produced. The most extensively studied remaining alloy is a-Si:Te, while only a little is known about a-Si:Se.

Amorphous silicon-telluride and silicon-selenide were first produced in 1966 by Hilton et al. through sealed-melt quenching [7]. a-Si:Te has also been fabricated by co-evaporation [153], sputtering of polycrystalline Si_2Te_3 [154], and twin-roller melt quenching [155]. a-Si:Se has been fabricated by evaporation of sintered SiSe in an ultra-high vacuum (UHV) [156], and by co-evaporation in a UHV enviroment [156,157].

Because data on a-Si:Se is quite limited, the following discussion will focus mainly on a-Si:Te, and any similarities or disparities displayed by a-Si:Se simply pointed out.

Whereas crystalline silicon-selenide exhibits a typical 1:2 stoichiometry for a 4a:6a compound, $SiSe_2$ (the other common form being in a 1:1 ratio like GeTe) [154]; silicon-telluride exhibits the very rare form of Si_2Te_3 (the only other known 4a:6a compounds of this type are Ge_2S_3, Sn_2S_3 and Sn_2Se_3). This crystal form is highly defective and ionic, and displays a large unpaired spin concentration [154]. This is in sharp contrast to the amorphous form, which does not display a significant unpaired spin concentration, and so appears to be fully covalently bonded [154].

Most work on a-Si:Te has been in the form of structural studies, where it has been concluded that the amorphous material consists of tetrahedral Si

atoms interconnected by zig-zag chains of divalent Te atoms (the length of a typical chain varying directly with the Te content) [159,160]. No structural studies of a-Si:Se have been undertaken.

A-Si:Te and a-Si:Se hydrolyze rapidly upon exposure to moist air according to the reactions [154,157]

$$SiSe_2 + 2H_2O \rightarrow SiO_2 + 2H_2Se$$

$$Si_2Te_3 + 4H_2O \rightarrow 2SiO_2 + 2H_2Te + Te + 2H_2$$

The occurrence of these reactions are easily discovered from the foul odour of H_2Te (or H_2Se). These reactions replace the surfaces of the alloys with SiO_2, which leads to surface and thickness effects in the electrical and optical properties of thin films of these materials [157], though bulk a-Si:Te appears to be unaffected by this reaction [154].

The optical gap of a-Si:Te decreases with increasing Te content above Te concentrations of 50 at.% Te as shown in Fig. 2.14. Peterson et al. found that E_o is a non-monotonic function of composition [154], and we have found a monotonic decrease [153]. a-Si:Se has only been studied in the range of a few at.% Se [156-158] (the exact composition was not known), so comparison with a-Si:Te is difficult. It appears, however, that even very low concentrations of Se can raise the optical gap from 1.25 eV to 1.8 eV [156]. This has been attributed to the Se compensating dangling bonds in a manner similar to hydrogen [156]. No change in E_o is observed in a-Si:Te below 50 at.% Te [153]. Photoconductivity (at room temperature and below) has been observed in a-Si:Te samples over a narrow composition range near that of a-$Si_{20}Te_{80}$ [153,154].

a-Si:Te is a p-type semiconductor, with an increasing conductivity with increasing Te content due to the decreasing band gap [154]. This conductivity is due to valence band conduction for temperatures down to 250 K. The activation energy for this process also appears to behave in a non-monotonic fashion [154], though only a very small composition range has been studied. The (hole) mobility is approximately 1.0 $cm^2/Vsec$, and is temperature independent, indicating the absence of small polaron effects [154]. Also, memory-type switching has been found in Te-rich a-Si:Te materials [154,161]. a-Si:Se, for low Se concentrations, has been found to exhibit two activation energies over different temperature ranges; 0.76 eV above room temperature, and 0.41 eV below [158]. Little else is known about these materials.

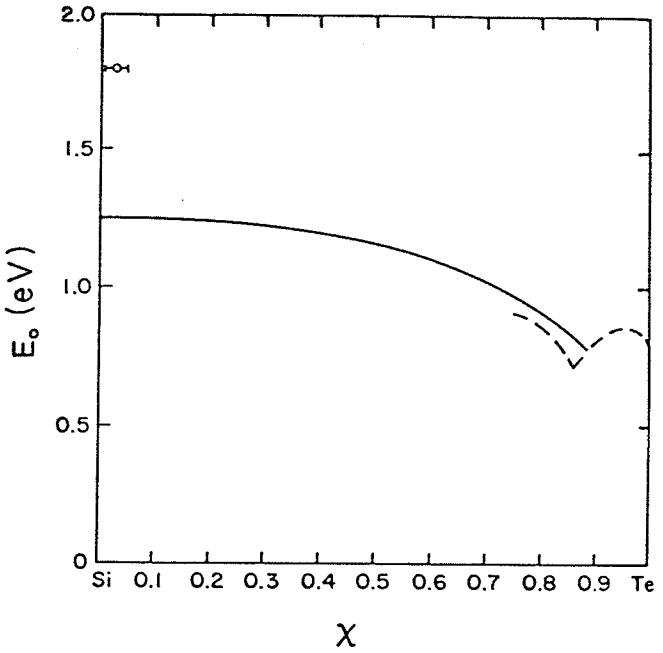

FIGURE 2.14: Optical energy gap of a-$Si_{1-x}Te_x$ alloys as a function of composition. Also included is a-$Si_{0.95}Se_{0.05}$ (o) [156]. Solid curve is taken from Ref 153, dashed curve from Ref. 154.

2.2.5. Amorphous Silicon-Column 7a Element Alloys

Alloys such as a-Si:F and a-Si:Cl are of principal interest as alternatives to a-Si:H, in which F or Cl serve as dangling bond terminators, similar to the role played by H atoms.

a-Si:H:F alloys have been reviewed by Madan [23], and have been shown to exhibit attractive photovoltaic properties [23,162], which are attributed to the large electronegativity of F as compared to H. This difference presumably makes F more effective in the termination of Si dangling bonds. a-Si:H:F has been prepared by RF glow discharge in SiF_4/H_2, $SiH_4/SiF_4/Ar$ and $SiF_4/H_2/Ar$ ambients, by sputtering in SiF_4 and by chemical vapour deposition in SiF_2 [162]. This material contains a large number of incorporated SiF_4 molecules [163]. The density of localized states in the energy gap can be reduced below 10^{17} $cm^{-3}eV^{-1}$ with the appropriate gas mixture. These films are also free from photostructural changes [164]. Theoretical calculations for the electronic structure of a-Si:H:F incorporating Si-F, $Si-F_2$, $Si-F_3$, $(Si-F)_n$ and $(Si-F_2)_n$ complexes were recently reported by Agrawal and Agrawal [165]. These results are in good agreement with photoemission data.

a-Si:H:Cl alloys have been discussed by Chevallier et al. [166]. Cl was found to be effective in the termination of dangling bonds, since, like F, its electronegativity exceeds that of H. The Cl gives rise to an optical gap of 1.8 eV, a substantial increase from a-Si:H without Cl. Both Si-Cl and $Si-Cl_2$ bonds appear to be present in the IR absorption data. Several H and Cl atoms may be attached to the same Si atom. Approximately 6-8 at.% Cl is bonded into the network, as compared to 5 at.% H, in establishing the 1.8 eV optical gap observed in this study [166].

2.2.6. Selected Ternary Amorphous Silicon Alloys

There is a vast number of multi-component amorphous alloys which contain Si as one component. This is especially true in the case of glassy metals, where Si is often used to enhance the glass forming ability of an otherwise metallic alloy [5]. The most common of these are a-Si:Pd:X and a-Si:Fe:X alloys (where X is any one of a variety of metallic elements). In virtually all such cases the Si content is less than 20 at.%. The sheer range of different behaviours exhibited by these alloys precludes their inclusion in this review. This also applies for the large number of multi-component chalcogenides which contain Si as one component. There are, however, a few ternary amorphous alloys of Si which exhibit unique properties of their own, in which Si plays a major role, and are treated as separate alloy systems in their own right (unlike the Si-containing chalcogenides, for example). Such ternary amorphous alloy systems are considered in this section.

Amorphous Si:Ge:B:H alloys were first produced by Murase et al. in 1982 by low-pressure CVD of $SiH_4/B_2H_6/GeH_4$ gas mixtures (diluted with He and H_2) at 500 °C [73]. So far, Murase et al. have been the only researchers to study this material [28,73,167]. This section summarizes their results, contained in Ref. [73]. Though referred to as a-Si:Ge:B alloys by these authors, the large amounts of H_2 present during fabrication imply that the films contain a significant H concentration, and may be better described as a-Si:Ge:B:H alloys.

This material exhibits a number of peculiar optical and electronic properties. These properties will be discussed in this section, while other unusual properties (oxidation and Schottky contact behaviours) will be discussed in the context of their applications to microelectronics in section 2.3. of this review.

This alloy exhibits considerable optical absorption even at very low photon energies, which makes it impossible to calculate an optical gap. The conductivity of these films is also very high ($\approx 0.4\ (\Omega\,\mathrm{cm})^{-1}$). These and other measurements [73] indicate that a-Si:Ge:B alloys are characterized by a very high density of localized states distributed throughout the energy gap. In fact, the density of localized gap states is so great that conduction in these alloys, even above room temperature, is dominated by variable-range hopping through these states. This fact appears to be a consequence of the fabrication process rather than the material, since LP-CVD a-Si:B:H also has this property [73], while RF-GD a-Si:B:H does not ($E_o > 1.4$ eV) [149].

The density of these localized gap states has been estimated at the Fermi level (pinned near the center of the gap) to be approximately $5\times10^{20}\ \mathrm{eV}^{-1}\mathrm{cm}^{-3}$. The nature of these gap states changes significantly with composition. Boron is incorporated into the alloy mainly in a threefold coordination, which gives the network the freedom to form a continuous random network (CRN). This CRN structure results in a very thermo-stable material. However, these threefold B atoms also produce a very *strained* amorphous network, which leads to augmented potential fluctuations that produce a high concentration of localized gap states through Anderson localization. On the other hand, the addition of Ge as a third component reduces the strain, and allows the spacial extent of the localized-state wavefunctions to increase. This has been observed through sudden increases in the conductivity and dielectric constant with increasing Ge content. As a result, it may be possible to study a purely Anderson-type MIT at room temperatures simply by increasing the Ge concentration in these films. This may have already been observed [73], but no detailed studies were undertaken. A possible complication in such a study is the tendency of Ge to induce crystallization (if present in large concentrations), though the addition of B partially counteracts this process.

Though neither a-Si:S or a-Si:Zn binary alloys have yet been produced, a study of the ternary alloy a-Si:S:Zn:H was recently reported [168]. These films were produced by reactive rf and rf magnetron sputtering of Si and ZnS composite targets in an Ar/H_2 ambient. It was found that S was preferentially incorporated into Si-rich films, while Si-poor films consisted of approximately stoichiometric ZnS. With increasing ZnS content, E_o increased from 1.7 eV to 3.2 eV. The addition of ZnS also reduced the spin density and photoconductivity $\eta\mu\tau$ product. It was concluded that this material is tetrahedrally

coordinated in both the Si-rich and Si-poor compositional regions, while a partial chalcogenide glass structure is exhibited for intermediate compositions [168].

2.3. Device Applications

Amorphous silicon alloys have found many applications as electronic, optical and optoelectronic device materials. Many of these applications were previously exploited using the simpler a-Si:H technology, in which case the use of silicon alloys simply served to increase the efficiency of the device. An example is the improvement in the photovoltaic solar cell realized through the incorporation of a-Si:C:H and a-Si:Ge:H, rather than pure a-Si:H, as an active layer of the device [169]. In some cases, the use of amorphous silicon alloys has made possible applications which were not practical with a-Si:H material, thereby giving rise to new devices. An example of the latter situation is the use of a-Si:C:H in visible light-emitting diodes (LEDs), as described by Kukimoto [3].

The following subsections outline the many applications for amorphous silicon alloys which have been realized commercially, are being investigated in the research laboratory, or remain as potential device applications presently served by a-Si:H alone.

2.3.1. Photovoltaic Solar Cells

This has been the primary application for a-Si:H materials in the past, and has served as a driving force for research and development in amorphous silicon and its alloys. Excellent reviews are available of a-Si:H solar cells [3,28,170]; we confine our attention exclusively to amorphous silicon alloys and their influence on the performance of these devices.

Since photovoltaic effects were first observed in a-Si:H [171], there has been a continuous improvement in the photovoltaic efficiency from 1% in 1974 to 5.5% in 1977 (small-area devices), to the present value in excess of 10% for large-area devices (> 1 cm^2) [3]. The recent advances and the present admirable efficiency, however, have depended upon the incorporation of a-Si:C:H and/or a-Si:Ge:H alloys as active materials in the devices. The incorporation of a-Si:Ge:H, with its reduced energy gap, and a-Si:C:H with its increased energy gap, as compared to a-Si:H, can give rise to enhanced open-circuit voltages as well as larger short-circuit currents. Both factors increase conversion efficiency.

The increased open-circuit voltage results from an overall increase in the diffusion potential of the heterojunction device, with its associated reduction in dark current. This is primarily due to the increased energy gap of a-Si:C:H.

The short-circuit current may also be enhanced as a result of the the optical absorption in a-Si:Ge:H which extends further into the infrared due to its small energy gap. This beneficial effect is difficult to exploit as a consequence of a low minority carrier lifetime in the narrow a-Si:Ge:H layer [3].

a-Si:C:H layers were first incorporated into solar cells by Tawada et al. [169]; a-Si:Ge:H layers by Nakamura et al. [171]. The devices of Catalano et al. [172] which incorporate a-Si:C:H as a window layer in a p-i-n structure exhibit 10.1% efficiency for 1.2 cm^2 solar cells. Nakamura et al. [173] have realized 8.6% efficient solar cells of 100 cm^2 area by using a-Si:Ge:H in a multilayer device.

2.3.2. Electronic Devices

The electronic properties of hydrogenated amorphous silicon and its alloys are compatible with a number of active device phenomena such as fast switching in diodes and appreciable gain in transistors. Furthermore, these materials exhibit many advantages over traditional crystalline silicon in several of these applications. Among their advantages are the ability to fabricate reliable devices of large area and high power handling capability, wide operational temperature range, relative immunity to chemical and structural defects, radiation tolerance, and an enlarged range of electronic properties, particularly in the case of amorphous alloys.

Both Schottky barrier and pin diodes have been manufactured with a-Si:H; these devices exhibit rectification ratios as large as 10^9 and have a very fast response [28]. The rapid response is a consequence of the small minority-carrier lifetime in the material; this response can be in the picosecond range [174]. The use of amorphous alloys provides for; (i) tailoring of the forward-bias threshold voltage due to variation of the energy gap, and (ii) modification of reverse-bias breakdown voltage and response time.

a-Si:H insulated gate field-effect transistors or thin-film transistors have been investigated by many workers; see, for example [3,28,175,176]. These devices have realized all of the advantages over crystalline devices that were cited above. The same material has also been employed in the manufacture of charge-coupled devices [28,177]. Among the many applications for the FET devices have been address circuitry for liquid crystal display panels and other logic circuits [3,28].

Amorphous silicon alloys are alternatives to a-Si:H as the active material in these devices; since the transistor parameters derive from the carrier mobility, dielectric constants, etc. they may again be tailored to the applications. Secondary considerations such as temperature dependence and radiation tolerance will also be sensitive to alloy composition. Further improvements and fabrication ease arise from the use of silicon alloys such as a-Si:N:H as a gate dielectric, deposited in situ upon the base material of the FET device.

2.3.3. Optoelectronic Devices

Amorphous silicon and its alloys have found many applications in electrophotography or xerography, media for laser printers, etc.. These applications have recently been reviewed by Shimizu [3]. They depend on a photoinduced discharge, which turns out to rely upon a large ratio of photoconductivity to dark conductivity in the material. Although no commercial devices employing alloys have yet been realized, it is known that alloys such as a-Si:N:H with $\sigma_{ph}/\sigma_d > 10^6$ [137] offer potential improvements over a-Si:H. This was discussed in section 2.2.3.1. Similar comments apply to image pickup tubes (discussed by Ishioka [3]) and large-area image sensors (discussed by Kaneko [3]). Photodetectors, modulators and LEDs with fast response times (discussed by Phelan [3]) have been fabricated in a-Si:H and, in some cases, in alloys such as a-Si:C:H [3,106]. Since these topics were recently reviewed for a-Si:H [3], we restrict our discussion once again to the advantages of amorphous silicon alloys.

Amorphous silicon alloys exhibit advantages over their crystalline counterparts, for optoelectronic applications, in the relaxation of $\mathbf{k}$ conservation rules with the attendant increase in optical absorption or luminescence efficiency. Their improvements over a-Si:H stem from the ability to extend the useful wavelength range to shorter wavelengths, as for example, with a-Si:C:H [106] or to longer wavelengths with, for example, with a-Si:Ge:H [28]. These abilities apply to either photoconductive, photovoltaic or luminescent phenomena. Further advantages in stability, reliability, temperature range and other considerations are expected to accrue due to a mature fabrication technology in amorphous silicon alloy materials.

2.3.4. Optical and Electronic Recording

The application of a-Si:H and its alloys to archival storage media, in which data is written and read by either optical (laser) beams or electron-beams, has been the topic of considerable recent study [3,178]. Information storage is accomplished by either ablative hole formation, hydrogen effusion, bubbling, or other energetically induced phenomena in the material.

In the case of electron-beam addressable material, the critical properties are the correlation of conductivity to H content or structure. In laser addressable systems, the optical absorption, refractive index and thermal properties of the films are the important parameters. All of these features are sensitive to the alloy composition, and this nascent research area holds tremendous potential in view of the insatiable demands of modern computer systems for extended memory.

2.3.5. Other Applications

A host of other applications have been explored in the laboratory for a-Si:H and its alloys. These include ambient sensors (discussed by D'Amico and Fortunato [3]), optical waveguides [179], strain gauges [180] and various other sensors and transducers. A still more pervasive set of applications is found in microfabrication technology (discussed by Murase and Mizushima [28]), and in particular for high-resolution VLSI processing.

In the latter area of microfabrication, amorphous silicon alloys are beginning to find a variety of roles to play [28]. These include enhanced oxidization rates using a-Si:Ge:B:H, whose resultant oxides provide excellent passivation, self-aligned electrodes, and patterning material for directional reactive-ion etching in submicron feature definition.

A variety of other preliminary applications studied for amorphous silicon alloys are not included in this review, since it is too early to forecast their eventual commercial potential.

2.4. Summary

There is a great variety of methods available for the fabrication of amorphous silicon alloys. RF GD remains the standard to which all other techniques are compared. Presently, only this and a few other chemical techniques can be used to produce device quality material on a large scale. Thus, to optimize the fabrication process for other alloys, effort must focus on the search for new gases to allow the production of more alloys by chemical techniques. Research into other fabrication systems will center on the production of materials inaccessible by glow discharge methods and the optimization of their quality.

A number of significant problems in the characterization of amorphous silicon alloys should be apparent from section 2.2. We feel that there are a few basic experiments crucial to the understanding and application of a-Si based alloys that should be carried out in all studies, until they are thoroughly understood. These experiments are (as argued in section 2.2) room temperature optical absorption and the temperature dependence of the dc conductivity. These relatively simple measurements should be standard characterization procedures, as they are for a-Si and a-Si:H. From these experiments, a good estimate of the first-order electronic structure of the material can be obtained, and variations between samples (of different compositions, alloys or from different research groups) may be compared. We would also suggest, in order to catalog properties for future work, that the spectral, temperature and composition dependence of any photoconductivity which may be present, be established.

Another characterization problem, especially important in chemically-produced materials, is the need to distinguish between the effects of alloying and those of hydrogenation. This problem must be solved through direct measurement. It is now well established that the H content of an alloy does not remain constant as the composition is varied. Further, it is clear that gas-phase ratios are not always directly related to the actual composition. Such composition values, if not corroborated by direct measurements, are often wrong or misleading.

One should always remember that amorphous materials, especially those based upon silicon, are often very unstable in air. Hydrolyzation and impurity absorption (due to voids and dangling bonds) can lead to artificial temporal and thickness dependences in many electronic and optical properties.

The following amorphous silicon alloys appear to be particularly deserving of increased investigation at present:

(1) metal-rich a-Si:M alloys offer a unique opportunity to study the metallic phase of Si; for example, in the observation of superconductivity due to Si in noble metal-rich a-Si alloys,

(2) the tetrahedral hydrogenated alloys (section 2.2.2) and the silicon-column 5a alloys (section 2.2.3) hold the greatest immediate potential for semiconductor device improvements, and for new structures such as superlattices,

(3) the a-Si:Ge:B:H system may prove to be an excellent vehicle for the study of a purely Anderson-type metal-insulator transition at room temperature.

It is hoped that the present review will stimulate additional systematic research in what is already an exciting and promising area for future semiconductor devices.

References for Chapter II

[1] R.C. Chittick, J.H. Alexander, H.F. Sterling, J. Electrochem. Soc. 116, pp. 77, 1969.

[2] W.E. Spear, P.G. Le Comber, Sol. St. Comm. 17, pp. 1193, 1975.

[3] J.I. Pankove (ed.), *Semeconductors and Semimetals vol. 21, pt. D,* Academic Press Inc., Orlando, 1984.

[4] N.F. Mott, E.A. Davis, *Electronic Processes in Non-Crystalline Materials, 2nd ed.,* Clarendon Press, Oxford, 1979.

[5] F.E. Luborsky (ed.), *Amorphous Metallic Alloys,* Butterworths' & Co. (Pub.) Ltd., London, 1983.

[6] H. Beck, H.-J. Güntherodt, *Glassy Metals 2,* Topics in Applied Physics 53, Springer-Verlag, Berlin, 1983.

[7] A.R. Hilton, C.E. Jones, M. Brau, (pp. 105), A.R. Hilton, C.E. Jones, (pp. 112), A.R. Hilton, C.E. Jones, R.D. Dobrott, H.M. Klein, A.M. Bryant, T.D. George, (pp. 116), Phys. & Chem. Glasses 7, 1966.

[8] W. Klement, R.H. Willens, P. Duwez, Nature 187, pp. 869, 1960.

[9] P. Duwez, Trans. ASM 60, pp. 607, 1967.

[10] R. Pond Jr., R. Maddin, Trans. Met. Soc. AIME 245, pp. 2475, 1969.

[11] S.T. Picraux, D.M. Follstaedt, Presented at MRS meeting, Boston (Nov. 1982).

[12] G. Fuxi, S. Baorong, W. Hao, J. Non-Cryst. Sol. 56, pp. 201, 1983.

[13] R. Tsu, R.T. Hodgson, T.Y. Tan, J.E. Baglin, Phys. Rev. Lett. 42, pp. 1356, 1979.

[14] M. Von Allmen, S.S. Lau, M. Mäenpää, B.Y. Tsaur, Appl. Phys. Lett. 36, pp. 205, 1980.

[15] L.I. Maissel, R. Glang, (eds.), *Handbook of Thin Film Technology,* McGraw-Hill Book Co., New York, 1970.

[16] J.L. Vossen, W. Kern, (eds.), *Thin Film Processes,* Academic Press, New York, 1978.

[17] J.I. Pankove (ed.), *Semiconductors and Semimetals, vol. 21, pt. A,* Academic Press. Inc., 1984.

[18] W. Pries, R.D. McLeod, T.V. Herak, S.R. Mejia, H.C. Card, K.C. Kao, J. de Physique, 1985, in press.

[19] G. Talukder, J.A. Cowan, D.E. Brodie, J.D. Leslie, Can. J. Phys. 62, pp. 848, 1984.

[20] M. Shindo, S. Sato, I. Myokan, S. Mano, T. Shibata, J. Non-Cryst. Sol. 59/60, pp. 747, 1983.

[21] M. Hanabusa, M. Suzuki, Appl. Phys. Lett. 39, pp. 431, 1981.

[22] K.L. Chopra, *Thin Film Phenomena,* McGraw-Hill Book Co., New York, 1969.

[23] J.D. Joannopoulos, G. Lucovsky (eds.), *Physics of Hydrogenated Amorphous Silicon I,* Topics in Applied Physics 55, Springer-Verlag, Berlin, 1984.

[24] J.J. Hanak, J. Mater. Sci. 5, pp. 964, 1970.

[25] R.A. Rudder, J.W. Cook Jr., G. Lucovsky, Appl. Phys. Lett. 45, pp. 887, 1984.

[26] H. Itozaki, N. Fujita, T. Igarashi, H. Hitotsuyanagi, J. Non-Cryst. Sol. 59/60, pp. 589, 1983.

[27] C. Coluzza, D. Della Sala, G. Fortunato, S. Scaglione, A. Frova, J. Non-Cryst. Sol. 59/60, pp. 723, 1983.

[28] Y. Hamakawa (ed.), JARECT 16, *Amorphous Semiconductor Technologies & Devices,* OHMSHA Ltd. & North-Holland Pub. Co., 1984.

[29] D. Bäuerle, P. Irsigler, G. Leyendecker, H. Noll, D. Wagner, Appl. Phys. Lett. 40, pp. 819, 1982.

[30] M. Meunier, J.H. Flint, D. Adler, J.S. Haggerty, J. Non-Cryst. Sol. 59/60, pp. 669, 1983.

[31] Y. Mishima, Y. Ashida, M. Hirose, J. Non-Cryst. Sol. 59/60. pp. 707, 1983.

[32] M. Konagai, T. Tanaka, K.W. Yeol, K. Takahashi, presented at the MRS Conf., Strasbourg, June, 1984.

[33] J.P.M. Schmitt, J. Non-Cryst. Sol. 59/60, pp. 649, 1983.

[34] M.P. Rosenblum, M.J. Thompson, R.A. Street, AIP Conf. Proc. 73, R.A. Street, D.K. Biegelsen, J.C. Knights (eds.), pp. 42, 1981.

[35] I. Kato, H.C. Card, K.C. Kao, S.R. Mejia, L. Chow, Rev. Sci. Instr. 53, pp. 214, 1982.

[36] I. Kato, S. Wakana, S. Hara, H. Kezuka, Jpn. J. Appl. Phys. 21, pp. L470, 1982.

[37] J.F. Currie, P. Depelsenaire, J.P. Huot, L. Paquin, M.R. Wertheimer, A. Yelon, C. Brassard, J. L'Ecuyer, R. Groleau, J.P. Martin, Can. J. Phys. 61, pp. 582, 1983.

[38] S.R. Mejia, R.D. McLeod, K.C. Kao, H.C. Card, J. Non-Cryst. Sol. 59/60, pp. 727, 1983.

[39] S.R. Mejia, R.D. McLeod, W. Pries, P. Shufflebotham, J. White, J. Schellenberg, K.C. Kao, H.C. Card, Proc. of the 11th Int'l. Conf. Amorph. & Liq. Semicond., Rome, 1985, in press.

[40] W.E. Spear, P.G. Le Comber, S. Kalbitzer, G. Müller, Phil. Mag. B 39, pp. 159, 1979.

[41] W. Beyer, R. Fischer, H. Overhof, Phil. Mag. B 39, pp. 205, 1979.

[42] D.J. Bishop, E.G. Spencer, R.C. Dynes, Sol. St. Elect. 28, pp. 73, 1985.

[43] J.B. Holt, D.C. Ankeny, C.F. Cline, Scripta Met. 14, pp. 959, 1980.

[44] D. Malterre, J. Durand, G. Marchal, J. Non-Cryst. Sol. 61/62, pp. 1137, 1984.

[45] N.T. Bagraev, L.S. Vlasenko, M.M. Mezdrogina, Sov. Tech. Phys. Lett. 7, pp. 80, 1981.

[46] P. Duwez, R.H. Willens, R.C. Crewdson, J. Appl. Phys. 36, pp. 2267, 1965.

[47] U. Köster, P. Weiss, J. Non-Cryst. Sol. 17, pp. 359, 1975.

[48] U. Mizutani, Prog. in Mater. Sci. 28, no. 2, 1983.

[49] E. Huber, M. von Allmen, Phys. Rev. B 28, pp. 2979, 1983.

[50] K. Morigaki, Phil. Mag. B 42, pp. 979, 1980.

[51] M. Dayan, N. Croitoru, Y. Lereah, Phys. Lett. A 82, pp. 306, 1981.

[52] T. Shimizu, M. Kumeda, I. Watanabe, Y. Noumi, Phil. Mag. B 44, pp. 159, 1981.

[53] T. Luciński, J. Baszyński, Phys. Stat. Sol. A 87, pp. K191, 1985.

[54] X. Le, C.L. Foiles, D.K. Reinhard, J. Non-Cryst. Sol. 47, pp. 355, 1982.

[55] R.W. Fane, Y. Zaka, J. Phys. D: Appl. Phys. 16, pp. 1993, 1983.

[56] L. Xu, C.L. Foiles, D.K. Reinhard, Phil. Mag. B 49, pp. 249, 1984.

[57] A.D. Inglis, J.R. Dutcher, N. Savvides, S.P. McAlister, C.M. Hurd, Sol. St. Comm. 47, pp. 555, 1983.

[58] S.B. Dierker, H. Gudmundsson, A.C. Anderson, Sol. St. Comm. 29, pp. 767, 1979.

[59] T. Luciński, J. Baszyński, Phys. Stat. Sol. A 84, pp. 607, 1984.

[60] P. Mangin, G. Marchal, C. Mourey, C. Janot, Phys. Rev. B 21, pp. 3047, 1980.

[61] A. Inoue, T. Masumoto, H.S. Chen, J. Phys. F: Met. Phys. 13, pp. 2603, 1983.

[62] A.S. Edelstein, S.R. Ovshinsky, H. Sadate-Akhavi, J. Wood, Sol. St. Comm. 41, pp. 139, 1982.

[63] C. Suryanarayana, A. Inoue, T. Masumoto, J. Mater. Sci. 15, pp. 1993, 1980.

[64] K. Akitmoto, K. Watanabe, Appl. Phys. Lett. 39, pp. 445, 1981.

[65] R.H. Crewsdon, Calif. Tech. Rep. , CALT-221-20, pp. 21, 1966.

[66] N.F. Mott, *Metal-Insulator Transitions,* Taylor & Francis Ltd., London, 1974.

[67] Sol. St. Elect. 28, no. 1/2 (Ja/Fe), 1985.

[68] N. Nishida, T. Furubayashi, M. Yamaguchi, K. Morigaki, H. Ishimoto, Sol. St. Elect. 28, pp. 81, 1985.

[69] A. Möbius, H. Vinzelberg, C. Gladun, A. Heinrich, D. Elefant, J. Schumann, G. Zies, J. Phys. C: Sol. St. Phys. 18, pp. 3337, 1985.

[70] M.M. Collver, Sol. St. Comm. 23, pp. 333, 1977.

[71] J.C. Slater, *Quantum Theory of Molecules and Solids, vol. 2,* McGraw-Hill Book Co., New York, 1965.

[72] A. Hiraki, A. Shimizu, M. Iwami, T. Narusawa, S. Komiya, Appl. Phys. Lett. 26, pp. 57, 1975.

[73] K. Murase, A. Takeda, Y. Mizushima, Jpn. J. of Appl. Phys. 21, pp. 561, 1982.

[74] W. Buckel, R. Hilsch, Zeit. für Phys. 138, pp. 109, pp. 118, 1954.

[75] B. Stritzker, H.L. Luo, J. Less Com. Met. 73, pp. 301, 1980.

[76] N. Nishida, M. Yamaguchi, T. Furubayashi, K. Morigaki, H. Ishimoto, K. Ono, Sol. St. Comm. 44, pp. 305, 1982.

[77] D. Dew-Hughes, V.D. Linse, J. Appl. Phys. 50, pp. 3500, 1979.

[78] C.C. Tsuei, Appl. Phys. Lett. 33, pp. 262, 1978.

[79] T. Masumoto, A. Inoue, S. Sakai, H. Kimura, A. Hoshi, Trans. Jpn. Inst. Met. 21, pp. 115, 1980.

[80] C. Suryanarayana, W.K. Wang, H. Iwasaki, T. Masumoto, Sol. St. Comm. 34, pp. 861, 1980.

[81] G. Wei-Yan, C. Xi-Shen, W. Zu-Lun, Y. Sun-Sheng, L. Ying, Acta Phys. Sin. 31, pp. 485, 1982. (in Chinese)

[82] C.J. Mogab, W.D. Kingery, J. Appl. Phys. 39, pp. 3640, 1968.

[83] J. Stuke, W. Brenig (eds.), *Amorphous and Liquid Semiconductors vol. 1,* Taylor & Francis Ltd., London, pp. 601, 1973.

[84] K. Nair, S.S. Mitra, J. Non-Cryst. Sol. 24, pp. 1, 1977.

[85] D.A. Anderson, W.E. Spear, Phil. Mag. 35, pp. 1, 1977.

[86] D. Caffier, M. Le Contellec, J. Richard, J. de Physique Coll C4 42, supp. 10, pp. 1037, 1981.

[87] R.S. Sussmann, R. Ogden, Phil. Mag. B 44, pp. 137, 1981.

[88] Y. Tawada, K. Tsuge, M. Kondo, H. Okamoto, Y. Hamakawa, J. Appl. Phys. 53, pp. 5273, 1982.

[89] I. Watanabe, Y. Hata, A. Morimoto, T. Shimizu, Jpn. J. Appl. Phys. 21, pp. L613, 1982.

[90] A. Morimoto, T. Miura, M. Kumeda, T. Shimizu, J. Appl. Phys. 53, pp. 7299, 1982.

[91] J. Bullot, M. Gauthier, M. Schmidt, Y. Catherine, A. Zamouche, Phil. Mag. B 49, pp. 489, 1984.

[92] Y. Catherine, G. Turban, Thin Sol. Films 60, pp. 193, 1979; ibid. 70, pp. 101, 1980

[93] T.E. Hartman, I.C. Blair, C.A. Mead, Thin Sol. Films 2, pp. 79, 1968.

[94] D.D. Allred, D.C. Booth, B.R. Appleton, P.D. Miller, C.D. Moak, J.P.F. Sellschop, C.W. White, A.L. Wintenberg, IEEE Trans. Nuclear Sci. NS-28, pp. 1838, 1981.

[95] R. Dutta, P.K. Banerjee, S.S. Mitra, Phys. Stat. Sol. B 113, pp. 277, 1982.

[96] S. Iida, S. Ohki, Jpn. J. Appl. Phys. 21, pp. L62, 1982.

[97] T. Shimada, Y. Katayama, K.F. Komatsubara, J. Appl. Phys. 50, pp. 5530, 1979.

[98] M. Le Contellec, J. Richard, A. Guivarch, E. Ligeon, J. Fontenille, Thin Sol. Films 58, pp. 407, 1979.

[99] B. Abeles, T. Tiedje, K.S. Liang, H.W. Deckman, H.C. Stasiewski, J.C. Scanlon, P.M. Eisengerger, J. Non-Cryst. Sol. 66, pp. 351, 1984.

[100] D. Engeman, R. Fischer, J. Knecht, Appl. Phys. Lett. 32, pp. 567, 1978.

[101] A. Yamada, J. Kenne, M. Konagai, K. Takahashi, Appl. Phys. Lett. 46, pp. 272, 1985.

[102] Y. Katayama, T. Shimada, K. Usami, Phys. Rev. Lett. 46, pp. 1146, 1981.

[103] W.-Y. Lee, J. Appl. Phys. 51, pp. 3365, 1980.

[104] R. Dutta, P.K. Banerjee, S.S. Mitra, Phys. Rev. B 27, pp. 5032, 1983.

[105] H. Munekata, A. Shiozaki, H. Kukimoto, J. Luminesc. 24/25, pp. 43, 1981.

[106] H. Munekata, H. Kukimoto, Appl. Phys. Lett. 42, pp. 432, 1982.

[107] H. Matsunami, M. Yoshimoto, Y. Fujii, J. Saraie, J. Non-Cryst. Sol. 59/60, pp. 569, 1983.

[108] A. Onton, H. Wiecker, D. Chevallier, C.R. Guarnieri, Proc. 7th Int'l. Conf. Amorphous and Liquid Semiconductors, Edinburgh, W.E. Spear (ed.), Stevenson Ltd., pp. 357, 1977.

[109] D. Hauschildt, R. Fischer, W. Fuhs, Phys. Stat. Sol. B 102, pp. 563, 1980.

[110] G. Nakamura, K. Sato, H. Kondo, Y. Yukimoto, K. Shirahata, J. de Physique Coll. C4 42 supp. 10, pp. 483, 1981.

[111] M.C. Cretella, J. A. Gregory, J. Electrochem. Soc. 129, pp. 2850, 1982.

[112] B. von Roedern, D.K. Paul, J. Blake, R.W. Collins, G. Moddel, W. Paul, Phys. Rev. B 25, pp. 7678, 1982.

[113] G. Nakamura, K. Sato, Y. Yukimoto, Solar Cells 9, pp. 75, 1983.

[114] L. Chahed, C. Senemaud, M.L. Theye, J. Bullot, M. Galin, M. Gauthier, B. Bourdon, M. Toulemonde, Sol. St. Comm. 45, pp. 649, 1983.

[115] J. Bullot, M. Galin, M. Gauthier, B. Bourdon, J. de Physique 44. pp. 713, 1983.

[116] C. Y. Huang, S. Guha, S.J. Hudgens, J. Non-Cryst. Sol. 66, pp. 187, 1984.

[117] J. Chevallier, H. Wieder, A. Onton, C.R. Guarnieri, Sol. St. Comm. 24, pp. 867, 1977.

[118] W. Paul, D. K. Paul, B. von Roedern, J. Blake, S. Oguz, Phys. Rev. Lett. 46, pp. 1016, 1981.

[119] A. Morimoto, T. Miura, M. Kumeda, T. Shimizu, Jpn. J. Appl. Phys. 20, pp. L833, 1981.

[120] N. Van Dong, T.H. Danh, J.Y. Leny, J. Appl. Phys. 52, pp. 338, 1981.

[121] P.K. Banerjee, R. Dutta, S.S. Mitra, J. Non-Cryst. Sol. 50, pp. 1, 1982.

[122] K.C. Kao, R.D. McLeod, C.H. Leung, H.C. Card, H. Watanabe, J. Phys. D: Appl. Phys. 16, pp. 1801, 1983.

[123] S.Z. Weisz, M. Gomez, J.A. Muir, O. Rest, R. Perez, Y. Goldstein, B. Abeles, Appl. Phys. Lett. 44, pp. 634, 1984.

[124] D. Beaglehole, M. Zavetova, J. Non-Cryst. Sol. 4, pp. 272, 1970.

[125] D.L. Staebler, C.R. Wronski, J. Appl. Phys. 51, pp. 3262, 1980.

[126] C.R. Wronski, R.E. Daniel, Phys. Rev. B 23, pp. 794, 1981.

[127] C. Vérié, J.F. Rochette, J.P. Rebouillat, J. de Physique Coll. C4 42 Supp. 10, pp. 667, 1981.

[128] M. Vergnat, M. Piecuch, G. Marchal, M. Gerl, Phil. Mag. B 51, pp. 327, 1985.

[129] A.H. Mahan, D.L. Williamson, A. Madan, Appl. Phys. Lett 44, pp. 220, 1984.

[130] B. Von Rodern, A.H. Madan, R. Könenkamp, D.L. Williamson, A. Sanchez, A. Madan, J. Non-Cryst. Sol. 66, pp. 13, 1984.

[131] Y. Kuwano, M. Ohnichi, H. Nishiwaki, S. Tsuda, F. Fukatsu, K. Enomoto, Y. Nakashima, H. Tarui, Proc. 16th IEEE PV Specialists Conf., San Diego, pp. 1338, 1982.

[132] D.L. Williamson, S.K. Deb, J. Appl. Phys. 54, pp. 2588, 1983.

[133] A.A. Andreev, O.A. Golikova, F.S. Nasredinov, P.V. Nistiryuk, P.P. Seregin, Sov. Phys.: Semicond. 16, pp. 715, 1982.

[134] J. Baixeras, D. Mencaraglia, P. Andro, Phil. Mag. 37, pp. 403, 1978.

[135] R.W. Griffith, F.J. Kampas, P.E. Vanier, M.D. Hirsch, J. Non-Cryst. Sol. 35/36, pp. 391, 1980.

[136] H. Watanabe, K. Katoh, M. Yasui, Jpn. J. Appl. Phys. 21, pp. L341, 1982.

[137] H. Watanabe, K. Katoh, M. Yasui, Thin Sol. Films 106, pp. 263, 1983.

[138] H. Watanabe, K. Katoh, M. Yasui, Y. Shibata, J. Non-Cryst. Sol. 59/60, pp. 605, 1983.

[139] H. Watanabe, K. Katoh, M. Yasui, Jpn. J. Appl. Phys. 23, pp. 1, 1984.

[140] T.V. Herak, R.D. McLeod, K.C. Kao, H.C. Card, H. Watanabe, M. Katoh, M. Yasui, Y. Shibata, J. Non-Cryst. Sol. 69, pp. 39, 1984.

[141] T.V. Herak, R.D. McLeod, M.G. Collett, K.C. Kao, H.C. Card, H. Watanabe, M. Katoh, M. Yasui, Y. Shibata, Can. J. Phys., in press.

[142] W.Y. Xu, Z.L. Sun, Z.P. Wang, D.L. Lee, J. de Physique Coll. C4 42, supp. 10, pp. 695, 1981.

[143] S.M. Pietruszko, K.L. Narasimhan, S. Guha, Phil. Mag. 43, pp. 357, 1981.

[144] H. Kurata, M. Hirose, Y. Osaka, Jpn. J. Appl. Phys. 20, pp. L811, 1981.

[145] T. Noguchi, S. Usui, A. Sawada, Y. Kanoh, M. Kikuchi, Jpn. J. Appl. Phys. 21. pp. L485, 1982.

[146] G. Sasaki, M. Kondo, S. Fujita, A. Sasaki, Jpn. J. Appl. Phys. 21, pp. 1394, 1982.

[147] G. Sasaki, S. Fujita, A. Sasaki, Appl. Phys. Lett. 54, pp. 2696, 1983.

[148] J.D. Joannopoulos, G. Lucovsky (eds.), *The Physics of Hydrogenated Amorphous Silicon II*, Topics in Applied Physics 56, Springer-Verlag, Berlin, pp. 301, 1984.

[149] C.C. Tsai, Phys. Rev. B 19, pp. 2041, 1979.

[150] J.C. Knights, Phil. Mag. 34, pp. 663, 1976.

[151] D. Leidich, E. Linhart, E. Niemann, H.W. Grueninger, R. Fischer, R.R. Zeyfang, J. Non-Cryst. Sol. 59/60, pp. 613, 1983.

[152] B.G. Yacobi, R.W. Collins, G. Moddel, P. Viktorovitch, W. Paul, Phys. Rev. Lett. B 24, pp. 5907, 1981.

[153] P.K. Shufflebotham, K.C. Kao, H.C. Card, to be published.

[154] K.E. Peterson, U. Birkholz, D. Adler, Phys. Rev. B 8, pp. 1453, 1973.

[155] H.S. Chen, C.E. Miller, Rev. Sci. Instr. 41, 1237, 1970.

[156] F.G. Wakim, A. Al-Jassar, S.A. Abo-Namous, J. Non-Cryst. Sol. 53, P.11, 1982.

[157] F.G. Wakim, A. Al-Jassar, M.A. Hasan, K.Z. Botros, J. Non-Cryst. Sol. 59/60, pp. 617, 1983.

[158] F.G. Wakim, S.A. Abo-Namous, A. Al-Jassar, M.A. Hassan, Appl. Phys. Lett. 42, pp. 523, 1983.

[159] F.R.L. Schoening, J. Mater. Sci. 14, pp. 2397, 1979.

[160] G.E.A. Bartsch, H. Bromme, T. Just, J. Non-Cryst. Sol. 18, pp. 65, 1975.

[161] S.A. Altunyan, V.S. Minaev, M.S. Minazhdinov, B.K. Sachkov, Sov. Phys.: Semicond. 4, pp. 1906, 1971.

[162] A. Madan, W. Czybatyj, J. Yang, J. McGill, S.R. Ovshinsky, J. de Physique Coll. C4 42, pp. 463, 1981.

[163] M. Kumeda, Y. Yonezawa, T. Shimizu, Jpn. J. Appl. Phys. 23, pp. L540, 1984.

[164] A. Madan, S.R. Ovshinsky, E. Benn, Phil. Mag. B 40, pp. 259. 1979.

[165] B.K. Agrawal, S. Agrawal, Phys. Rev. B 29, pp. 6870, 1984.

[166] J. Chevallier, S. Kalem, S. Al Dallal, J. Bourneix, J. Non-Cryst. Sol. 51, pp. 277, 1982.

[167] K. Murase, Y. Amemiya, Y. Mizushima, Jpn. J of Appl. Phys. 21, pp. 1559, 1982.

[168] A. Morimoto, S. Takamori, T. Shimizu, presented at The 11th Int'l. Conf. on Amorph. and Liq. Semicond., Rome, Sept., 1985.

[169] Y. Tawada, M. Kondo, H. Okamoto, Y. Hamakawa, Proc. IEEE Phot. Spec. Conf. 15, pp. 245, 1981.

[170] M.H. Brodsky (ed.), *Amorphous Semiconductors,* Springer-Verlag, Berlin, pp. 287, 1981.

[171] D. Reidel (ed.), Proc. 4th Europ. Commun. Photov. Solar. Energy Conf., Stressa, Doredrecht, Holland, pp. 616, 1982.

[172] A. Catalano, R.V. D'Aiello, J. Dresner, B. Faughnan, A. Firester, J. Kane, H. Schade, Z.E. Smith, G. Schwartz, A. Triano, Proc. IEEE Phot. Spec. Conf. 16, pp. 1421, 1982.

[173] G. Nakamura, K. Sato, T. Ishihara, M. Usui, K. Okaniwa, Y. Yukimoto, J. Non-Cryst. Sol. 59/60, pp. 1111, 1983.

[174] D.H. Auston, P. Lavallard, N. Sol, D. Kaplan, Appl. Phys. Lett. 36, pp. 66, 1980.

[175] Y. Hirai, K. Sakai, Y. Osada, K. Aihara, T, Nakagiri, J. Non-Cryst. Sol. 59/60, pp. 1191, 1983.

[176] A.J. Snell, P.G. Le Comber, K.D. MacKenzie, W.E. Spear, A. Doghmane, J. Non-Cryst. Sol. 59/60, pp. 1187, 1983.

[177] S. Kishida, Y. Naruke, Y. Uchida, M. Matsumara, J. Non-Cryst. Sol. 59/60. pp. 1281, 1983.

[178] R.D. McLeod, W. Pries, H.C. Card, K.C. Kao, Appl. Phys. Lett. 45, pp. 628, 1984.

[179] J.M. Berger, J.P. Ferraton, B. Yous, A. Donradieu, Thin Sol. Films 86, pp. 337. 1981.

[180] S. Kodato, S. Nishida, M. Konagai, K. Takahashi, J. Non-Cryst. Sol. 59/60, pp. 1207, 1983.

[181] K. Murase, T. Tamama, M, Sukave, T. Ogino, Y. Amemiya, Y. Mizushima, J. Non-Cryst. Sol. 59/60, pp. 1211, 1983.

CHAPTER III

FABRICATION OF a-Si:N:H BY ARE

Activated reactive evaporation (ARE) was originally developed in 1972 as a method of obtaining high rate deposition of compounds from electron beam evaporation of metals [11]. This process was successfully adapted to the fabrication of a-Si:H thin films independently by Werner Pries et al. [12,13] at the University of Manitoba, and G. Talukder et al. [14] at the University of Waterloo, both in 1983. They showed that the difficulty in incorporating atomic hydrogen into evaporated a-Si thin films could be overcome through the use of the ARE technique. It was also found that the atomic hydrogen incorporated by the ARE process (as opposed to the molecular hydrogen incorporated by conventional reactive evaporation techniques) was successful in partially suppressing the effects of impurities such as oxygen, a significant improvement on conventional e-beam systems.

The success obtained with hydrogen incorporation suggested that this process might be used to produce a variety of doped or alloyed a-Si thin films. This led directly to the present study of a-Si:N:H thin films produced by ARE. Unfortunately, the results of this study were negative; that is, no significant trends were found in any of the electrical or optical properties of the films as a function of the alleged composition. These results are presented in section 3.2 and are discussed in section 3.3, where possible solutions to this problem are also described.

3.1. Activated Reactive Evaporation

ARE consists simply of electron beam evaporation of pure silicon in an activated atmosphere of the desired alloying or dopant (reactant) gas. This system is simple, rugged and requires a minimum of gas handling equipment. Clearly, if feasible, such a system would be an attractive candidate for an industrial process. As a result, one of the primary aims of this research was to investigate the suitability of this system for the fabrication of quality a-Si alloy thin films. The other main purpose was to study the electrical and optical properties of films produced by this unusual method.

The feature that distinguishes ARE from ordinary e-beam evaporation is that it takes place in a (relatively) high-pressure activated reactive atmosphere. The reactant gas is brought into the chamber through a nozzle which is held at a positive dc potential. This nozzle sprays the gas molecules directly into the path of both the e-beam and the evaporated Si atoms. The positive potential on the nozzle draws primary (from the beam) and secondary (from the melt) electrons into collisions with the gas molecules, dissociating or ionizing (activating) them and making them more reactive. These species are then able to react with the evaporated Si atoms to form complexes which condense on the substrate, producing an amorphous silicon alloy thin film [11]. Of course, free gas molecules, atoms and ions will also be incorporated as they impinge on the growing film.

The ARE system used in this research was the same one used by Pries [12] to fabricate a-Si:H thin films. This system is shown schematically in Fig. 3.1. The vacuum chamber was bakeable to 200 °C, and was evacuated with a liquid N_2 cold trap-equipped diffusion pump. Evaporation was performed with a Varian 4 kW triple crucible electron gun. The substrates were mounted an optimal distance (with respect to film uniformity) of 20 cm above the melt, could be heated to 200 °C, and were protected from unwanted deposition by a movable shutter. The reactant gas was injected into the chamber through a nozzle which could be held at a positive potential up to 1500 Vdc. This nozzle was electrically isolated from the rest of the system by a section of glass tubing. The flow of gas into the chamber was controlled by a Matheson needle valve and flowmeter. Both the pressure and composition of the atmosphere in the chamber were monitored with a Varian partial pressure gauge (PPG).

The reactant gas used in these experiments was a mixture of 10% H_2 and 90% N_2 called Forming gas. This composition was confirmed using the PPG.

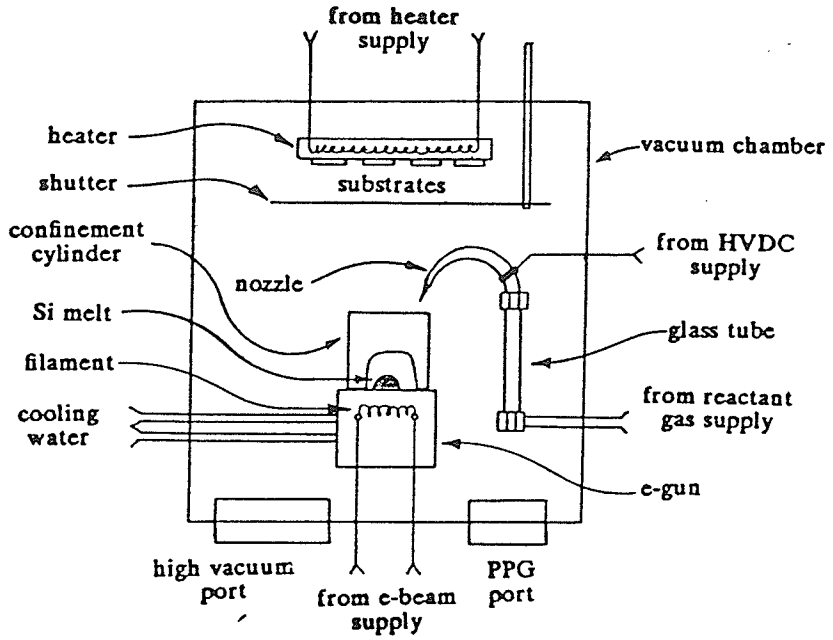

FIGURE 3.1: Schematic diagram of the ARE system used in the fabrication of a-Si:N:H thin films. Interior components only are shown.

The evaporant used was high purity polycrystalline silicon, etched in CP_4 to remove the oxide layer, and ground into a coarse powder. Six substrates were used; 4 glass, 1 quartz, and 1 <111> boron doped (p-type) c-Si wafer. These were thoroughly cleaned in organic solvents and an ultrasonic bath before use.

Before each deposition, the chamber was thoroughly cleaned, baked, flushed with reactant gas and evacuated to less than 10^{-6} Torr. The evaporant Si was also fully melted in advance in order to remove any remaining impurities.

All depositions were carried out with an e-beam power of 1 kW (250 mA @ 4 kV), at a substrate temperature of 200 °C. These values were found to give positive results in the work on a-Si:H by Pries [12], and were retained in these experiments (a planned study of substrate temperature and deposition rate effects was abandoned when it became clear that no N or H incorporation had occurred). The composition of the samples was varied by changing the Forming gas partial pressure and the nozzle potential for each deposition. Nozzle potentials of 0 V, 500 V and 1 kV were combined with a range of partial pressures up to 10^{-4} Torr (above which neither the PPG or e-gun could be used). These values covered most of the safe operating conditions possible with this system; so the full range of its capabilities was investigated.

3.2. Characterization

The a-Si:N:H thin films were characterized with X-ray diffraction, visible and IR spectrophotometry, ellipsometry and temperature-dependent conductivity.

The thickness of the films was measured with a Sloan Dektak mechanical stylus instrument. Samples ranged in thickness from 0.2 μm to 1.5 μm, with 1 μm being a typical thickness. The (monotonic) variation across a sample was usually about 15 %.

X-ray diffraction measurements showed that the films were completely amorphous over the entire range of investigated deposition conditions.

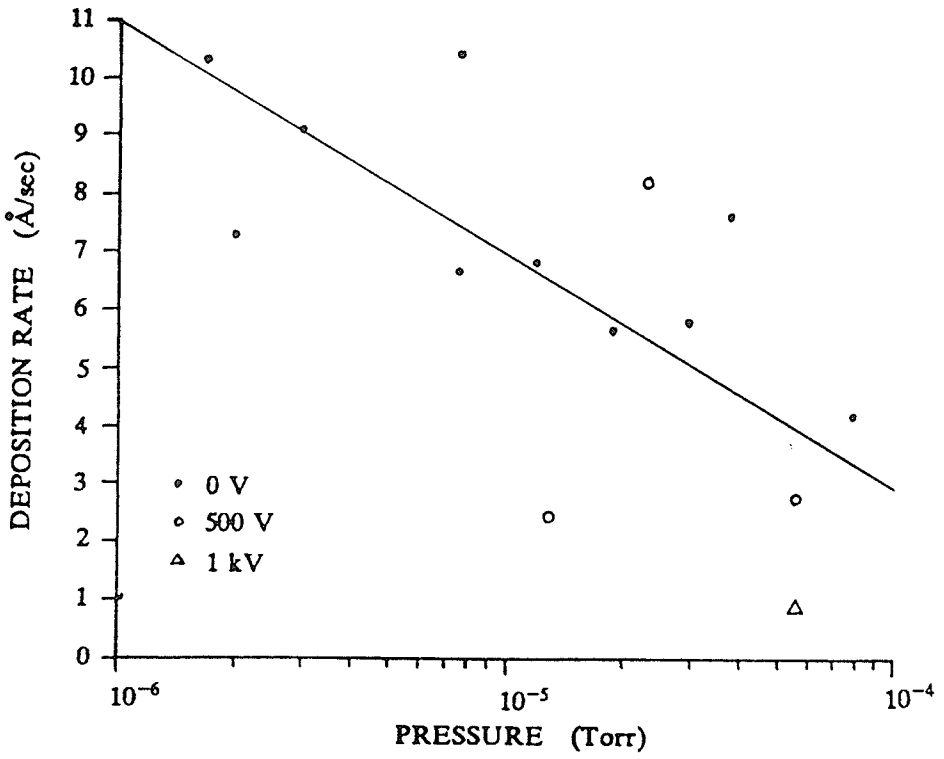

FIGURE 3.2: Deposition rate vs pressure, as a function of nozzle potential, at an e-beam power of 1 kW.

Fig. 3.2 shows the effects of the Forming gas partial pressure and the nozzle potential on the deposition rate. The scatter of the data was a result of the sensitivity of e-beam evaporation to a wide range of variables; two particularly important ones were the size and shape of the melt. The downward trend with increasing pressure was due to the reduction of the mean free path length. It is also apparent from the figure that the large nozzle potentials used

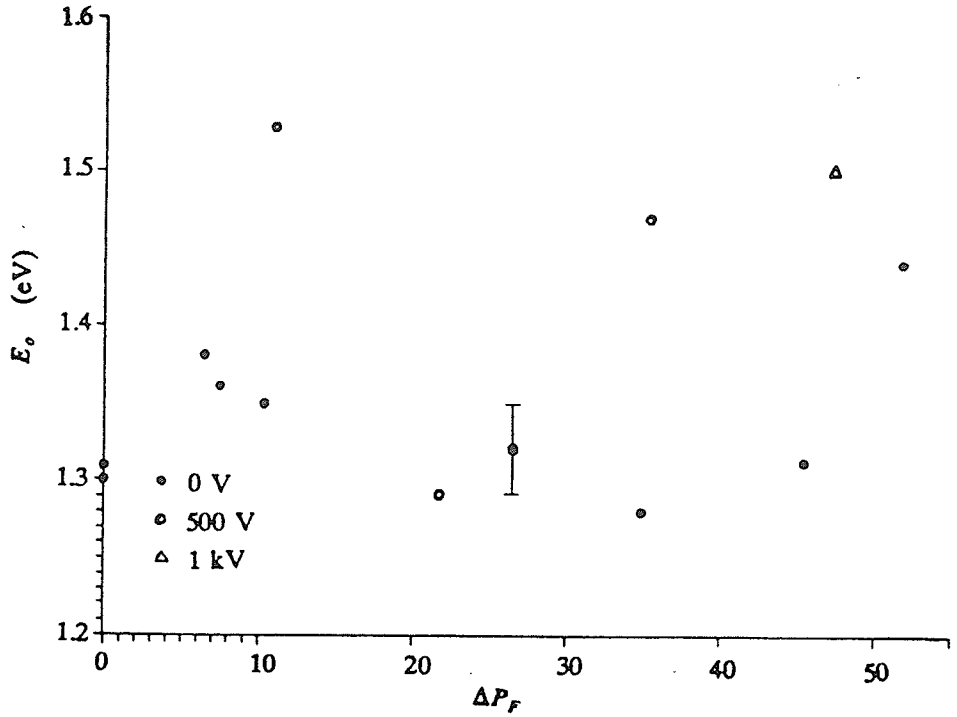

FIGURE 3.3: Optical gap vs Forming gas partial pressure, as a function of nozzle potential. Measurement error in E_o is ± 0.03 eV.

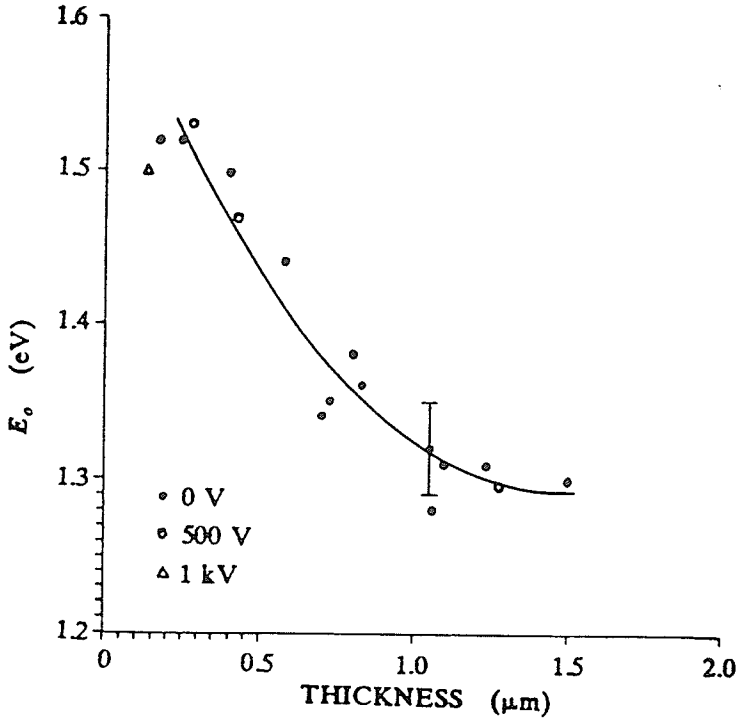

FIGURE 3.4: Optical gap vs film thickness. Measurement error in E_o is ± 0.03 eV.

in these experiments (as opposed to the 200 V used by Pries) tended to reduce the deposition rate still further. This could have been due to the large positive potential stripping electrons from the beam, reducing the heating power incident on the melt. Finally, it was observed that for a certain range of flow rates (50-75 %) and nozzle potentials (> 800 V) a glow discharge formed in the glass tubing section of the gas supply (see Fig. 3.1). The importance of this observation will be discussed in section 3.3.4.

Fig. 3.3 shows the optical gap, E_o, as a function of Forming gas partial pressure* and nozzle potential. It would appear from this figure that some N or H incorporation may have occurred at high pressures and nozzle voltages, but this was not the case. In fact, E_o does not depend significantly on the deposition conditions, but primarily on the *thickness* of the film, as shown in Fig. 3.4. Because films produced with high pressures and nozzle potentials were made at lower deposition rates, they tended to be thinner, and thus have larger optical gaps. A model to explain this phenomenon will be presented in section 3.3.3.

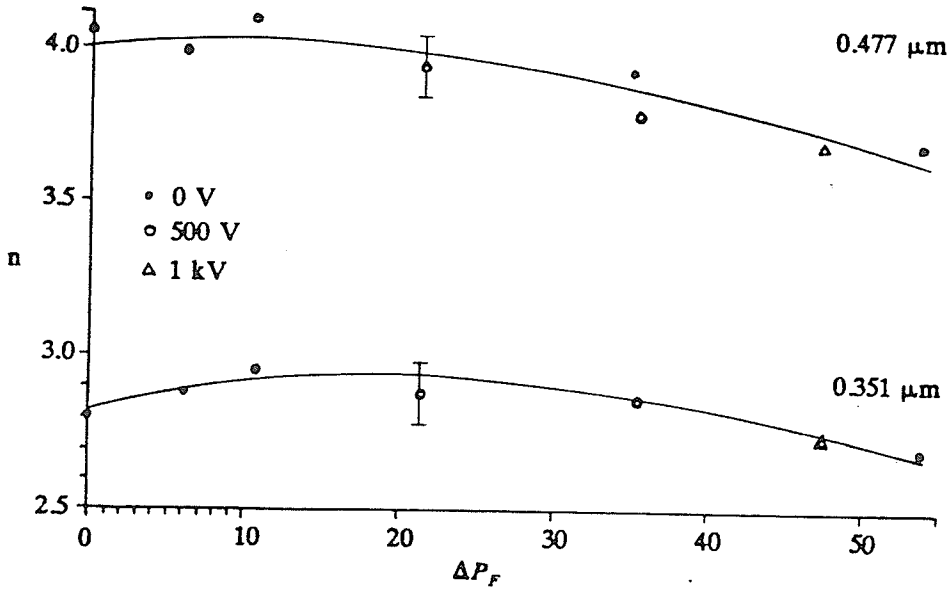

FIGURE 3.5: Refractive index vs Forming gas partial pressure, as a function of nozzle potential, for 2 wavelengths in the visible range. Measurement error in n is ± 0.1.

* $\Delta P_F = \frac{\text{Forming gas partial presssure}}{\text{base pressure}}$

Fig. 3.5 gives the dependence of the refractive index on the Forming gas pressure and the nozzle potential, at wavelengths of 0.351 μm and 0.477 μm, as obtained from ellipsometry measurements. No evidence of substantial N or H incorporation was found.

The dark conductivity of the a-Si:N:H thin films was measured in the ohmic region as a function of temperature using Al contacts in a gap cell geometry. These results are given in Fig. 3.6. Activation energies obtained from the temperature dependence of the dark conductivity are shown in Fig. 3.7. Neither figure shows evidence of significant N or H incorporation.

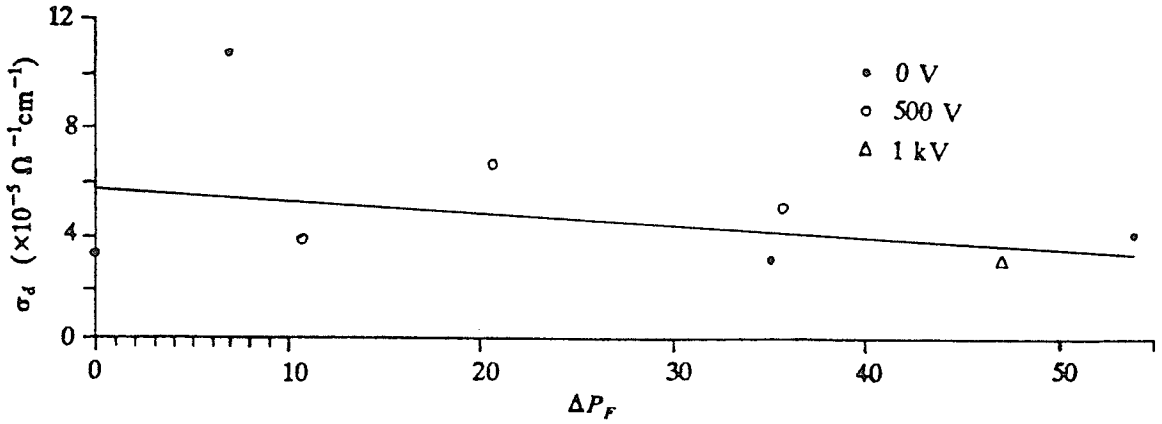

FIGURE 3.6: Dark conductivity vs Forming gas partial pressure, as a function of nozzle potential, at 30 °C.

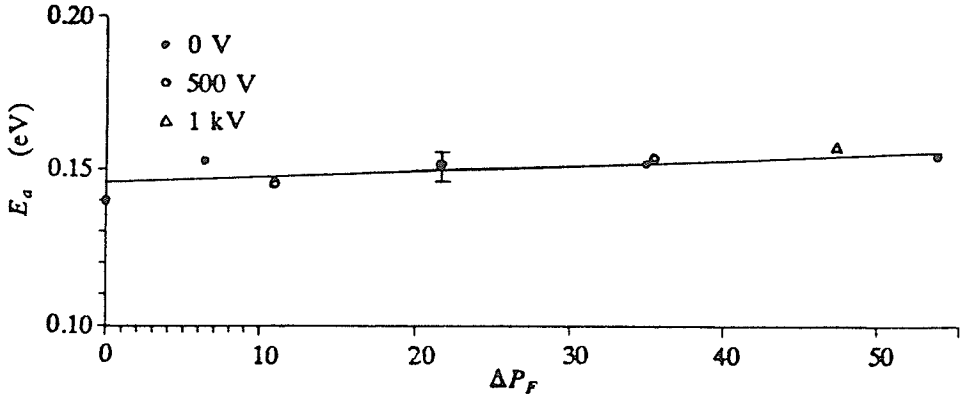

FIGURE 3.7: Activation energy vs Forming gas partial pressure as a function of nozzle potential. The experimental error in E_a is ± 0.01 eV.

Finally, no detectable photoconductivity or photoluminescence was found in any of these films.

3.3. Discussion

3.3.1. Failure of N or H Incorporation by ARE

The results of section 3.2 clearly demonstrate that no significant amounts of nitrogen or hydrogen were incorporated into the a-Si thin films by the ARE process. This appears to have been due solely to the use of an inappropriate (unreactive) reactant gas. This was further aggravated by having too small a reaction zone.

In the ARE process, reactions between the evaporant and reactant gas can occur on the melt, in the vapour phase, or on the substrates. Reactions on the melt are unimportant since the high temperatures present dissociate any compounds that form [11,15]. Reactions in the vapour phase and on the substrates occur whenever a reactant gas is present, the rate being determined by the degree of reactivity of the reactant species with Si. These reactions did not occur to a significant extent, and thus the ARE process failed. The reasons for this failure are discussed below.

In the original, and all subsequent work on ARE it was assumed that vapour phase reactions would dominate [11]. In order for this to be true, the source-substrate distance, l, must be equal to or greater than the mean free path length, λ, ensuring that many collisions occur, so that there will be many opportunities for reactions to take place [11,15]. Yet this has not been the case in any of the systems used, including the present one. Typical source-substrate distances were ≈ 20 cm, while λ at 10^{-4} Torr is 40 cm [15]. The fraction of particles undergoing a collision is then [15]

$$\frac{N_c}{N_o} = 1 - e^{-l/\lambda} \approx 30\% \qquad (3.3)$$

which is a rather low rate. That these collisions do occur to some extent can be seen from the drop in the deposition rate with increasing pressure.

Even so, the occurrence of collisions does not guarantee that reactions take place, as the reactivity of the colliding species must be considered. These reactions were to be enhanced by activation of the reactant gas, as described in section 3.1. However, it has been shown in sputtering experiments with Si in N_2 and NH_3 ambients that N_2 is *extremely* unreactive with Si (p.4-30 [15]). N_2 is not chemisorbed by Si at all; N_2^+ and N^+ ions are required. The great stability* of the N_2 molecules ensured that these species were not present in

* The relative stability of these molecules with respect to dissociation or ionization

large numbers. This lack of activation of the N_2 was also indicated by the small current drawn by the nozzle, and the absence of the glow characteristic of activation processes [11]. However, it was found from the sputtering experiments that ammonia, NH_3, was very reactive, being easily dissociated into the required N^+ ions [15].

Even if all the colliding species react, the nature of the collisions themselves must also be considered. While the depression of the deposition rate indicates that some collisions did occur, it also indicates that the colliding particles were *scattered away from the substrates*. Any Si:N complexes that may have formed then impinged on other surfaces, where they condensed. Thus, these complexes did not partake in the growth of the films.

The conclusion is that vapour phase reactions were not significant contributors to the composition of the films. This conclusion is contrary to the assumption held by all previous ARE researchers.

The only remaining place for a significant number of reactions to occur is on the substrate surfaces. Such reactions did not occur for N_2 for the same reason of lack of reactivity outlined above. Obviously, reactions did occur to some extent for H_2, since positive results were obtained for H incorporation into a-Si by ARE in an H_2 ambient [12-14]. This is to be expected since H_2 is much easier to dissociate than N_2. This also indicates that appreciable N and H incorporation should be possible with ammonia (NH_3), which is even easier to dissociate than H_2.

Ammonia has already been used in non-activated reactive evaporation to make a-Si:N:H films [16], where some success was obtained. The use of activated NH_3 should significantly improve those results.

3.3.2. Incorporated Impurities

In section 3.3.3 it will be described how the great porosity of evaporated a-Si leads to the absorption of large amounts of impurities from the atmosphere. There are, however, other sources of impurities intrinsic to the ARE fabrication process. It is these incorporated impurities which are discussed in this section.

---

was compared on the basis of their equilibrium constants.

There were two main sources of incorporated impurities: residual gasses and vapours (which gave rise to the 10^{-6} Torr base pressure), and dust or oils on interior surfaces (which sublimated or evaporated upon heating). The effects of the latter were minimized through the use of rigorous cleaning procedures and bakeouts. The residual gasses could not be removed, however, and contributed significant amounts of impurities to the growing films.

The residual gas was simply air that had leaked into the system. Dry air is 79 vol.% N_2 and 21 vol.% O_2. In normal air a considerable fraction of this is replaced by H_2O vapour, the actual amount being determined by the local humidity. From these, the main contamination of a-Si comes from H_2O and O_2, since they are substantially more reactive with Si than is N_2.

Silicon is oxidized by O_2 and H_2O according to the following reactions [17]:

$$Si + O_2 \rightarrow SiO_2$$

$$Si + 2H_2O \rightarrow SiO_2 + 4H_2$$

The steam reaction is generally an order of magnitude faster than the O_2 reaction at any given temperature [17], though H_2O was likely present only in small quantities.

These facts indicate that the ARE-produced a-Si films contained oxygen and some hydrogen as deposited impurities; the oxygen incorporated substitutionally, while the hydrogen was trapped as H_2 gas in the void network [18].

The concentration of impurities incorporated into the films was estimated from the residual gas pressure and corresponding deposition rate. The impingement rates for the Si atoms and impurity molecules were found from the nomogram provided on page 1-82 of [15]. For a residual gas pressure of $\approx 10^{-6}$ Torr, the impingement rate was $\approx 5\times10^{14}$ impurity molecules/cm^{2}sec. For a corresponding Si deposition rate of 11 Å/sec, the impingement rate was 5×10^{15} Si atoms/cm^{2}sec. The impingement ratio of impurities to Si was thus 0.1. However, this is not generally the same as the impurity concentration, since this also depends on how much of the impurity is actually chemisorbed by the growing film. This dependence is known in the case of Si evaporation in an O_2 ambient, and coincidently gives an oxygen concentration of ≈ 10 at.% [15].

In summary, the ARE-produced a-Si thin films contain approximately 10 at.% impurities, consisting mainly of substitutional O with some H_2 gas trapped in the void network. These results are consistent with previous impurity studies performed on ARE produced a-Si:H material [12-14].

3.3.3. Thickness Effects

All thin-film growth begins with a nucleation process. Subsequent coalescence of the nuclei produces a continuous film. The inhomogeneities implied by this growth process produce extreme thickness dependences in virtually all electrical and optical properties of the film. Even once the film is homogeneous, there is still scattering of the charge carriers by the surfaces, which produces a thickness dependence in the transport properties as the relative contribution of surface scattering to the total scattering changes. These effects are generally found only in films less than 300 Å thick [15]. Since the ARE-produced a-Si thin films are at least an order of magnitude thicker than this, some other mechanism must be found to explain the thickness dependence of E_o seen in Fig. 3.4.

Thickness dependences in the electrical and optical properties of ARE produced a-Si:H thin films were also found by the Waterloo group [14]. In fact, their results for E_o were virtually identical to those seen in Fig. 3.4. They also found that the resistivity and activation energy were thickness dependent, increasing dramatically for films less than 0.3 μm thick. No such dependence was found here, because the conductivity was not measured on samples of such small thickness.

In Waterloo, it was found that these thickness effects were produced by hydrogen-rich layers at both surfaces of the films [14]. The combined thickness of these layers (about 0.1 μm) remained constant even as the overall film thickness decreased. Thus, in a thinner film, only the bulk layer was reduced, and the surface layers contributed more to the overall properties of the film. It was suggested that the higher H content of these layers gave rise to a larger E_o, and thus a larger resistivity also. A simplified two-layer model was used to study these thickness dependences. It was found that this model was successful in explaining all observed electrical and optical thickness phenomena. Since the a-Si:N:H films made for this study were deposited using the same process and displayed similar properties, a similar mechanism must have been involved.

A question immediately arises as to how these hydrogen rich layers would be formed, since even samples made "pure" (no reactant gas present) displayed these thickness effects. It is well known that evaporated a-Si is a very porous material, consisting of a large number of voids (~ 100 Å diameter) interconnected by a network of micropores (~ 10 Å diameter). This makes a-Si highly gas-absorbent, even at room temperature and atmospheric pressure. These gas impurities can penetrate more than 0.1 μm into the film, significantly affecting its properties [19].

Because of these facts, the following hypothesis is proposed: there exist impurity rich surface layers in ARE deposited a-Si thin films caused by impurities absorbed by the void network and incorporated into the film upon exposure to air. The impurity layer on the substrate side results from absorption by the film of gasses previously adsorbed by the surface of the substrate. As a result, the cumulative thickness of these layers is dependent on the porosity of the film and the duration of exposure, rather than the thickness of the film as a whole. These surface layer impurities consist mainly of O and H_2, for the same reasons described in the previous sections. Significant support for this hypothesis has been obtained from IR spectroscopy measurements performed on evaporated a-Si:Te thin films, as discussed in section 4.2. Those measurements revealed the presence of a small but constant O contamination in all films (incorporated during deposition), along with additional O and H_2 impurities whose concentration was found to be dependent on the extent (or duration) of exposure to air.

The Waterloo researchers found that the surface layers contained a high concentration of hydrogen. Unfortunately, no other impurities were profiled, and the actual composition of these layers is still largely unknown. However, it is significant that thickness effects were found only in samples where the (layer) hydrogen content was larger than the (bulk) oxygen content [14]. Also, no explanation as to why hydrogen should be concentrated at the surfaces was given. It is the author's opinion that the trapped H_2 (from the absorbed water vapour) would be responsible for the high H concentrations found by the Waterloo group. Further, it is suggested that it is in fact the oxygen that is mainly responsible for the different properties of these surface layers. It is important to note that this would not be the same as an oxide layer on c-Si, but would be a graded layer of a-Si:O_x alloy on top of a purer a-Si bulk region. As a result, it would display properties consistent with a-Si:O_x

materials: high resistivity, large E_a and large E_o.

To see how these surface layers affect the optical absorption coefficient, the simple 2-layer model shown in Fig. 3.8 was used.

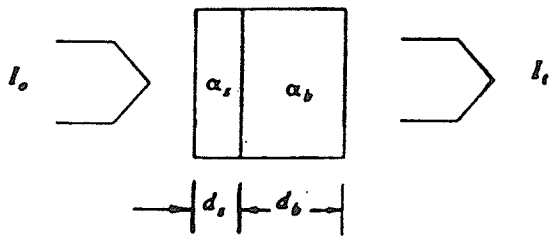

FIGURE 3.8: Simple 2-layer model used to study the effects of surface layers on the optical properties of the sample.

The optical gap is obtained from the energy dependence of the absorption coefficient in the highly absorbing region near the band edges. The absorption coefficient is found from the ratio of the transmitted light I_t, to the incident light I_o. In the simple 2-layer model of Fig. 3.8, assuming no reflections, this is given by

$$I_t = I_o e^{-(\alpha_s d_s + \alpha_b d_b)} \tag{3.4}$$

where s and b refer to the surface and bulk regions, respectively.

It is easily seen that the absorption properties of the sample are dependent on the relative magnitudes of the absorption coefficients and layer thicknesses. Since E_o depends on the form of α, it will also depend on how much the layers contribute to the absorption; ie, how they compare in thickness.

The most definitive evidence for these surface layers would come from a complete impurity profile of the ARE a-Si thin films, with emphasis on O and H. Also, the properties of thin ARE a-Si films should be systematically compared with the bulk properties of alloy films such as a-Si:O_x and a-Si:H, in order to determine which of the impurities is actually responsible for the modified properties in these surface layers.

3.3.4. System Improvement

As mentioned in section 3.2, it was observed that under certain conditions a glow discharge was formed inside the insulating glass tube portion of the reaction nozzle. The reactant gas was passed through the tube at a reduced pressure, while a large dc electric field was applied along the length, as shown in Fig. 3.9(a). This configuration corresponds to a crude plasma tube, such as in Fig. 3.9(b), within which a glow discharge can be formed for appropriate values of pressure (flow rate) and field strength (nozzle potential).

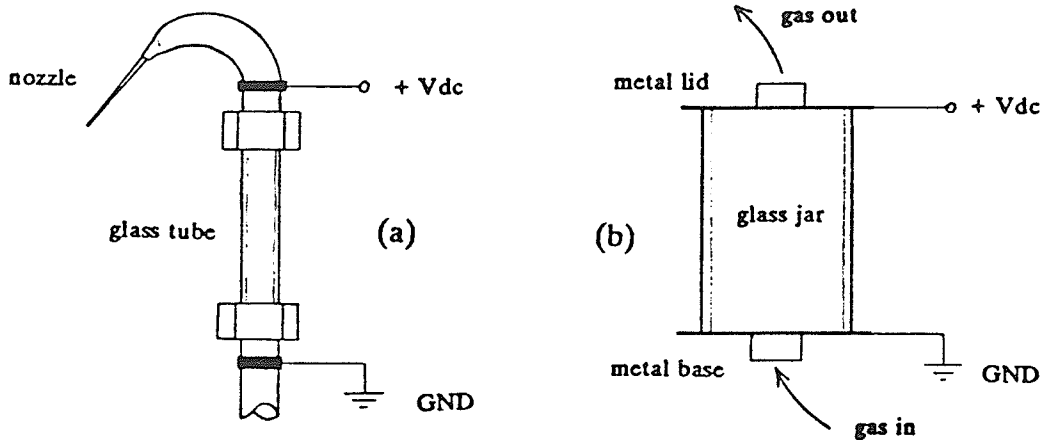

FIGURE 3.9: Actual (a) and schematic (b) configuration of the glass tube used to insulate the reaction nozzle from the rest of the system, which is grounded.

When there was no flow of reactant gas, the pressure inside the nozzle was equal to the system pressure. With a reactant gas flowing at a constant rate, the pressure inside the tube reached a steady state value. The constricted opening of the nozzle and the generally narrow pathway provided by the tubing ensured that this steady state pressure was greater than the system pressure. For a certain pressure range, on the order of milli-Torr, a glow discharge occurred upon application of sufficiently high fields. This field was produced by the high positive potential at one end of the tube with respect to the system ground at the other end. The glow discharge was observed over a restricted range of pressures (corresponding to flow rates of 50-75%), and for nozzle voltages over 800 V (for a 4 cm tube length, this corresponded to a field strength of 200 V/cm).

If the reactant gas was in the form of a plasma, then it was obviously fully activated. Unfortunately, this plasma was not sustained through the metal nozzle, where there was no field present. Thus, with the present nozzle

configuration it was not expected that the plasma would affect the properties of the films. This was supported by the experimental results.

If the plasma could be made to impinge directly upon the growing film, then it would be expected that a great deal of reactant incorporation should occur, as in other plasma activated processes such as sputtering and RF glow discharge. This could be accomplished using a different nozzle configuration, which will be called a plasma injector, like that shown in Fig. 3.10.

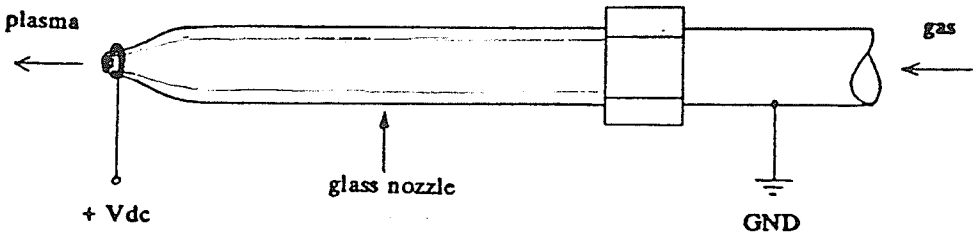

FIGURE 3.10: A suggested design for a plasma injector, which would activate the reactant gas with a glow discharge, and immediately spray this plasma onto the substrates.

This injector would spray the plasma formed within the glass plasma tube directly onto the substrates, hopefully before the activated constituents could recombine into more stable forms, so they could then react with the condensed Si to form a-Si alloy films.

In fact, similar deposition methods have already been used by some researchers [20,21], and are variations of the primary ion beam deposition technique (see section 2.1.2.3). A-Si:H thin films formed by this process strongly resemble RF glow discharge produced materials. It was found that this process incorporated mainly atomic H, and was capable of reducing oxygen incorporation to less than 0.1 at.% [20]. Clearly, this process should produce equally dramatic results with ammonia used as the plasma medium.

CHAPTER IV

FABRICATION AND PROPERTIES OF a-Si:Te*

In this chapter we present the results of an experimental study of the fabrication (by vacuum co-evaporation of Si and Te) and physical properties of a-Si:Te alloys. Co-evaporation is a common and well understood technique for the deposition of layered, graded or alloy thin films [15]. This technique has recently been applied with considerable success to the fabrication of amorphous silicon alloy thin films (as discussed in section 2.1.2.1). Co-evaporation is performed in simple, rugged systems, yet is capable of producing amorphous films over wide compositional ranges. As a result, it is an excellent fabrication technique with which to investigate the first-order properties of new amorphous alloy systems such as a-Si:Te.

To my knowledge, this is the first report of the use of an evaporation technique to produce a-Si:Te thin films. Also, this is the first reported study that covers the composition range below 75 at.% Te, and is only the third study of the electrical and optical properties of this material.

The study of a-Si:Te has been restricted almost entirely to the determination of the structure of these alloys in the bulk glass-forming region (75-85 at.% Te [22]) [23-34]. The only work done at other compositions has been on Te-doped c-Si material [35]. Since no study of the *microscopic* structure of a-Si:Te was undertaken as part of this research, a brief summary of the present understanding of the structure of this material will initially be presented.

From detailed radial distribution analysis [23,25,26,29], IR spectroscopy [24,28,29,36], thermal properties [24,27,32-34,36] and other structural studies [30,31,36], it has been concluded that a-Si:Te consists of four-fold coordinated Si atoms and two-fold coordinated Te atoms linked together in a fully coordinated expanded tetrahedral structure, as shown in Fig. 4.1 [23]. This network consists of tetrahedral Si atoms joined by spiral chains of Te atoms. The average number of Te atoms in the chains is directly proportional to the Te concentration [23]. Note that both right and left handed chains are present

* The contents of this chapter have been submitted for publication to the Journal of Applied Physics.

(intersecting Si atoms at right angles), unlike in crystalline Te, where all chains in a single crystal have the same rotational sense [23]. It is the presence of both types of chains that allows the Si atoms to assume tetrahedral configurations. This structure satisfies all local bonding requirements, again unlike the crystalline form, which is highly defective and ionic in character [36]. This leads to considerable chemical instability of Si_2Te_3 crystals, whereas amorphous a-Si:Te is quite stable (though some defects are expected in freshly evaporated thin films due to X-ray and ion bombardment during deposition; recall the results of Chapter 3) [36]. Though the location of Te atoms in Si-rich a-Si:Te has not been examined, recent studies of the location of Te in doped c-Si [35] have shown that Te is substitutionally incorporated as a double donor impurity. Therefore it is expected that the tetrahedral model (with two-fold coordinated Te) presented above remains valid for most compositions, gradually moving toward a substitutional doping model (with four-fold coordinated Te) with decreasing Te content.

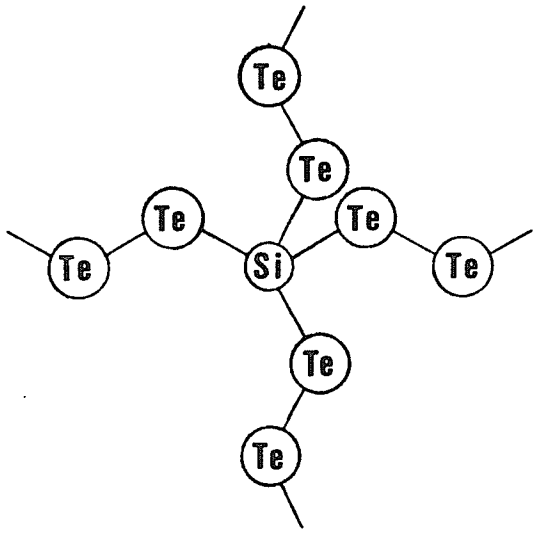

FIGURE 4.1: Expanded tetrahedron model for the structure of a-Si:Te. Note that the Si atom is intersected at right angles by Te chains of opposite rotational senses, allowing it to assume a nearly perfect tetrahedral configuration.

The electrical and optical properties of c-Si_2Te_3 and a-Si:Te over the composition range of 75 to 98 at.% Te (in bulk and thin film form) has been studied by Peterson et al. [36]. A limited study of the pressure and temperature dependence of the optical gap and activation energy of bulk a-$Si_{20}Te_{80}$ has also been performed by Fagan et al. [37]. The thin films were produced by

sputtering polycrystalline Si_2Te_3 [36], while the bulk a-Si:Te was produced by sealed-melt quenching [36,37]. These two papers are, to my knowledge, the only other reports on the electrical and optical properties of a-Si:Te, besides the one presented here. Detailed comparisons with the results of Peterson et al. [36] will be made throughout the remainder of this chapter.

4.1. Co-Evaporation

The co-evaporation system used in this research is shown schematically in Fig. 4.2. The vacuum chamber was bakable to 200 °C, and was evacuated with a liquid N_2 cold trap-equipped diffusion pump. Evaporation of the Si was performed with a Varian 4kW triple-crucible electron gun. Evaporation of the Te was performed with a temperature-controlled resistive heater mounted directly beside the Si source. The substrates were mounted 20 cm above the sources (in order to ensure uniform coverage of all substrates), these substrates could be heated to 200 °C, and were protected from unwanted deposition by a movable shutter.

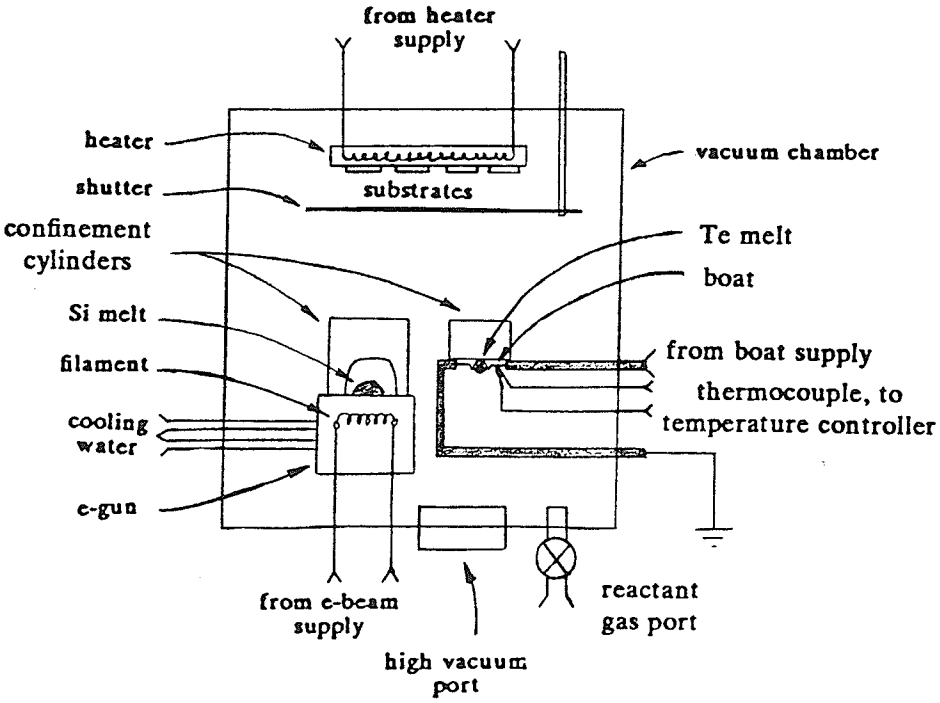

FIGURE 4.2: Schematic diagram of the co-evaporation system used in the fabrication of a-Si:Te thin films. Interior components only are shown.

The Te source consisted of a large Mo boat coated with aluminum oxide (Al_2O_3). This is the recommended configuration for Te evaporation [15]. The boat was suspended next to the Si source by heavy copper strips, which also carried the heater current to the boat. The temperature of the boat was monitored with a Pt/Pt:13% Rh thermocouple. The evaporation rate of the Te was controlled via the boat temperature using a West set-point temperature controller. The evaporation rate of the Si was controlled via the e-beam current.

The overall composition of the films was varied by changing the relative evaporation rates of the two sources. A gas port was also available for reactive co-evaporation, but was not used in this research.

The evaporant materials used were high purity polycrystalline Si and Te, ground into coarse grains. The Si was etched in CP_4 before grinding in order to remove the oxide layer. 5 substrates were used; 2 glass, 1 quartz, 1 aluminum and 1 crystalline salt (KI) disc. All except the KI disc were thoroughly cleaned in organic solvents and an ultrasonic bath before use. The KI discs were polished and dessicated before use.

Prior to each deposition, the chamber was thoroughly cleaned, baked and evacuated to less than 10^{-6} Torr. Both the evaporant Si and Te were fully melted in advance in order to remove any remaining impurities (especially the oxide layer on the Te granules).

All depositions were carried out at a substrate temperature of ≈ 50 °C. Higher temperatures were found to inhibit condensation of the Te and would have resulted in Te crystallization in most films, while lower temperatures were observed to reduce the quality of Si rich films (by increasing the number of defects) and to leave the deposition process susceptible to variations in the ambient temperature. The pressure in the chamber was continuously monitored with an ionization gauge.

Finally, it should be noted that there were some difficulties involved with the use of Te in an evaporation environment. First, metallic Te is a mildly toxic substance, and can become very toxic under special circumstances. The toxicity of Te and recommended safety procedures for its handling are discussed in Appendix A. Second, and more importantly for the experimental results, Te has a high vapour pressure and low melting point, which led to difficulties in maintaining optimum operating conditions over the course of several depositions. As an example, Te deposits tended to form throughout the vacuum system, fouling the thermocouple contact and performance of the vacuum pumps and gauges. These difficulties made prediction of either the deposition rate or composition from the deposition parameters difficult, and may have led to compositional grading in the depth profile of some of the samples.

4.2. Characterization

The a-Si:Te thin films were characterized with X-ray diffraction, scanning electron microscopy (SEM), X-ray energy dispersive spectroscopy (EDS), Fourier Transform infrared (FTIR) spectroscopy, visible and IR spectrophotometry, temperature-dependent conductivity and photoconductivity.

4.2.1. Structural and Chemical Analysis

The thickness of the thin films was measured with a Sloan Dektak mechanical stylus instrument. Samples ranged in thickness from 0.5 to 1.5 μm, with 0.8 μm being a typical thickness. The (monotonic) variation across a sample was usually about 5%. The deposition rate averaged about 20 Å/sec, but varied from 10 to 30 Å/sec depending on the evaporation rates chosen and the condition of the melts.

The degree of crystallinity of the thin films was determined by X-ray diffraction [38] using the Philips X-ray diffractometer in the Metallurgical Sciences Laboratory (MSL) of the Department of Mechanical Engineering. The pure Te samples were found to be fully microcrystalline, which was to be expected since the crystallization temperature of Te is approximately 10 °C [36]. Suprisingly, the 41 and 57 at.% Te samples were also found to display relatively sharp peaks characteristic of microcrystallinity [38]. However, it should be pointed out that the peaks were of relatively low intensity, so it was not expected that the microcrystallites would make up a significant portion of the film. These peaks were positively identified as being due to the presence of Te microcrystallites in the films. The 82 at.% Te sample displayed a single very broad peak due to a-Te. Crystallite identification was made using both the locations and relative intensities of the four peaks observed (using tabulated data available in the MSL). The sharpness of these peaks decreased with increasing Te content, indicating a corresponding decrease in microcrystallite size. All other samples were completely amorphous. These observations and their implications will be discussed in section 4.3.2.

A number of properties of a-Si:Te thin films deposited onto Al substrates were studied with a JEOL JSM-840 SEM equipped with Tracor-Northern image and EDS analysis system (in the Metallurgical Sciences Laboratory). No appreciable surface structure in the thin films could be observed up to the maximum resolvable magnification of 35,000.

The overall composition of the films was obtained by a quantitative X-ray EDS technique (also known as X-ray microanalysis). In this technique the sample is bombarded by the electron beam in a SEM, causing the atoms to flouresce at characteristic X-ray wavelengths (a continuous spectrum is also produced, but is not used) [39]. In this case, the composition was calculated with an iterative, standard-based ZAF package (ZAF is described below) available on the Tracor-Northern system. Since strong signals were always detected from the Al substrates, it was clear that the entire thickness of the thin films was analysed by this technique.

The ZAF technique is a widely used quantitative compositional analysis method. This technique involves first measuring the relative intensities of selected characteristic X-ray peaks, and then correcting them as follows to arrive at the proper composition. First, selected emission lines (Si Kα and Te Lα) from both the sample and from appropriate standards (pure Si and Te) are compared and their intensity* ratio is calculated:

$$K = \frac{\text{intensity of sample line}}{\text{intensity of standard line}} \tag{4.1}$$

This ratio is then iteratively corrected through the use of the following equation (for Te, in this case);

$$C_{Te} = \frac{K_{Te}}{K_{Si} + K_{Te}} ZAF \tag{4.2}$$

where Z is the atomic number correction factor, A the absorption factor and F the flourescence factor [39]. Together, these parameters constitute the so-called "ZAF factor". It was estimated that the composition values obtained in this manner for the a-Si:Te thin films were accurate to ± 5 at.%.

The compositional homogeneity of several representative a-Si:Te films was studied with the X-ray mapping utility available on the Tracor-Northern system. These results are shown in Fig. 4.3(a). The minimum feature size detectable by this technique was approximately 0.1 μm across.

From Fig. 4.3(a) it can be seen that samples in the 50 at.% range (30-70 at.%) can be considered essentially homogeneous, containing a few isolated

* the intensity of a characteristic X-ray peak is the area under the peak in the spectrum: number of counts (detected photons) vs energy.

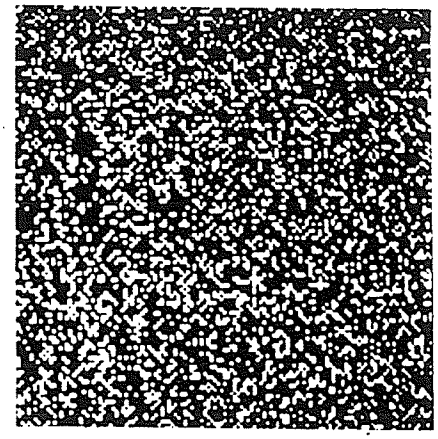

(i)

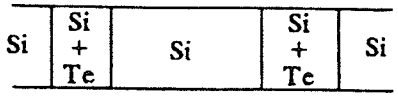

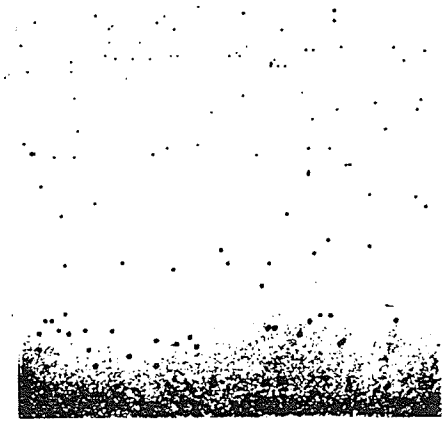

(ii)

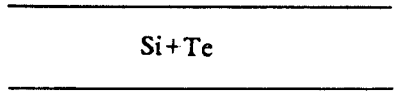

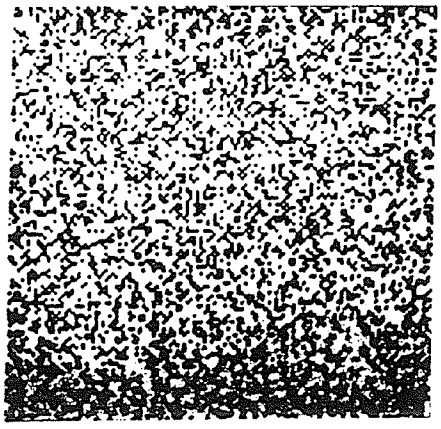

(iii)

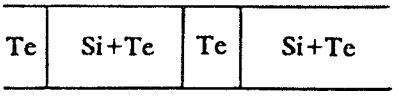

(a) (b)

FIGURE 4.3: X-ray composition maps (a) and proposed depth profiles (b) for three representative a-Si:Te thin films: (i) 12 at.% Te, (ii) 41 at.% Te, (iii) 82 at.% Te. Light regions are Si+Te, dark regions either Si or Te. 1 cm = 40 μm.

pockets of pure Si or Te in a matrix of relatively homogeneous a-Si:Te. However, this is not true of samples having a large excess of one element. In this case, islands of one composition were embedded in a matrix of different composition.

It should be noted that the only information provided by these maps was a top-view picture of the distribution of different atoms in a three dimensional sample. Thus, neither the exact composition nor the depth profile of the Si+Te regions is known. Clearly, however, the regions containing a single element must be homogeneous in order to completely penetrate the film; this explains the compositional depth profiles suggested in Fig 4.3(b).

It is interesting that both pure Si and pure Te regions were not found in any single sample. It appears that Si+Te regions were formed until the minor component was exhausted, leaving separate regions of Si+Te and the (pure) excess element. This fact, and the ability of the Si+Te regions to cover large areas (as in Fig. 4.3 (ii)), would seem to indicate that a homogeneous amorphous compound (within a certain composition range) has been formed, rather than some type of inhomogeneous vertical stacking of small, elemental regions. Thus it will be assumed that these are indeed (macroscopically) homogeneous regions of a-Si:Te.

Finally, it was noted that the electron beam of the SEM tended to "burn" Te-rich a-Si:Te samples. No attempt to characterize this effect was made, though there are obvious implications for archival storage applications; especially if the burning effect is not related to the common ablative hole technique used with pure Te films. Indeed, a-Si:Te has been shown to exhibit memory-type switching (believed to be due to current-induced thermal modifications) in sandwich structures [32,33,36]. The possibility of inducing such effects with an electron beam is a topic which should be pursued in future research.

The IR absorption spectra of the a-Si:Te thin films was measured using the Nicolet FTIR spectrophotometer in the Department of Chemistry. Films deposited on crystalline KI substrates were used for these measurements as the substrates are transparent in the IR region.

IR absorption takes place when the electric field of the incident radiation is in resonance with a vibrational mode of one of the bonding configurations that make up the material. The IR absorption spectrum provides a unique "fingerprint" of the material, from which information about the composition

and structure of the material may be obtained [40]. In particular, the frequency (or wavenumber) at which the absorption band occurs determines which elements are present and how they are bonded, while the height of the peak is directly proportional to the concentration of the absorbing species in the sample [40].

Table 4.1 lists all absorption bands observed in a-Si:Te, along with their postulated sources. The IR absorption spectra for the a-Si:Te thin films produced in this study are shown in Fig. 4.4.

TABLE 4.1: IR absorption bands observed in a-Si:Te thin films deposited by co-evaporation. Also included are all other absorption bands observed in a-Si:Te.

Wavenumber (cm^{-1})	Absorbing Species	Reference
1041-1080	Si-O stretching in a-Si:Te:O	28
787	Si-O stretching in SiO_2	28
907	Si-H_2 bending	41
862	Si-H_2 bending	41
719	Te-O in TeO_2	28
578	Te-O in TeO_2	28
400-455	Te-O in TeO_2	28
370	Te-Te (tentative assignment)	24
165	Te-Te stretching in Te chains	24
87	Te-Te bending in Te chains and ν_4 of $SiTe_4$ tetrahedra	24
328	ν_3 of $SiTe_4$ tetrahedra	24,28
310	Si-Te nonlinear symmetric stretching	28,36

One feature of this figure that should be noted immediately is that the absorbances are very small, which accounts for the wide variation in the background level in these curves. This made it impossible to determine with any confidence the presence of any shifts (to smaller wavenumbers) which might have indirectly indicated the presence of Si-Te bonding [28]. Also, although there was some structure visible below 750 cm^{-1}, it was not possible to determine whether or not it represented actual absorption or was an artifact of the measurement process. However, the fact that its strength is strongly correlated with that of the feature near 670 cm^{-1} (which was due to an atmospheric impurity present in the measurement enclosure) suggests that the latter possibility is more likely. The lower limit of this spectrophotometer was 400 cm^{-1}, so the most interesting bands (due to Si-Te and Te-Te) were completely

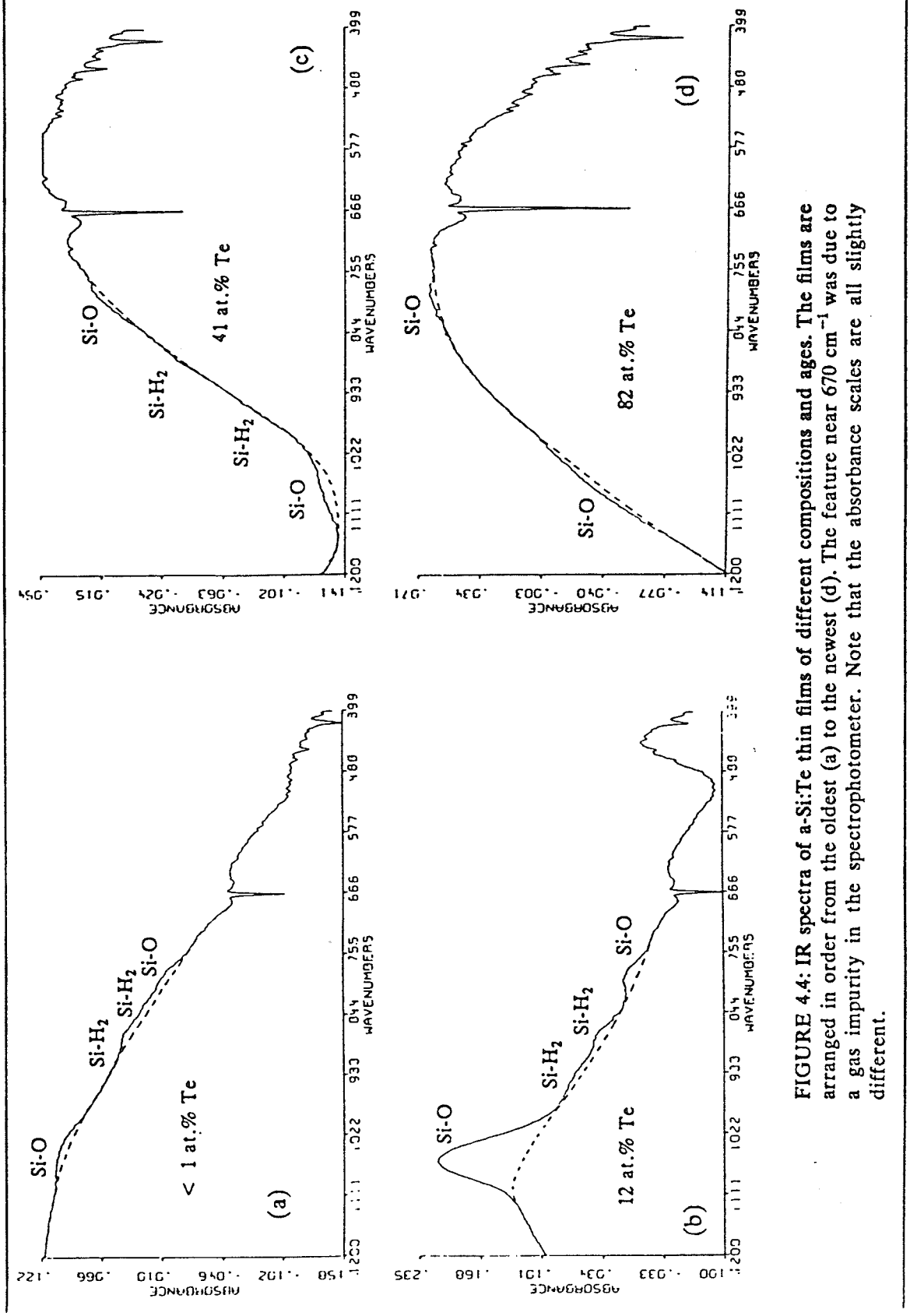

FIGURE 4.4: IR spectra of a-Si:Te thin films of different compositions and ages. The films are arranged in order from the oldest (a) to the newest (d). The feature near 670 cm^{-1} was due to a gas impurity in the spectrophotometer. Note that the absorbance scales are all slightly different.

inaccessible.

The prominent peak near 1050 cm^{-1} is attributed to the Si-O stretching mode in a-SiO rather than in SiO_2, since the wavenumber for this mode (or for interstitial O in Si) is too large (> 1070 cm^{-1}) [28].

The IR spectra were not able to provide unambiguous results concerning bonding in the a-Si:Te; they were, however, quite informative about the impurities incorporated into this material. These results lend support to the model of impurity incorporation presented in sections 3.3.2 and 3.3.3. According to this model, a small but constant amount of O was incorporated during deposition, while variable amounts of O and H_2 were incorporated by atmospheric absorption through the void network. The degree of impurity incorporation by the latter process was a function of the duration of exposure, as well as the condition of the film and atmosphere. In Fig. 4.4, the age of the films is inversely proportional to the Te concentration, with about 1 week between samples. Indeed, it can be seen from the figure that there is a small band due to O impurities which is constant (the one exception will be discussed shortly), and a band due to Si-H_2 bonds which increases as the age of the films increases.

The most convincing evidence in support of this model (which also rules out any compositional dependence) arises from the samples displaying significantly larger impurity peaks in Fig. 4.4(b). These films, unlike the others, exhibited extensive cracking and peeling after deposition, a problem which worsened with age. As a result, these samples had a much greater surface area exposed to the atmosphere, thus more atmospheric impurities were absorbed, producing the exaggerated peaks seen in the Fig. 4.4.

4.2.2. Optical and Electrical Properties

The compositional dependence of the optical gap, E_o, is shown in Fig. 4.5. E_o was obtained using the standard procedure outlined in section 1.1.3. Also included in this figure are the results of Peterson et al. [36], who found a minimum in E_o at 80 at.% Te (corresponding to the eutectic composition [42]). The present work fills out the complete range of compositions. The optical gap of the crystallized Te films was found to be approximately 0.44 eV. The large difference in this value and that found for a-Te was also noted by Peterson et al. [36].

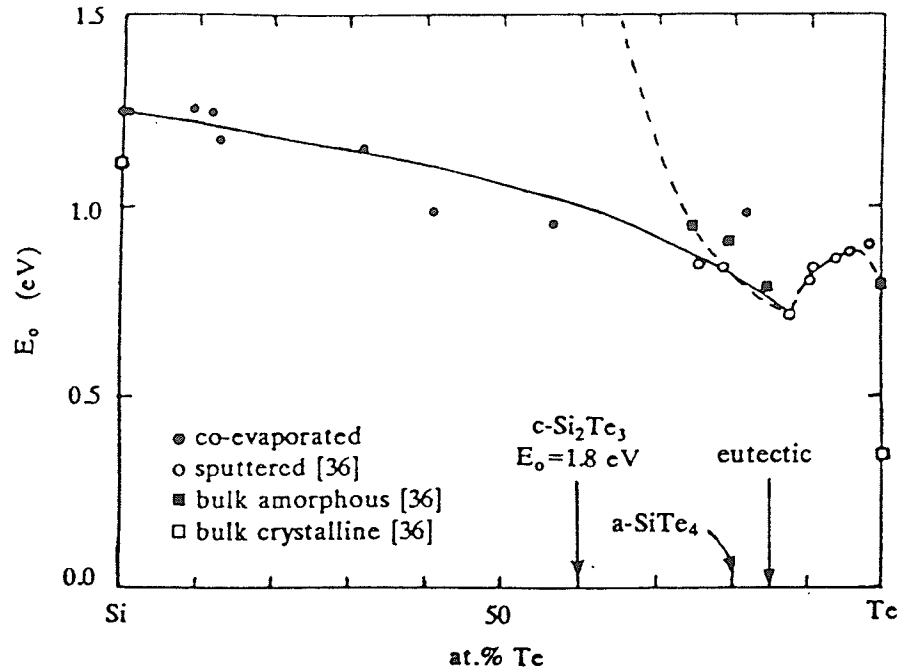

FIGURE 4.5: Optical energy gap of co-evaporated a-Si:Te thin films vs composition. Dashed line is that suggested by Peterson et al. [36], solid line by the author. Measurement error in E_o is ± 0.03 eV.

The temperature dependence of the dc dark conductivity of the a-Si:Te thin films was measured using Al contacts in a gap-cell geometry, and is shown as a function of composition in Fig. 4.6. This data was analyzed using the techniques outlined in section 1.1.2.

The dark conductivity of all samples, σ_d, was dominated by extended state conduction for temperatures above 250 K, while variable range hopping through localized states near the Fermi level dominated below 250 K. The compositional dependence of σ_d for these two conduction regimes has been clarified by replotting the data in the form of Fig. 4.7.

As expected, the room temperature conductivity increases with increasing Te content, due mainly to the decrease in E_o. The activation energy for extended state conduction is shown in Fig. 4.8. E_a was obtained using the procedure described in section 1.1.2. The linear region of the $\ln\sigma_d$ vs $1000/T$ graph extends from 325 K to approximately 250 K, as seen in Fig. 4.6. The low values of E_a correspond to the relatively large values of σ_d. The fact that the increase in E_a near 60 at.% Te did not produce a corresponding decrease in σ_d was due to compensation by changes in the pre-exponential factor, σ_0. Because there is much disagreement on the exact nature of σ_0, no attempt will

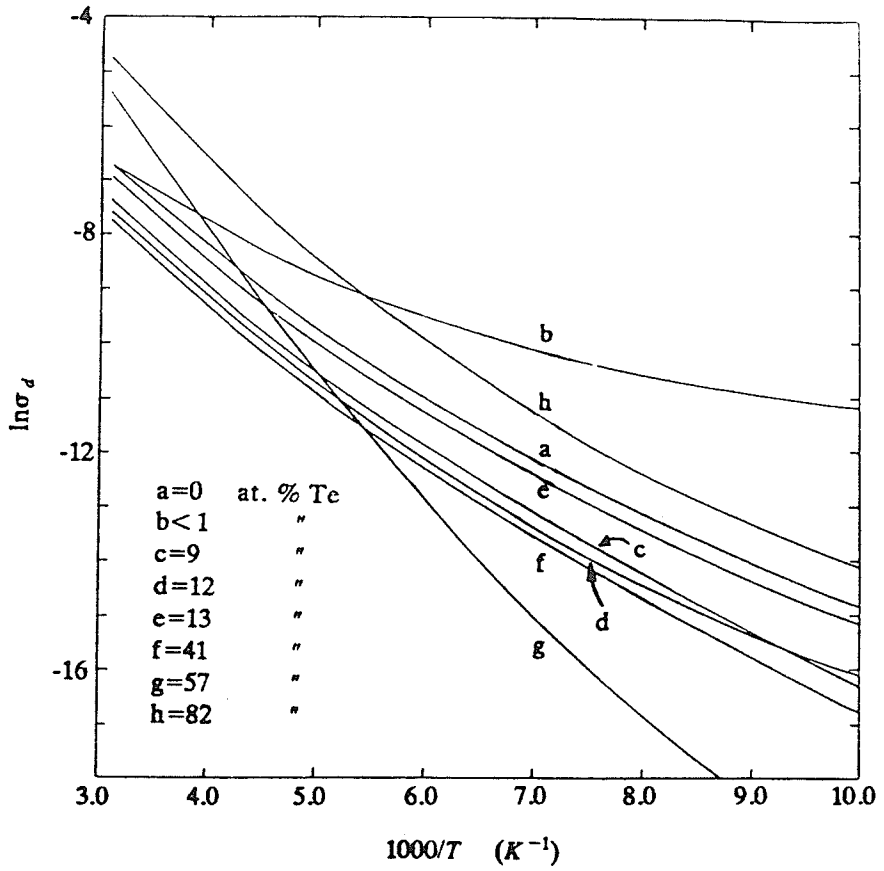

FIGURE 4.6: $\ln\sigma_d$ vs $1000/T$ as a function of composition. Note that the linear region extends from 325 K to approximately 250 K, indicating the dominance of extended state conduction over this temperature range.

be made to propose a mechanism for this change. Since bulk a-Si:Te contains a very small number of defects [36], it is expected that E_a should be larger than in evaporated thin films. The main point to note is that both materials exhibit a peak in E_a, which will be discussed further in section 4.3.3.

Suprisingly, however, the low temperature σ_d (Fig. 4.7) shows considerable structure. This is attributed to variations in the density of states, DOS, as conduction at low temperatures is dominated by hopping through localized states near the Fermi level. The presence of this conduction process is revealed by a linear graph of $\ln(\sigma_d T^{1/2})$ vs $T^{-1/4}$, as shown in Fig. 4.9. Estimates of $N(E_F)$ derived from the temperature dependence of σ_d in this regime (by the methods outlined in section 1.1.2) confirm this fact, as can be seen from Fig. 4.10.

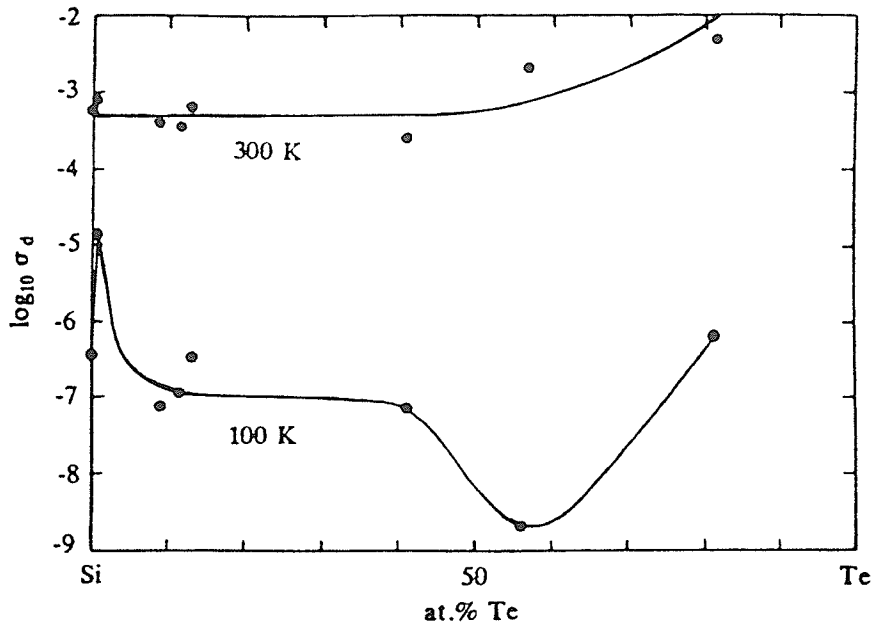

FIGURE 4.7: DC dark conductivity of a-Si:Te thin films vs composition for high temperature (extended state conduction) and low temperature (hopping conduction) regions. Experimental error in σ_d is less than the dot size at 300 K and approximately ± 10 % at 100 K.

The a-Si:Te thin films displayed a modest photoconductivity, generally observable only at low temperatures. The magnitude of σ_{ph} ranged from 10^{-8} to 10^{-5} $(\Omega\,\mathrm{cm})^{-1}$. These values were measured at 100 K using the 514.5 nm line from a Spectra-Physics Ar^+ ion laser. The laser was operated at an output power of 0.02 W, corresponding to approximately 1.5×10^{17} photons/cm^{2}sec incident on the gap-cell (appropriate corrections were made to account for mirror and window loss, and the fraction of the beam spot incident on the gap).

The ratio of photoconductivity to dark conductivity is shown in Fig. 4.11. This figure clearly shows a strong peak for films containing approximately 60 at.% Te. Peterson et al. [36] also found a strong photoresponse in samples containing 80 at.% Te, though they either could not or did not measure the photoconductivity in samples of other compositions. This peak also correlates well with the drop in the density of gap states at this concentration, since these states are expected to act as non-radiative recombination centers.

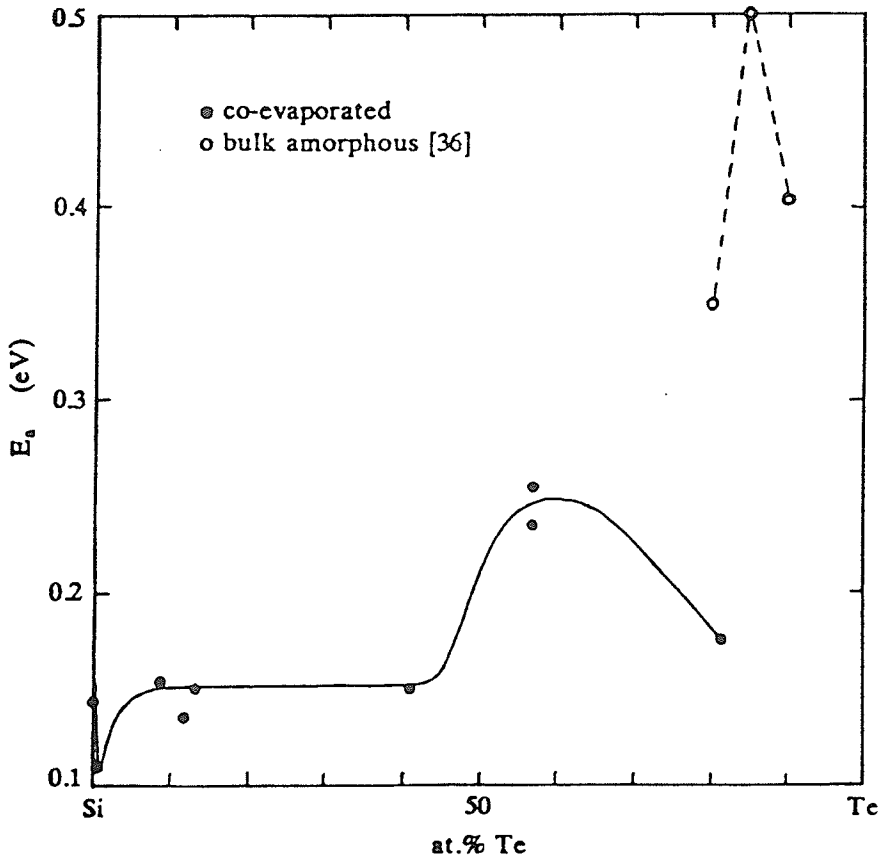

FIGURE 4.8: Activation energy of a-Si:Te thin films vs composition. Measurement error in E_a is ± 0.01 eV.

4.3. Discussion

4.3.1. Effects of Homogeneity

The compositional homogeneity of the a-Si:Te thin films was measured directly using the qualitative X-ray mapping technique discussed in section 4.2.1. These results, as shown in Fig. 4.3, indicate that not all the films produced were homogeneous. Only films in the range of approximately 30 to 70 at.% Te could be considered as a homogeneous a-Si:Te material. Films of less than 5 at.%, or more than 95 at.% Te could be considered essentially homogeneous as well, though the latter were subject to crystallization of the Te. The non-homogeneous films existed in two different varieties: Si-rich and Te-rich. In the first case, the films consisted of small islands of a-Si:Te embedded in an a-Si matrix. In the second case, a-Te islands were embedded in an a-Si:Te matrix. This non-homogeneity must be distinguished from the microcrystallinity, which was found only in the (macroscopically) homogeneous films in

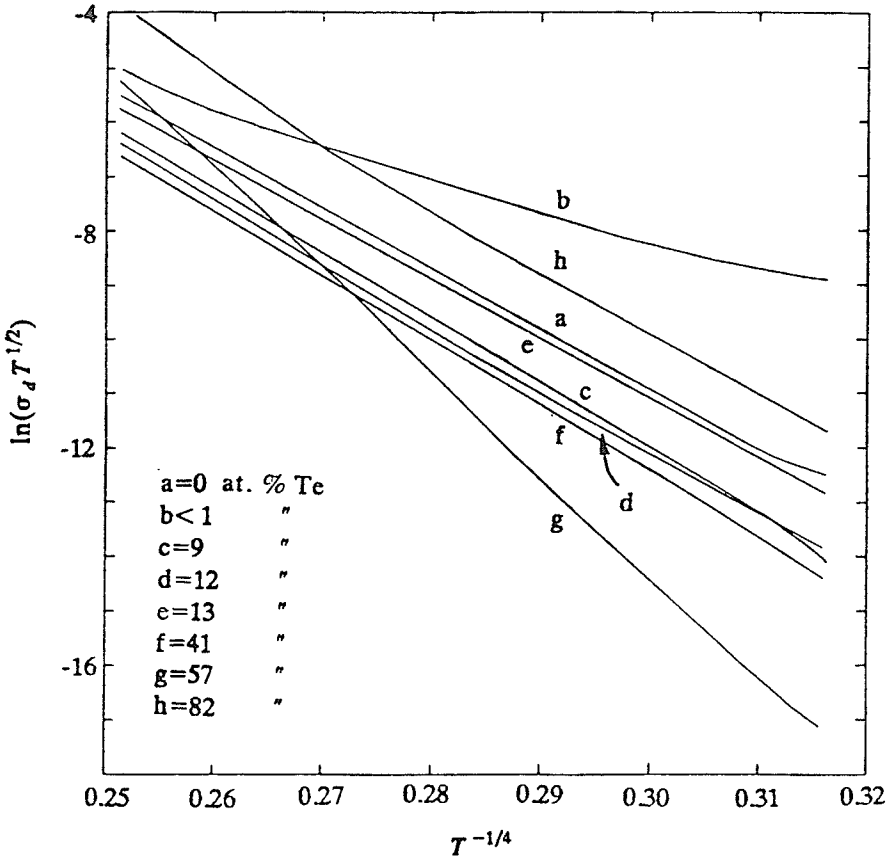

FIGURE 4.9: $\ln(\sigma_d T^{1/2})$ vs $T^{-1/4}$ as a function of composition. Note that the linear region extends below approximately 250 K, indicating the dominance of variable range hopping conduction at the Fermi level over this temperature range.

the 30 to 70 at.% Te range. Clearly, the Te microcrystallites constitute a non-homogeneity as well, but their small size and low concentration ensured that their effect on the measured electrical and optical properties was negligible, as will be discussed further in the next section.

The degree of homogeneity of the thin films had a strong effect on their optical and electronic behaviour. In this research, the properties that were measured characterized the dominant material phase. In the case of homogeneous films, this was representative of the entire film. In the case of non-homogeneous films, only the properties of a single phase were measured; any features of the remaining phase were swamped by those of the dominant phase for that particular measurement.

The optical data was obtained from transmission measurements. In this case, the regions with the lowest absorption dominated the overall film

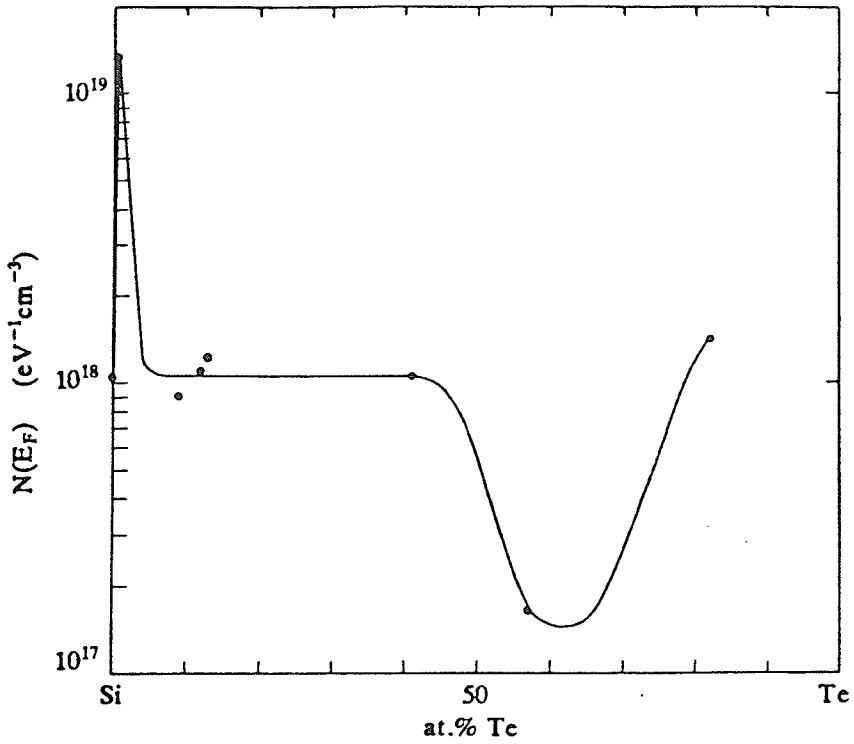

FIGURE 4.10: Estimated DOS at the Fermi level for a-Si:Te thin films vs composition. Measurement error in $N(E_F)$ is approximately ± 20 %.

properties. It was not possible to measure the properties of the domains individually because of their small size (on the order of μm). Si-rich non-homogeneous films appeared to possess the optical properties of pure a-Si (which has a larger E_o than a-Si:Te), and any downward trend that may have occurred in E_o was not observed. Similarly, Te-rich, non-homogeneous films appeared to possess the properties of a-Si:Te, and again the trend was lost. The overall effect was to produce a generally flat plot of E_o vs composition (non-homogeneous regions), interrupted by apparently sudden changes (homogeneous regions). This type of behaviour is clearly visible in Fig. 4.5.

The electrical measurements were also dominated by a single phase in non-homogeneous samples. In this case, the dc conductivity was dominated by the matrix phase. The island material, being below the percolation threshold, contributed to σ_d in a minor way. In order to examine the properties of the island material, ac conductivity measurements may provide better information. Therefore, conduction in the Si-rich films proceeded mainly through the a-Si matrix, while a-Si:Te dominated conduction in the Te-rich sample (though in this case the a-Si:Te appeared to be Si-dominated in turn). Again the overall

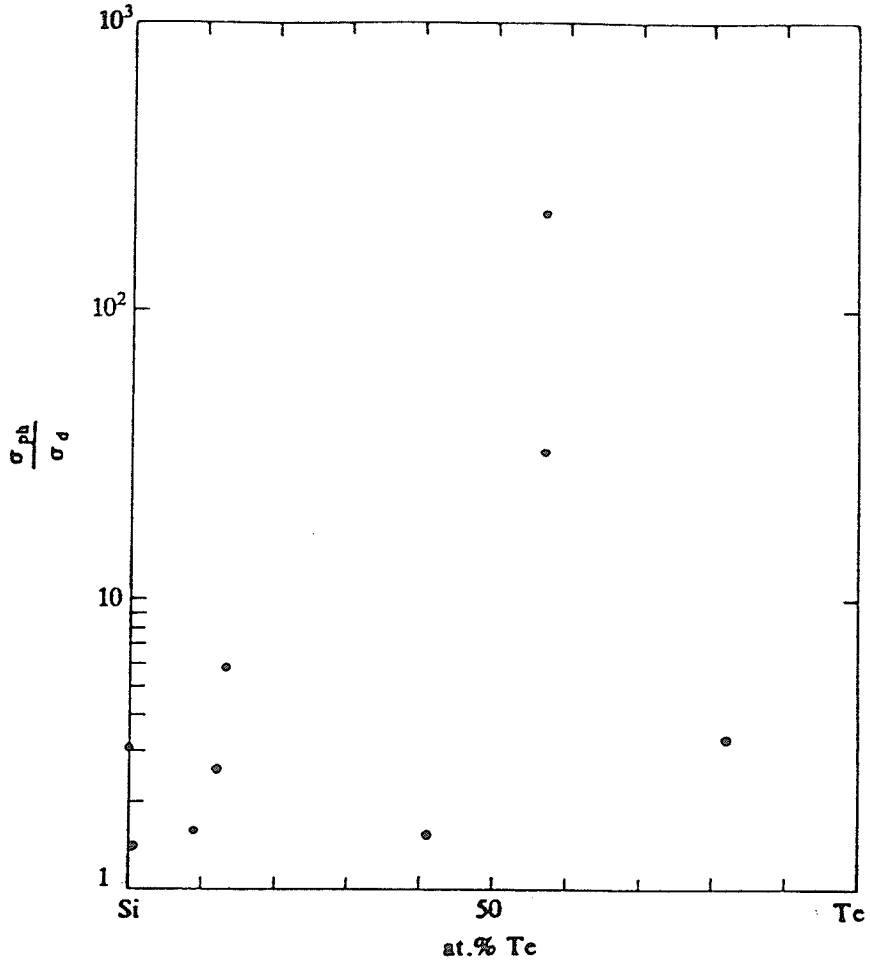

FIGURE 4.11: Photoconductivity to dark conductivity ratio of a-Si:Te thin films vs composition. Measurement error in this ratio is less than ± 5.

effect was to wash out any trends that may have been more apparent if all the films were homogeneous. This also can be seen in the conductivity results.

In section 4.3.3, some interesting features that were observed in the electrical data will be discussed in detail. The preceeding discussion does not apply to this section as the properties discussed were found only in fully homogeneous films.

4.3.2. Microcrystallinity

The presence of Te microcrystallites in the a-Si:Te thin films was not expected to significantly affect their optical and electrical properties for reasons similar to those given in the preceeding section. The maximum dimensions of the Te microcrystallites was on the order of 100 Å [43], and was thus

infinitesimally small compared to the scales of measurement (conductivity gap-cell dimensions of mm^2, for example). This, combined with the fact that these films were found to be homogeneous a-Si:Te from the X-ray mapping procedure, and that the concentration of microcrystallites was very low, implies that the microcrystallites were in the form of isolated islands embedded in an a-Si:Te matrix. Because of their small size and low concentration, and the fact that they were well below any percolation threshold, the microcrystallites could not contribute significantly to the measured properties. This can be seen from the similarity in the properties of the 41 and 82 at.% Te samples and most of the remainder of the films (despite significant differences in the degree of microcrystallinity). Thus the different properties of the 57 at.% Te sample were not due to the presence of Te microcrystallites.

That there were microcrystallites at all in these films was quite suprising. The nearly pure (> 90 at.% Te) a-Te samples were expected to become microcrystalline, since the crystallization temperature for Te is approximately 10 °C [36]. It is also interesting that the sharpness of the peaks (corresponding directly to the microcrystallite size) *decreases* with increasing Te content. Perhaps the close contact with the Si atoms expected in homogeneous films at these compositions forced the Te chains to adopt more ordered configurations. However, this remains a point of conjecture.

4.3.3. Optical and Electrical Properties

The a-Si:Te thin films studied in this research were produced by co-evaporation and were therefore expected to contain a large concentration of defects such as voids and dangling bonds (in both Si and Te). These defects are expected to produce a high density of localized states in the pseudo-gap. The experimental data for these films confirms this assumption. The high dark conductivities, small activation energies and large $N(E_F)$ are all characteristic features of the highly defective amorphous films produced by evaporation processes. However, the compositional dependence of the physical properties shows some interesting features for compositions of <1 and 60 at.% Te. The physical origins of each of these features will be discussed in turn.

For <1 at.% Te there is a minima in E_a and a maximum in $N(E_F)$. This would appear to indicate that Te is acting predominantly as a substitutional donor (fourfold coordinated); the decrease in E_a is due to the two electrons donated by each substitutional Te atom, moving the Fermi level slightly closer

to the conduction band mobility edge. This is similar to the behaviour of most other elements when incorporated into a-Si at these concentrations (see section 2.2.). The dramatic increase in $N(E_F)$ at this composition could be due to the additional trap levels produced by the donors (at 0.41 and 0.14 eV in Te-doped c-Si [35]) contributing to $N(E_F)$. However, it is also likely that a significant fraction of the Te atoms did not adopt a fourfold coordination, but retained their usual two-fold habit. If this was the case, then a significant number of Si dangling bonds may also have been produced by this highly non-optimum bonding situation, contributing directly to $N(E_F)$.

Therefore, a-Si:Te thin films of <1 at.% Te appear to consist of a-Si containing substitutional Te atoms incorporated both as double donors and in their normal two-fold coordination; the net effect being a more defective and n-type film.

For approximately 60 at.% Te there is a maximum in E_a and σ_{ph}, and a minimum in $N(E_F)$. These features indicate that the films have become less defective. This was almost certainly due to the formation of the more fully coordinated network characteristic of a-$SiTe_4$. As mentioned at the beginning of this chapter, the bulk form of this material contains very few dangling bonds [36], thus $N(E_F)$ should be considerably smaller than in samples of different compositions. Though somewhat Si-rich, evaporated films near 60 at.% Te were homogeneous, and probably approached this optimum case more closely than did the very non-homogeneous samples closer to the optimum composition of 80 at.% Te (corresponding to a-$SiTe_4$). The satisfaction of a significant number of dangling bonds is supported by the increase in E_a. Since these localized states are located close to the conduction band, they cause pure a-Si to become n-type. Any reduction in the dangling bond concentration results in a decrease in this doping effect by reducing $N(E_F)$, which in turn allows the Fermi level to move back towards the center of the gap, thereby increasing E_a (as in the case of hydrogenation of a-Si, for example). The increase in σ_{ph}/σ_d also supports this hypothesis, as a reduction of the number of dangling bonds is also a reduction of the number of non-radiative recombination centers present in the gap.

Therefore, samples having a composition near 60 at.% Te appear to have formed a somewhat Si-rich but homogeneous approximation to the optimum a-$SiTe_4$ material. This material forms a nearly fully-coordinated amorphous network, which reduces the concentration of dangling bonds present in the

film. This trend may also have been observed by Peterson et al. [36] in bulk a-Si:Te, since their sample of 80 at.% Te exhibited a strong peak in E_a (see Fig. 4.8).

Unfortunately, it was not possible to unambiguously identify the dominant carrier type. However, Peterson et al. [36] found that a-Si:Te was dominated by hole conduction above about 60 at.% Te. Thus a transition from n-type to p-type conduction is expected at some composition, though the high defect concentration found in the co-evaporated thin films may have prevented this occurrence.

There are few applications presently foreseen for this unusual material. Some interest has been shown in a-$SiTe_4$ as a memory-type (or ovonic [7]) switch [32,33,36]. As mentioned earlier, there is now the possibility that a-$SiTe_4$ could also be used in archival storage applications in a manner similar to a-Si:H [3]. In the consideration of other potential applications for a-Si:Te, it should be remembered that this material can be made in bulk form, can be quite stable chemically and thermally, and can display room temperature photoconductivity. In addition, the wide range of diverse properties that this material possesses may foster its application in devices such as those based upon amorphous multilayers, for example.

4.3.3. System Improvements

During the course of this research it became apparent that the co-evaporation system being used possessed some major shortcomings. These did not preclude the production of a-Si:Te thin films, but did make for difficult, unpredictable operation and generally low quality films (with respect to homogeneity). These problems were mainly the result of two particular faults. The most important was the lack of a proper current-limited power supply for the very low resistance Mo boat required for Te evaporation. The other problem was that maintaining a constant temperature at the boat did not guarantee a constant evaporation rate. The result of these two system faults were chronic boil-over of the Te during warm-up, a highly variable evaporation rate (due to temperature overshoot and changes in melt conditions) and contamination of the vacuum system by excessive amounts of Te vapour.

To solve these problems, a number of relatively simple equipment modifications are required. To reduce Te contamination, a basket-type boat should be used to enforce beaming of the Te vapour stream onto the

substrates. A proper, current-limited power supply must be used with the boat to ensure controllability of the evaporation process. This control should be provided directly through the use of rate controlled (rather than temperature controlled) evaporation. The use of separate deposition rate monitors and controllers for the Si and Te sources will enable accurate prediction and direct control of the deposition rate, composition and compositional gradient of the films.

The results of such improvements will be greatly improved predictability, controlability and versatility of this system. The films produced will be more homogeneous, and the controlled production of graded or layered films will become possible.

Finally, to produce amorphous films above compositions of approximately 80 at.% Te, cryogenically cooled substrates must be used to prevent crystallization of the Te. These substrates must be held significantly below the crystallization temperature of 10 °C both during and after deposition, or the subsequent annealing (even at room temperature) will crystallize the films.

CHAPTER V

CONCLUSIONS

The fabrication, properties and applications of amorphous Si based alloys was reviewed. It was found that these materials exhibit a fascinating range of behaviours, and possess properties suitable for many applications. Based on this work, the following recommendations were proposed:

1. A more standardized approach to the characterization of these materials should be adopted in order to facilitate comparison between the results of different researchers. This could be accomplished by including in all studies a few basic, simple experiments. These include measurement of the optical gap, determination of the dc dark conduction mechanisms and demonstration of the presence or absence of photoconductivity.
2. More effort should be made by researchers to distinguish between the effects of alloying and hydrogenation. Any results claimed to be due to alloying in a hydrogenated alloy can only be regarded with suspicion if no consideration to possible variations in the H content are made.
3. There are several promising avenues of research that have yet to receive due consideration from researchers:

   (i) the possibility of studying the metallic phase of Si in metal-rich a-Si:M alloys,

   (ii) the possibility of studying directly the Anderson metal-insulator transition in a-Si:Ge:B:H alloys,

   (iii) the exploitation of the relatively well known properties of the hydrogenated tetrahedral alloys toward the improvement of existing devices and the implementation of new ones.

The fabrication of a-Si:N:H alloys by activated reactive evaporation was attempted. The electrical and optical properties of these thin films were characterized, and the following conclusions reached:

1. Activated reactive evaporation of silicon with a 90% N_2, 10% H_2 reactant gas (Forming gas) is not capable of producing a-Si:N:H alloy thin films. The films produced were found to consist of impure and highly porous amorphous silicon.

2. This failure of the ARE process (with Forming gas) to incorporate either N or H into a-Si thin films is attributed to several cooperative effects:
   (i) the very low reactivity of N_2 with Si,
   (ii) the great difficulty in activating N_2,
   (iii) the absence of sufficient quantities of the more reactive H_2.
3. It was also found that the longstanding assumption of previous ARE researchers that vapour phase reactions dominate the fabrication process is incorrect. Only the particles impinging on the substrates can significantly affect the composition of the film. Therefore, it is substrate reactions which dominate film growth in the ARE process.
4. Bulk impurities incorporated into these a-Si thin films during fabrication are thought to consist of approximately 10 at.% oxygen (as SiO and SiO_2), with some hydrogen also (as H_2 gas trapped in the void network).
5. It was found that the highly porous nature of these a-Si films led to significant contaminant absorption upon exposure to the atmosphere, producing a constant thickness (≈ 0.1 μm) surface layer possessing a higher optical gap than the bulk region. This surface layer (thought to be O and H_2 rich) contributes significantly to the overall properties of thinner films, producing an increased optical gap in these samples. Additional support for this theory was obtained from IR absorption measurements made on evaporated a-Si:Te thin films.

Despite the negative results of this work, it is thought that ARE remains a promising technique for the fabrication of alloys where one or more of the constituents is in a gaseous form. To bring the performance of the ARE process up to expectations, the following recommendations are given:

1. To improve the existing ARE system, it is recommended that ammonia, NH_3, be used as the reactant gas, since it is easily dissociated into species that will react with Si. Current plans are to extend the ARE work in this direction in the near future.
2. To improve the ARE process, it also is recommended that a glow discharge be used to fully activate the reactant gas. This plasma is to be produced in an insulating nozzle, so that the activated species can be injected directly into the growing film.

Thin films of a-Si:Te were successfully fabricated by co-evaporation over the composition range 0 to 82 at.% Te. There has been very little work done on the electrical and optical properties of this material. As a result, this work has significantly extended the knowledge of this material. This is the first study to use an evaporation technique to produce a-Si:Te thin films, is the first study of a-Si:Te with less than 75 at.% Te, and is only the third study of the electrical and optical properties.

In this report, the structural, optical and electrical properties of co-evaporated a-Si:Te thin films were characterized, and the following conclusions reached:

1. The films were found to be non-homogeneous over a significant range of compositions. Consideration of this fact was extremely important in developing an understanding of this material.
2. A-Si:Te thin films with compositions above 90 at.% Te were crystalline, and could not be utilized in this study. Homogeneous thin films in the 30-70 at.% Te range were also found to exhibit a small degree of micro-crystallinity which was not expected to significantly affect the properties of these films. However, it is interesting that the crystallite size decreased with increasing Te content in these films.
3. A-Si:Te exhibited two radically different behaviours depending on the concentration of Te in homogeneous thin films:

   (i) for very low concentrations, $<$ 1at.% Te, the presence of Te reduced E_a and increased $N(E_F)$. This was attributed to four-fold coordinated Te atoms acting predominantly as substitutional double donors in a-Si. Such doping behaviour is typical of most elements when incorporated into a-Si at these concentrations.

   (ii) for compositions near 60 at.% Te, an increase in E_a and a decrease in $N(E_F)$ was found. This was attributed to the Si and Te forming a Si-rich, homogeneous approximation to the optimal a-$SiTe_4$ network. These films therefore formed a more fully coordinated amorphous network. A strong peak in the photoconductivity for these films also supports this hypothesis.

4. Presently, there are only a few applications foreseen for a-Si:Te, as memory-type switches or possibly in archival storage. However, the fact that the coordination of Te can be changed from four-fold to two-fold depending on the concentration (with correspondingly drastic changes in the electrical and optical properties) demonstrates some potential for future multilayer devices and structures.
5. The co-evaporation system was found to have a number of shortcomings; the most important of these was the lack of rate monitored and controlled deposition (producing compositional grading and non-homogeneity) or cryogenic substrates (producing Te microcrystallinity).

REFERENCES

[1] H. Frizsche, *Noncrystalline Semiconductors,* Phys. Today, Oct. 1984, pp. 34.

[2] J.I. Pankove (ed.), *Semiconductors and Semimetals vol. 21, pt. D,* Academic Press Inc., Orlando, 1984.

[3] R.D. McLeod, W. Pries, H.C. Card, K.C. Kao, *Hydrogenated Amorphous Silicon for Archival Storage,* Appl. Phys. Lett. 45, pp. 628, 1984.

[4] R.D. McLeod, *Studies in Amorphous Silicon,* Ph.D. Thesis, University of Manitoba, 1985.

[5] Z. Zhao-bo, J. Jian-Sheng, S. Zhi-an, *Study of Amorphography by Using Fuzzy Symetric Group and Basic Structural Characteristic Parameters,* J. Non-Cryst. Sol. 59/60, pp. 105, 1983.

[6] R.D. McLeod, W. Pries, H.C. Card, *Hardware Experts for Computational Physics,* presented at the Canadian VLSI '85 Conf., Toronto, Nov., 1985.

[7] N.F. Mott, E.A. Davis, *Electronic Processes in Non-Crystalline Materials, 2nd ed.,* Clarendon Press, Oxford, 1979.

[8] P.W. Anderson, *The Absence of Diffusion in Certain Random Lattices,* Phys. Rev. 109, pp. 1492, 1958.

[9] W.E. Spear, P.G. Le Comber, *Substitutional Doping of Amorphous Silicon,* Sol. St. Comm. 17, pp. 1193, 1975.

[10] W.B. Jackson, S.J. Oh, C.C. Tsai, J.W. Allen, *Conduction Band Density of States in Hydrogenated Amorphous Silicon Determined by Inverse Photoemission,* Phys. Rev. Lett. 53, pp. 1481, 1984.

[11] R.F. Bunshah, A.C. Raghuram, *Activated Reactive Evaporation Process for High Rate Deposition of Compounds,* J. Vac. Sci. Tech. 9, pp. 1385, 1972.

[12] W. Pries, *Novel Fabrication Techniques and Applications for Amorphous Silicon,* Master's Thesis, University of Manitoba, 1984.

[13] W. Pries, R.D. McLeod, T.V. Herak, S.R. Mejia, H.C. Card, K.C. Kao, *Properties of a-Si:H Deposited by Activated Reactive Evaporation (ARE),* Journal de Physique, to be published.

[14] G. Talukder, J.A. Gowan, D.E. Brodie, J.D. Leslie, *Thickness and Doping Effects Observed in Impure Vacuum Deposited a-Si Films,* Can. J. of Physics 62, pp. 848, 1984.

[15] L.I. Maisel and R. Glang (eds.), *Handbook of Thin Film Technology,* McGraw-Hill Book Co., 1970.

[16] L. Kubler, J.J. Koulmann, R. Haug, A. Jaéglé, *Evaporated a-Si Films with Low ESR Defect Density by Hydrogenation Under NH_3 Ambient,* Sol. St. Comm. 48, pp. 61, 1983.

[17] S.M. Sze, *Physics of Semiconductor Devices, 2nd ed.*, John Wiley and Sons Inc., 1981.

[18] Y.J. Chabal, C.K.N. Patel, *Solid Hydrogen in Amorphous Silicon: Phase Transition,* Phys. Rev. Lett. 53, pp. 1771, 1984.

[19] J.C. Bean and J.M. Poate, *Evidence for Void Interconnection in Evaporated Amorphous Silicon from Epitaxial Crystallization Measurements,* Appl. Phys. Lett. 36, pp. 59, 1980.

[20] M. Shindo, S. Sato, I. Myokan, S. Mano, T. Shibata, *Preparation and Analysis of Reactively Evaporated a-Si:H,* J. Non Cryst. Solids 59-60, pp. 747, 1983.

[21] V. Grasso, A.M. Mezzasalma, F. Neri, *A New Method for Preparing Hydrogenated Amorphous Silicon Films,* Sol. St. Comm. 41, pp. 675, 1982.

[22] H.S. Chen, C.E. Miller, *A Rapid Quenching Technique for the Preparation of Thin Uniform Films of Amorphous Solids,* Rev. of Sci. Instr. 41, pp. 1237, 1970.

[23] F.R.L. Schoening, *The Structure of Amorphous Silicon Telluride,* J. of Materials Sci. 14, pp. 2397, 1979.

[24] G.E.A. Bartsch, H. Bromme, J. Zirke, *Infrared and Thermal Studies of Glassy Tellurium-Silicon Alloys,* in *The Physics of Non-Crystalline Solids, 4th Int'l. Conf., Clausthal-Zellerfeld, 1970,* G.H. Frischat ed., Trans Tech Pub., pp. 591, 1977.

[25] G.E.A. Bartsch, H. Bromme, T. Just, *Radial Distribution Studies of Glassy Tellurium-Silicon Alloys,* J. Non Cryst. Solids 18, pp. 65, 1975.

[26] G. Bartsch, T. Just, *On the Structure of the Amorphous Tellurium Alloy with 19 at.% Si,* Zeit. für Metallkde 63, pp. 360, 1972. (in German)

[27] A.R. Hilton, C.E. Jones, M. Brau, *Non-Oxide IVa-Va-VIa Chalcogenide Glasses. Pt. 1,* Phys. and Chem. of Glasses 7, pp. 105, 1966.

[28] A.R. Hilton, C.E. Jones, *Non-Oxide IVa-Va-VIa Chalcogenide Glasses. Pt. 2,* Phys. and Chem. of Glasses 7, pp. 112, 1966.

[29] A.R. Hilton, C.E. Jones, R.D. Dobrott, H.M. Klein, A.M. Bryant, T.D. George, *Non-Oxide IVa-Va-VIa Chalcogenide Glasses. Pts. 3,* Phys. and Chem. of Glasses 7, pp. 116, 1966.

[30] V.S. Minaev, V.T. Shipatov, *Use of the Mössbauer Effect to Investigate the Structure of Glasses in the Silicon-Tellurium System,* Inorganic Mater 16, pp. 1037, 1980.

[31] P.P. Seregin, E. Yu. Turaev, A.A. Andreev, B.T. Melekh, *Structure of the Short-Range Order in Glassy and Crystalline Si-Te and Ge-Te Alloys Using NMR and Electron Spectroscopy,* Sov. J. of Glass Phys. and Chem. 5, pp. 597, 1979.

[32] S.A. Altunyan, V.S. Minaev, M.S. Minazhdinov, B.K. Skachkov, *Formation of Glasses in the Si-Te System and Memory-Type Switching Diodes Made of Si-Te Semiconducting Glasses,* Sov. Phys. Semicond. 4, pp. 1906, 1971.

[33] L.N. Makhinya, *Influence of the Delay Time on the Nature of Switching in Glassy Chalcogenide Films,* Sov. Phys. Semicond. 14, pp. 464, 1980.

[34] H. Ruppersberg, C. Görlitz, B. Heck, *Structural Relaxations in $Ni_{35}Ti_{65}$ and $Te_{78}Si_{22}$ Glasses Studied by DSC Measurements,* J. Phys. F: Met. Phys. 14, pp. 309, 1984.

[35] K. Hofmann, M. Shulz, *Tellurium-Related Trap Levels in Silicon,* Appl. Phys. A 33, pp. 19, 1984.

[36] K.E. Petersen, U. Birkholz, D. Adler, *Properties of Crystalline and Amorphous Silicon Telluride,* Phys. Rev. B 8, pp. 1453, 1973.

[37] E.A. Fagen, S.H. Holmberg, R.W. Seguin, J.C. Thompson, H. Fritzsche, *Temperature and Pressure Dependence of the Optical and Electrical Gap in Chalcogenide Glasses,* in *Proc. of the 10th Int'l. Conf. on the Phys. of Semicond., Cambridge, 1970,* S.P. Keller, J.C. Hensel, F. Stern (eds.), U.S. Div. Tech. Inform., Oak Ridge, Tenn., pp. 672, 1970.

[38] H.P. Klug, L.E. Alexander, *X-Ray Diffraction Procedures for Polycrystalline and Amorphous Materials, 2nd ed.,* John Wiley and Sons, New York, 1974.

[39] I. Adler, *X-ray Emission Spectrometry in Geology,* Elsevier Pub. Co., Amsterdam, 1970.

[40] A.L. Smith, *Applied Infrared Spectroscopy,* John Wiley and Sons, New York, 1979.

[41] G. Lucovsky, W.B. Pollard, *Vibrational Properties of Amorphous Alloys,* in *The Physics of Hydrogenated Amorphous Silicon II,* J.D. Joannopoulos, G. Lucovsky (eds.), Topics in Applied Physics vol. 56, Springer-Verlag, Berlin, pp.301, 1984.

[42] L.G. Bailey, *Preparation and Properties of Silicon Telluride,* J. Phys. Chem. Solids 27, pp. 1593, 1966.

APPENDIX A

TOXICITY AND SAFE HANDLING OF TELLURIUM METAL [1]

Tellurium metal is a low toxicity substance, but can potentially become very dangerous under special circumstances. This material should not present a hazard if due precautions are taken.

Te metal is potentially hazardous when in the form of fine powders or flakes, as it can then enter the body through inhalation or ingestion. Once in the body, Te is converted to dimethyl telluride, which produces the following symptoms of mild Te poisoning: fatigue, loss of appetite, nausea, metallic taste in the mouth, and a garlic odour to breath and perspiration. In addition, Te can also cause mild skin and/or eye irritation. Symptoms of chronic exposure are fatigue, loss of appetite, bronchitis and dermatitis.

In general, one should avoid any skin contact (through the use of rubber gloves), or exposure to dust or powders (through the use of goggles and dust-masks or respirators).

In an emergency, the following steps should be taken immediately upon exposure:

(1) skin contact; wash thoroughly,
(2) if inhaled; keep patient warm and seek medical aid,
(3) if ingested; wash mouth, induce vomiting and seek medical aid.

Note that exposure of open wounds to *large* amounts of Te can be fatal. Therefore one should not work with this material if injured. If exposed, seek medical aid immediately.

Certain unusual situations can result in the production of highly toxic Te compounds, such as TeO_2 gas. Therefore, heating of Te should be done in a vacuum, or at least under a fume hood. Avoid entirely exposure of Te to acids.

Reference for Appendix A

[1] N.I. Sax (ed.), *Dangerous Properties of Industrial Materials, 5th ed.*, Van Nostrand Reinhold Co., New York, 1979.